Assessing and modeling night-time contrast perception of elderly drivers under conditions of glare

van Hoesel, Tom R.C.

Award date:
2023

Assessing and modeling night-time contrast perception of elderly drivers under conditions of glare

Tom Richardus Cornelis van Hoesel

Master thesis

Department of Industrial Engineering and Innovation Sciences
Human Technology Interaction

Supervisors
Raymond Cuijpers
Rik Spieringhs
Xiangzhen Kong

February 2023

Abstract

The global population is aging rapidly, which means more elderly drivers will be on the road. As we age, our visual system changes, and we become less sensitive to contrast and more susceptible to glare. It is of importance that road design standards take into account these characteristics of the elderly visual system to guarantee safe roads for all its users. One commonly used standard regarding the maximum amount of glare a road user can be exposed to is, however, based on the visual system of a 23-year-old. In this work, the luminance difference threshold of an elderly sample is investigated under conditions of glare in order to guide better future design standards. This is investigated with a psychophysical experiment, in which participants are exposed to a night-time driving scene, and have to indicate the direction of an arrow on the road that is present in the scene. Besides this, different models that predict the threshold are investigated. Results showed that on average, elderly participants have a luminance difference threshold that is 1.3x higher under conditions of glare compared to conditions without glare. Furthermore, comparing the data of this elderly sample with that of younger participants (under conditions of glare), it was found that the luminance difference threshold of the elderly participants is 2.5x higher than that of the younger ones. This highlights the need of improving road lighting standards to accommodate the aging population.

Keywords: visibility, road lighting, contrast perception, glare perception, image forming, luminance difference threshold

Contents

Introduction

"*We willen leven in een land waar we vlot en veilig van A naar B kunnen*."
Rijkswaterstaat (2022)

"*We want to live in a country where we can travel from A to B quickly and safely*" are the words from Rijkswaterstaat (2022), the Dutch Ministry of Infrastructure and Water Management. To achieve this goal, one has to constantly be aware of technological, societal, and demographical changes in the world. One of the most significant, challenging demographic changes right now is aging. This change started in high-income countries, but it is no longer exclusive to them: the aging of the population happens all over the world (WHO, 2021). One of the reasons for this is a decline in the fertility rate, in combination with an increase in life expectancy due to advancements in healthcare technology (WHO, 2010, 2022a).
In the Netherlands, aging is very prevalent. At the time of writing, 28% of the total population is 60 years or older, which is expected to rise to 34% in the next thirty years (WHO, 2022c). In the last twenty years, life-expectancy for people at the age of 60 has increased by three years (WHO, 2022b).

While an increase in people's lifespan is generally regarded as positive, it does propose other challenges. These challenges can be categorized into the categories of economy, healthcare, and social pressures (Sciubba, 2020). The economic challenge includes a continuous increase of the pressure on the welfare state, as the workforce is shrinking. There will be fewer 'young' people (i.e., working population) that have to provide for an increasing number of elderly (i.e. retired population). As a result, businesses will find difficulties in filling in their occupations. Shifting to the healthcare perspective, there will be an increase in people suffering from age-related diseases like diabetes, dementia, arthrosis, and cataracts (RIVM, 2019), which will increase the demand for healthcare and the pressure on the healthcare system. Lastly, these challenges might lead to societal tensions. For example, there might be intergenerational conflicts on whether or not to allocate government funds toward all these challenges (Hess et al., 2017).

For this study, the health issues, especially the problems related to vision, are most relevant. While indeed, healthcare has been improving over the last decades, and the chance of suffering from vision impairments has been reduced on an individual level, population growth in combination with aging causes our healthcare systems to not be prepared for the increasing amount of people suffering from vision impairments on a population level (Bourne et al., 2021). Or, as the WHO (2019) states in their *World report on vision*: "The global need for eye care is projected to increase dramatically in the coming decades, posing a considerable challenge to health systems" (p. x).

As Figure 1 shows, there is an expected increase in the number of people with a variety of vision impairments in the coming decades. Among these, the most common are cataracts, uncorrected refractive errors, glaucoma, macular degeneration, and corneal opacity, of which the risk of contracting increases with age (Ackland et al., 2017; WHO, 2019).

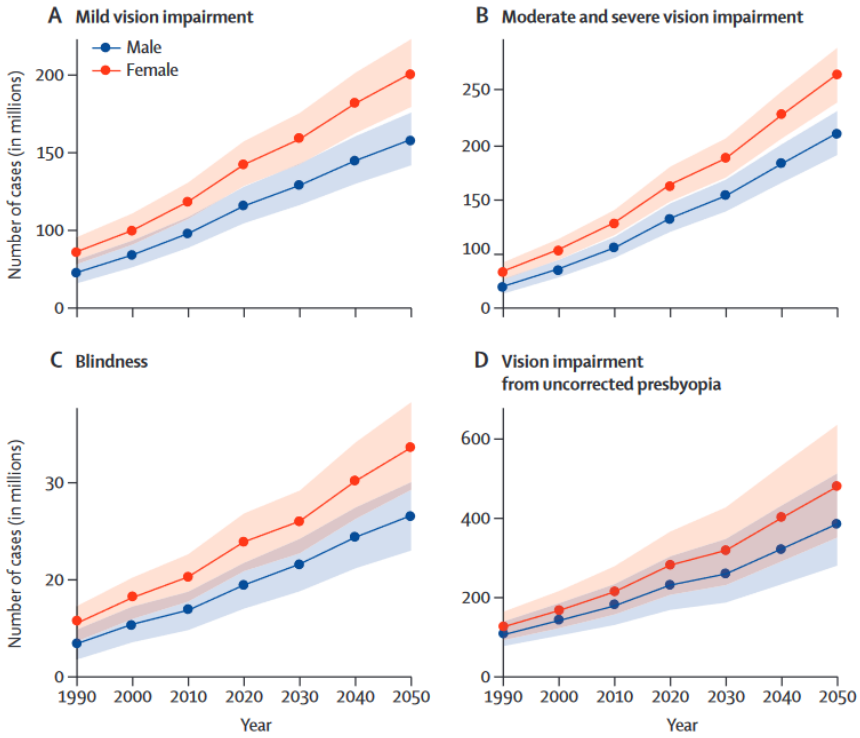

Figure 1. Forecast of people suffering from different vision impairments in the United States. Adapted from Bourne et al. (2021).

This increase in visual impairments may be detrimental to safety, especially when driving a motorized vehicle. Numbers from CBS (2022) show that in the Netherlands, more elderly are in the possession of a valid driver's license. In fact, compared to five years before, driver's license possession saw the sharpest increase in the age group of 75+, increasing by 38%. In addition to this, most casualties on the road fall in the age group of 65+ (Rijkswaterstaat, 2021; SWOV, 2022). Without going into the underlying causes of these numbers, but acknowledging the fact that elderly have a higher risk of dying anyway (being on the road or not), it is not controversial to conclude that the elderly are proportionally more at risk when driving a vehicle.

Nevertheless, even while aware of the fact that they are at risk and their driving skills (e.g. reaction time, quick hand and feet movements) are declining, elderly drivers still overestimated their driving skills, which was in turn related to an increase in unsafe driving behavior (Freund et al., 2005). The perception of

reduced driving skills is not the most important reason for elderly to stop driving, as when asked, the most frequently given reason for them to stop driving is on doctor's advice (Persson, 1993).

Considering an aging population, in which visual impairments are more common, and more elderly drivers are on the road (who are not planning on quitting driving any time soon), one might think that in road design this rapidly growing group is considered, and necessary safety precautions are taken to make the road a safe place for all its users. However, this is not the case.

A crucial aspect of road safety is lighting, which ensures the road, its markings (i.e., signs and stripes), and its users, are all visible during the nighttime. To ensure this, there are European Standards on road lighting like the NEN 13201-3 (2016) that guide designers in how to ensure the visibility of objects and create safe roads. These standards provide recommendations on, among lots of other things, the required luminance at different locations on the road surface, uniformity of the luminance, and the amount of acceptable glare as a result of the lighting.

One of the recommendations in this standard is questionable, given the current demographic changes. It concerns the parameters that are used in calculating the maximum amount of glare road users are allowed to perceive. As stated in the NEN 13201-3 (2016) under Chapter 8.5, *conventionally* they based their recommendations on the visual system of a 23-year-old person. The problem is that the visual system of a 23-year-old is not at all comparable to the visual system of an elderly person. Research has shown that the older we get, the worse our vision gets due to changes in different parts of our eyes and subsequent neural pathways (CIE, 2017; van Bommel, 2015). Two main effects of age on the visual system, are loss of contrast perception and increased susceptibility to glare, which cause the visual scene to be less clear (van den Berg et al., 2010). As an illustration, Figure 2 shows how the world is perceived when you experience reduced contrast perception, while Figure 3 illustrates the effect of age on the susceptibility to glare. As can be seen in these figures, they are not two independent phenomena: the more susceptible you are to glare, the lower the overall contrast in your visual field is. This becomes especially clear when comparing the visibility of the person in left and right picture of Figure 3.

Figure 2. The visual effects of a reduction in contrast perception, from low (left) to high (right) contrast. Adapted from Ising (2014).

Figure 3. The visual effects of being more susceptible to glare (on the right), compared to a normal eye (left). Adapted from van den Berg et al. (2010).

Considering these age-related effects on vision, an aging society, and road lighting installations designed for a 23-year-old, a reevaluation of these recommendations is necessary. Therefore, the main goal of this work will be to fill in this gap by investigating the contrast perception of elderly people under conditions of glare in a night-driving situation.

In the past, attempts have been made to model the contrast perception thresholds of elderly, for example in the work of Adrian (1989), whose model includes parameters like age and glare. However, this model is based on the perception of simplified stimuli: small uniformly lit circles on a uniformly lit background. In addition, only objects smaller than 1° were investigated (Joulan, Hautière, et al., 2011). We can imagine that this model would not be representative of the complex scenes we encounter when driving at night. First, the targets are much more complex and have various shapes (pedestrians, road markings, signs, etc.). Second, as shown in Figure 3, the object in focus (the pedestrian in the middle of the image) does not have a uniform luminance as its legs and face are brighter than its torso. The same holds for the background, it is also not uniformly illuminated, leading to different contrasts with the pedestrian at different parts of its body. Another limitation of Adrian's (1989) model is that only static parameters are allowed. For example, only one ‘background luminance’ can be used as input, which leads to problems in complex visual scenes: should this be an average luminance around the target, a minimum or maximum, or some kind of weighted average?

To deal with these limitations, other models of contrast have been proposed that do not depend on these assumptions. These are image-based models, for example, those of Joulan et al. (2011) or Tadmor and Tolhurst (2000), which are based on computer vision and simulate aspects of our visual system. In these models, complex images can be used as input, and using edge-detecting algorithms local contrasts across these edges are calculated. To the author's knowledge, none of the current image-based models however take into account how contrasts are perceived in situations with glare.

Combining the previously discussed unsatisfactory standards for contrast perception of elderly drivers under conditions of glare with the suboptimal models to predict their perception, we find ourselves with the following main research question:

RQ*: In a population of elderly drivers, what is the contrast perception of non-uniform objects in a complex scene under conditions of glare, and how can we model this?*

Besides this main research question, two different sub-questions will be answered. The first sub-question is answered using the work of Spieringhs and colleagues (2023) [Unpublished manuscript], who also investigated contrast perception in night-time driving under conditions of glare. Their target demographic, however, was younger, and can thus be used to answer the first sub-research question.

SRQ1: *How does the contrast perception under glare conditions differ in a young compared to an old population of drivers at night?*

The second sub-research question can be answered by using the data collected in this work.

SRQ2: *How does the contrast perception of elderly drivers at night differ in situations with glare compared to situations without glare?*

These questions will be investigated through a psychophysical experiment using a driving simulation. In this experiment, participants have to indicate the direction of an arrow on the road that is present in the scene under different conditions. The conditions include variations in road luminance, arrow luminance, arrow size, and, most importantly, the presence or absence of glare. The participants' performance in this experiment reveals their luminance difference threshold, that is, the amount of luminance contrast required for participants to distinguish between arrows pointing left and right. This threshold will in turn also be predicted by the models introduced earlier to investigate their usefulness in this context. It is expected that the luminance difference threshold of the elderly sample will be higher under conditions of glare compared to conditions without glare, and that the threshold of the younger sample is lower than that of the elderly sample. By answering all three research questions, a better understanding of contrast perception in complex situations is achieved, and more accurate contrast perception models can be developed, which in turn can guide the development of new road lighting standards, ultimately leading to safer roads for all its users.

This report will start with an elaborate *Theoretical Background* section, including an explanation of the human visual system, and its components that are relevant to the perception of contrast and glare. Following, several ways of mathematically modeling contrast and glare perception are described. This section ends with a more detailed description of how aging influences visual perception. Next, the *Method* section describes the design of this research, all used materials, and the QUEST+ psychometric paradigm. The *Results* section is structured the following way: after a short description of the effects of road luminance and arrow size on the luminance difference threshold, the effects of glare (i.e., SRQ1) and age (i.e, SRQ2) on the threshold are presented. Next, the applicability of the Adrian (1989), Tadmor and Tolhurst (2000), and Joulan et al. (2011) models are discussed respectively. Finally, the *Discussion* section follows the same structure to discuss the results found in this study and answers the main research question.

By having answered all three research questions, a better understanding of contrast perception in complex situations is achieved, and more accurate contrast perception models can be developed, which in turn can guide the development of new road lighting standards, ultimately leading to safer roads for all its users.

Theoretical Background

The human eye

The human eye is an intricate instrument that enables us to see our surrounding visual environment. In most everyday situations vision is our dominant modality, which highlights the importance of this instrument (Gazzaniga et al., 2014). Figure 4 shows a schematic anatomy of the human eye, where all its important structures are highlighted (Fiedler et al., 2009). In this section, these major structures will shortly be explained. Thereafter, more detailed attention will be paid to the structures involved in contrast and glare perception.

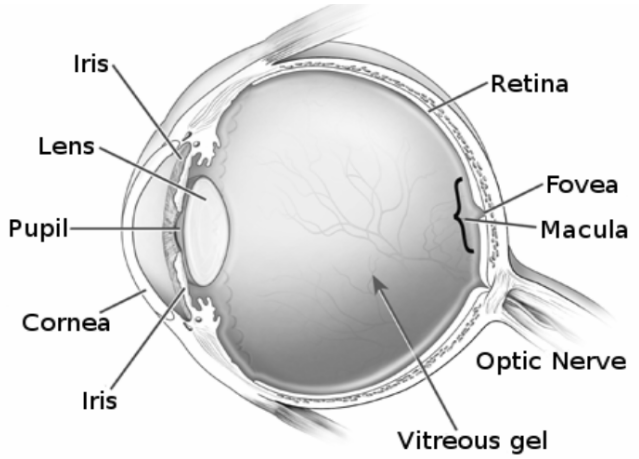

Figure 4. Schematic representation of the human eye, extracted from Fiedler et al. (2009).

When light from the outside world enters the eye, the cornea is the first structure it passes through. The cornea is a transparent membrane responsible for the largest refraction of light, focusing it on subsequent structures like the lens (Galloway et al., 2016; Mather, 2016). The lens and the ciliary muscles that are connected around it form the second major structure responsible for refracting light. The ciliary muscles can change the convexity of the lens, which is called accommodation. Accommodation allows us to focus on, that is, to see sharp, objects at different distances from our eyes (Mather, 2016). When we want to focus on nearby objects, our ciliary muscles contract, which thickens our lens; when we want to focus on the far field, the opposite occurs (Galloway et al., 2016). In between the cornea and lens, we find the pupil, an aperture whose size is regulated by muscles in the iris. Together, they regulate the amount of light that can pass into the subsequent eye-structures (Fairchild, 2013; Galloway et al., 2016). The area between the lens and the inner surface of the eye is filed with the clear vitreous gel, which maintains the spherical shape of the eye and assures that light can reach the retina (Mather, 2016). The retina is the inner surface of our eye, which consists of several neuronal layers, including three different photosensitive cells: rods,

cones, and intrinsically photosensitive retinal ganglion cells (ipRGCs) (Berson, 2003). These cells transduce light signals (photon streams) into electrical signals, which in turn get propagated to the brain via the optic nerve.

Contrast perception

The first aspect of human visual perception that will be discussed in more detail is contrast perception. To understand how we perceive contrast, it is important to examine the retina in more detail. Figure 5 presents a schematic overview of the retina (Discovery Eye Foundation, 2016). The following section describes the cellular organization of the retina, after which different models of contrast perception will be discussed.

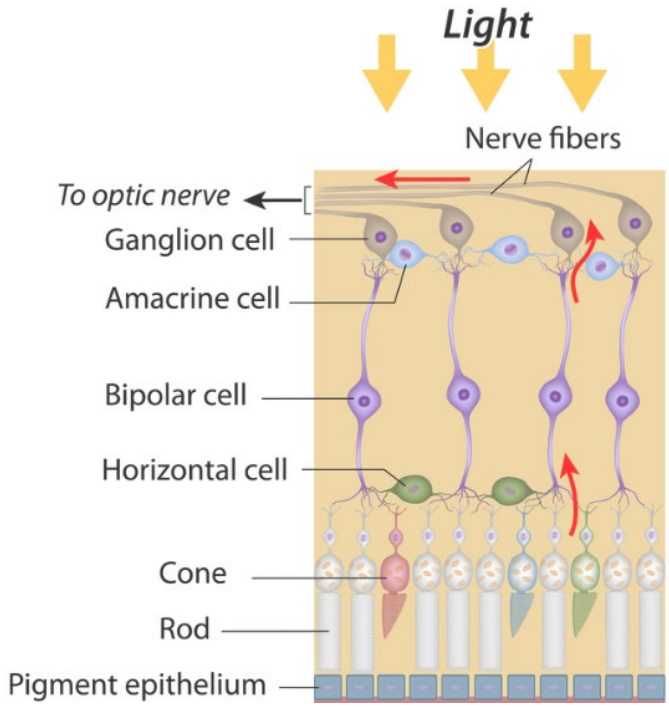

Figure 5. A schematic overview of the retina, extracted from Discovery Eye Foundation (2016) and slightly modified by the author.

Layers of the retina

Starting at the back of the eye, we find the pigment epithelium, an opaque structure consisting of cells that reduce light scattering back into the retina by absorbing light that was not absorbed by photoreceptors. Besides this function, it also nourishes neighboring cells, stimulating the regeneration of depleted photopigments (Fairchild, 2013; Galloway et al., 2016).

As explained earlier, photoreceptors transduce light signals, that is photons, into electric signals that are further processed in the brain. There are three types of photoreceptors: rods, cones, and intrinsically photosensitive retinal ganglion cells (ipRGCs). The ipRGCs are mainly important for non-image-forming

effects of light like regulating our circadian rhythms and alertness, and thus are less relevant for our current discussion (Berson, 2003; Lok et al., 2018). Rods and cones, however, do play an important role in image forming. They both contain photopigments, photopsin and rhodopsin respectively, which are sensitive to light and can absorb photons. Upon absorption, the membrane potential of the photoreceptor is changed, triggering a downstream action potential (Gazzaniga et al., 2014). Cones are mainly responsible for color vision, and come in three different types: long (L, red), medium (M, green), and short (S, blue), corresponding to the wavelength of maximum absorption of its specific photopigment. Photopigments in L cones are most sensitive to wavelengths of 558 nm, those in M cones to 531 nm, and those in S cones to 419 nm. For rhodopsin, the peak absorption is 496 nm (Hildebrand & Fielder, 2011). Figure 6 shows a graph of the spectral sensitivities of the different photoreceptors (Betts et al., 2013).

Besides differences in spectral sensitivity, there are more differences between the photoreceptors. Rods require way less stimulation to elicit a response, a single photon is enough. This allows rods to communicate information about the visual world at low light levels (scotopic vision). However, rhodopsin is depleted quickly, and therefore not useful at high luminance levels (Gazzaniga et al., 2014). Cones, on the other hand, require more stimulation and only get activated in environments with sufficient light (photopic vision), but have photopigments that quickly replenish. In between scotopic and photopic vision, we find mesopic vision. In mesopic vision, both rods and cones contribute to our visual perception.

Another difference is the amount and distribution of these photoreceptors: there are roughly 7 million cones which are mainly in the fovea, the center of our field of vision. As a result of this, we are able to distinguish the most visual details in the fovea. Our 120 million rods, on the other hand, are spread out over the entire retina, with the exception of the fovea (Fairchild, 2013). This distribution is visualized in Figure 7 (Lin et al., 2012), which also shows the blind spot: the location where the optic nerve connects to the retina and thus contains no photoreceptors of any kind.

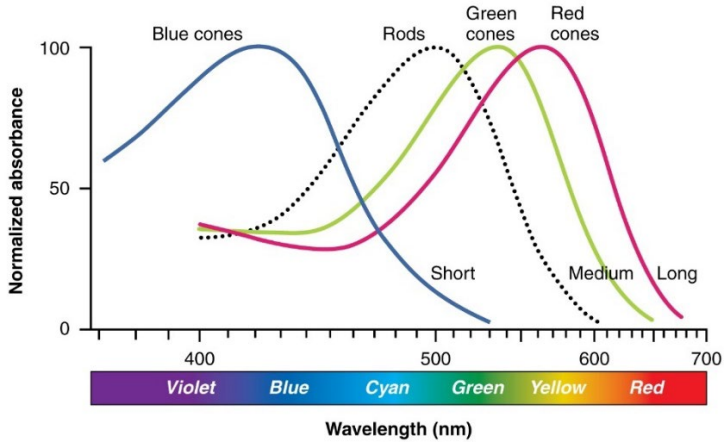

Figure 6. Spectral sensitivities of different photoreceptors in the retina. Adapted from Betts et al. (2013) and slightly modified by the author.

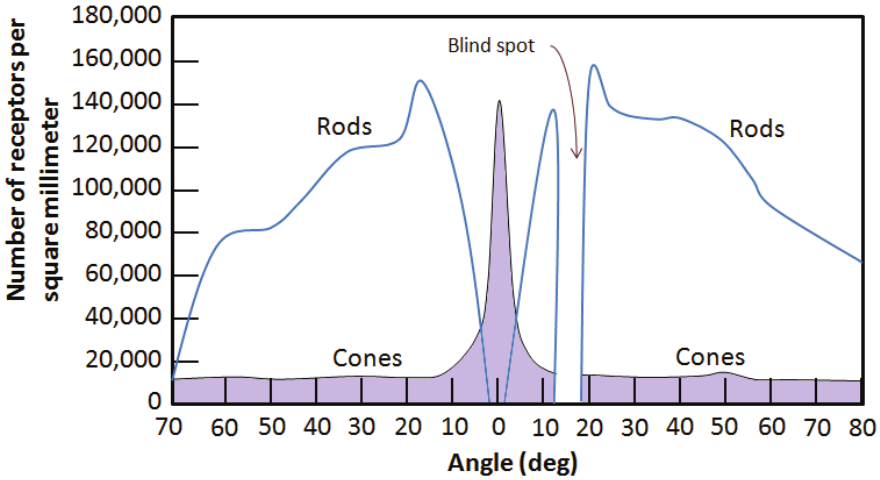

Figure 7. The photoreceptor distribution relative to the fovea (0°), adapted from Lin et al. (2012).

Upon absorption of photons by photoreceptors, the downstream signal will travel through the interneuron layer. This layer consists of different cells, all with the function of processing the photoreceptor signal and feeding it to the ganglion cells. There are three types of interneurons in this layer (Figure 5): bipolar cells, horizontal cells, and amacrine cells (Hildebrand & Fielder, 2011). The bipolar cells respond to an increase or decrease in photon catch by photoreceptors: ON-bipolars activate by an increase in photon catch, while OFF-bipolars activate by a decrease in photon catch (Mather, 2016). There are few cones connected to each cone bipolar (as few as a single cone), while for rod bipolars up to 70 rods can be connected (Hildebrand & Fielder, 2011). The horizontal cells connect photoreceptors and bipolar cells laterally to each other, and regulate their signals. They serve several functions, one of which is lateral inhibition: when a photoreceptor gets excited, the activity of neighboring photoreceptors is reduced (Demb & Singer, 2015). These cells also serve the ganglion cells (which are discussed in the next section) by ensuring their center-surround receptive field formation and responsiveness (Chaya et al., 2017). The last interneuron we consider is the amacrine cell, which comes in 30 different types (Hildebrand & Fielder, 2011). They connect to bipolar, ganglion, and other amacrine cells and have lots of different functions. A few of these functions are: support the center-surround responses of ganglion cells, exchange information between ON and OFF bipolar information streams, and direction-selective computations in the retina (Demb & Singer, 2015; Masland, 2012).

The next layer in the retina contains mostly ganglion cells, which receive the majority of their input from amacrine cells. The axons of these ganglion cells bundle into the optic nerve, which propagates the visual information into the brain. There are different types of retinal ganglion cells (RGCs), one of which has already been discussed (ipRGCs). The other main types of ganglion cells are midget and parasol ganglion cells, which together make up about 80% of all ganglion cells (Hildebrand & Fielder, 2011). Both

types of RGCs receive signals from cones, which means they are active under mesopic and photopic conditions, but only the parasol RGCs receive input from rods and thus are active under scotopic conditions (Mather, 2016). The information from the different RGCs is in turn projected onto different parts of the lateral geniculate nucleus (LGN), but this is beyond the scope of this thesis (Hildebrand & Fielder, 2011).

The most relevant property of both midget and parasol RGCs regarding contrast perception is the spatial response of the cells, which relates to the cells' receptive fields. A receptive field is "*a graphical representation of the area in the visual field to which a given cell responds*" (Fairchild, 2013, p. 16). The receptive fields of these RGCs are known to have a special property called spatial opponency, which is best illustrated in Figure 8 (Mather, 2016). As shown in the figure, there are two types of RCGs: ON- and OFF-center cells. In ON-center cells, an excitatory response is generated if a stimulus falls in the center of the receptive field, and an inhibitory response is generated when a stimulus falls in the surround of the receptive field. For OFF-center cells, the response is exactly the opposite. In the case of uniformly stimulated receptive fields (the center and surround are *both* stimulated, or *both* not stimulated), there is little response of the RCGs.

While both midget and parasol RGCs show spatial opponency, they differ in their receptive field sizes (Mather, 2016). This fact is crucial when it comes to understanding contrast perception, as different receptive field sizes allow for the processing of information with different spatial frequencies.

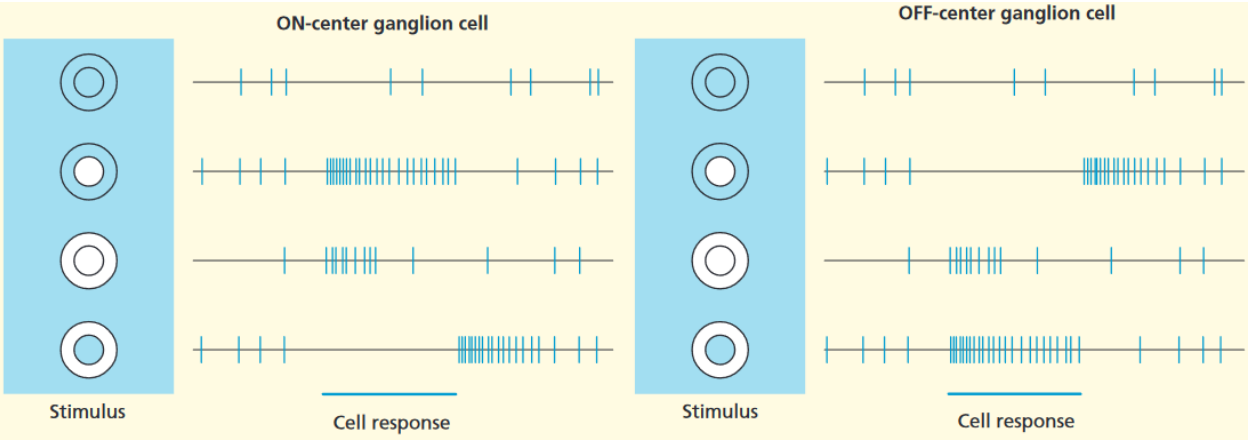

Figure 8. Spatial responses in retinal ganglion cells show their spatial opponency property. Left: white surfaces in the receptive fields indicate that there is a stimulus present in that area, while blue indicates the absence of a stimulus. Right: patterns of action potentials within the cell, corresponding to the patterns of stimuli in the same row. Image adapted from Mather (2016).

Spatial frequency and contrast sensitivity

The world as we perceive it consists of scenes that are filled with objects of different sizes, textures, and shapes. All these different objects provide our visual system with different types of information. This information is present on different spatial scales, which means different levels of detail. At one moment,

one might be interested in for example the texture of a tree bark, which is detailed information on a small spatial scale. At a different moment, one might look at the same tree only focusing on the tree trunk as a coherent chunk of information, for which more coarse information processing on a bigger spatial scale is required. In the lab, our perception of these different spatial scales is investigated using luminance gratings (top part of Figure 9). These luminance gratings have various properties (contrast, spatial frequency, orientation, spatial phase), which all can be experimentally manipulated to reveal properties of our visual system (Mather, 2016).

Two of these features are crucial for the understanding of contrast perception: spatial frequency and contrast. Spatial frequency can be defined as the number of light and dark cycles over a certain distance, and has as unit cycles per degree (cpd) (Campbell & Maffei, 1974). Figure 9 shows luminance gratings of different spatial frequencies: the one on the left contains few bars and represents a low spatial frequency, while the grating on the right contains way more bars within the same bar size, representing a higher spatial frequency.

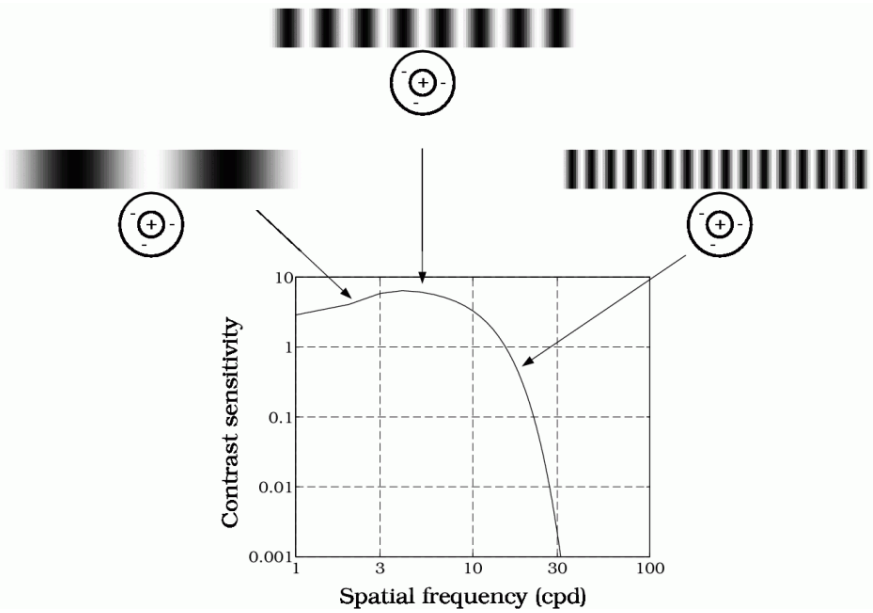

Figure 9. The contrast sensitivity function is related to the spatial frequency of the visual information, adapted from Wandell (1995).

Contrast relates to the difference in luminance between the brightest and the darkest parts of adjacent areas (Campbell & Maffei, 1974). In the luminance gratings in Figure 9, there is no difference in contrast between the gratings, as all gratings consist of the same black (the darkest) and white (the brightest) parts. The lower the difference between the darkest and brightest parts of adjacent areas, the lower the contrast, and the harder it is to distinguish these adjacent areas. The most basic quantification of luminance

contrast (Weber's contrast) is given in Equation 1, in which $C_0[-]$ is the luminance contrast between an object L_o $[\frac{cd}{m^2}]$and its background L_b $[\frac{cd}{m^2}]$ (Davoudian et al., 2014).

$$C_0 = \frac{|L_o - L_b|}{L_b} \tag{1}$$

A final consideration regarding luminance gratings is their waveform. The most commonly investigated are sinusoidal wave gratings (also called Gabor patches), and square wave gratings (Figure 10). In square wave gratings, there are sharp distinctions between high and low luminance patches, while in the sine wave gratings, there is a smooth transition between peak luminances. Theoretically, the sine wave is the more 'clean' stimulus when you want to investigate human perception, as it only consists of a single spatial frequency. The square wave on the other hand consists of a sum of sine waves, with a fundamental frequency and its odd-numbered multiples (Campbell & Robson, 1968).

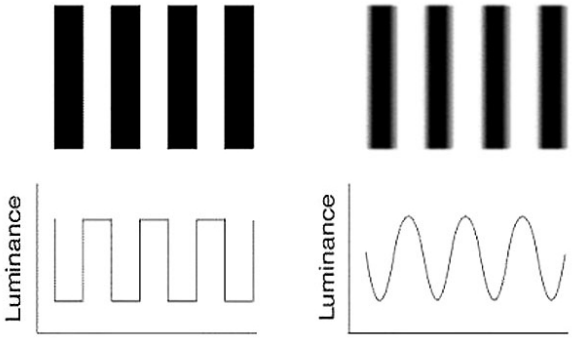

Figure 10. A square wave grating (left) and a sine wave grating (right) with their corresponding luminance patterns. Adapted from Kalloniatis & Luu (2005).

Our visual system is capable of processing information of different spatial frequencies due to the previously discussed receptive fields: smaller receptive fields allow us to capture detailed differences between visual areas, while bigger receptive fields allow the perception of more coarse structures. This is also shown in Figure 9: for the middle receptive field, corresponding to an ON-center cell, the bright area falls on the center while the surround area is covered by dark bars. This receptive field thus is perfectly tuned for this spatial frequency. Imagine what would happen when the same luminance grating would cover a bigger receptive field: a suboptimal center-bright and dark-surround match would make this cell less responsive to this specific spatial frequency. For each luminance grating, so each spatial frequency, there exist cells with receptive fields sensitive to its specific spatial dimensions.

Figure 9 also indicates that spatial frequency and contrast are not independent. Their relation is described with a contrast sensitivity function, and was first investigated by Campbell and Robson (1968). They found that the visual system is more sensitive to contrast at specific spatial frequencies than other spatial frequencies. As a general rule, one can state that our visual system is less sensitive to contrast at higher spatial frequencies, that is, when the spacing of the luminance gratings decreases. Also, below an optimal spatial frequency of 3 to 4 cycles per degree, contrast sensitivity tends to decrease (Campbell & Maffei, 1974). It can thus be thought of as a bandpass filter, with decreased sensitivity at both extremes. Figure 11 shows a similar contrast sensitivity function as in Figure 9, but with the spatial frequency visualized in the background (Kerofsky et al., 2015). It is important to note that the contrast sensitivity function of each individual is different, and aging, one of the factors that influences it, will be discussed later.

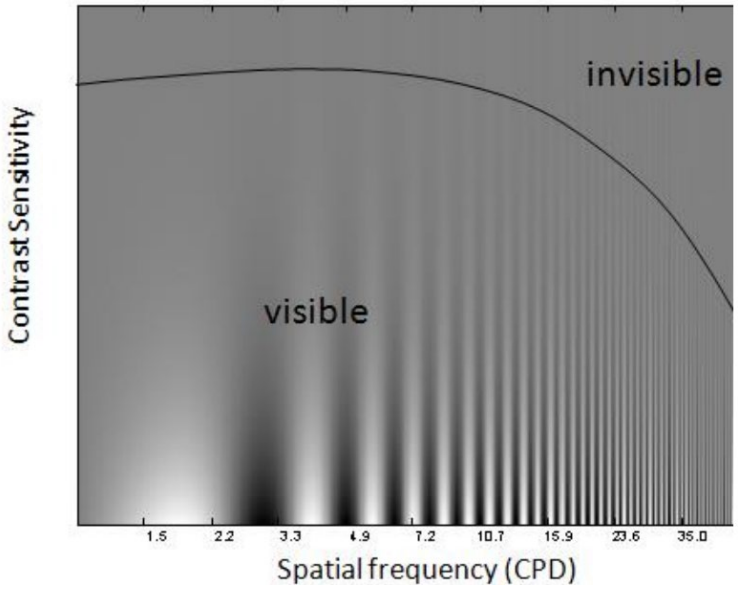

Figure 11. A contrast sensitivity function on top of luminance gratings with different spatial frequencies, adapted from Kerofsky et al. (2015)

Modeling contrast perception

When it comes to existing methods of modeling contrast, there are two main branches of models. The first is based on large-scale psychophysical experiments considering the visibility of targets on backgrounds (Adrian, 1989; Blackwell, 1946), while the second is rooted in characteristics of our visual system and computer vision (Joulan, Hautière, et al., 2011; Tadmor & Tolhurst, 2000). The first branch tries to predict contrast thresholds directly, while the second branch provides a more general indicator of contrast perception. Both of these branches will be discussed.

Adrian's psychometric model. Based on a lot of experimentally collected psychophysical data from, among others, Blackwell (1946), Adrian (1989) proposed a model that predicts the required luminance difference to detect contrasts with 99.93% certainty. This model is built on data coming from experiments in which homogenously illuminated targets and backgrounds were used (Brémond, 2020). The model, given by Equation 2 below, will be discussed in further detail.

$$\Delta L_{th} = AF \cdot PF \cdot EF \cdot k\left[\sqrt{L} + \frac{\sqrt{\phi}}{\alpha}\right]^2 \tag{2}$$

ΔL_{th} = difference in luminance between target and background at threshold visibility $[\frac{cd}{m^2}]$
AF = age factor
PF = contrast polarity factor
EF = exposure time factor
k = constant dependent on the experimental conditions $[-]$
L = luminance function [a.u.]
ϕ = luminous flux function [a.u.]
α = size of the object $[']$

The rightmost factor in Equation 2 constitutes the main component of the model. In this factor, two auxiliary functions based on two laws are introduced. A luminous flux function ϕ, following Ricco's law, and a luminance function L, following Weber's law (Adrian, 1989). Depending on the background luminance L_b, once should choose different variations of these auxiliary functions to make the model accurate (see Equations 3 - 5 below). In Figure 12, the luminance threshold required for contrast vision is plotted against object size α. In this figure, one can see both Ricco's and Weber's laws reflected.

For $L_b \leq 0.00418\frac{cd}{m^2}$:

$$\log\sqrt{L} = -0.891 + 0.5275\log(L_b) + 0.0277\log(L_b)^2$$
$$\log\sqrt{\phi} = 0.028 + 0.173\log(L_b) \tag{3}$$

For $0.00418\ \frac{cd}{m^2} < L_b < 0.6\frac{cd}{m^2}$:

$$\log\sqrt{L} = -1.256 + 0.319\log(L_b)$$
$$\log\sqrt{\phi} = -0.072 + 0.3372\log(L_b) + 0.0866\log(L_b)^2 \tag{4}$$

For $L_b \geq 0.6\frac{cd}{m^2}$:

$$\sqrt{L} = 0.05946 \cdot {L_b}^{0.466}$$
$$\sqrt{\phi} = \log(4.1925 \cdot {L_b}^{0.1536}) + 0.1684 \cdot {L_b}^{0.5867} \tag{5}$$

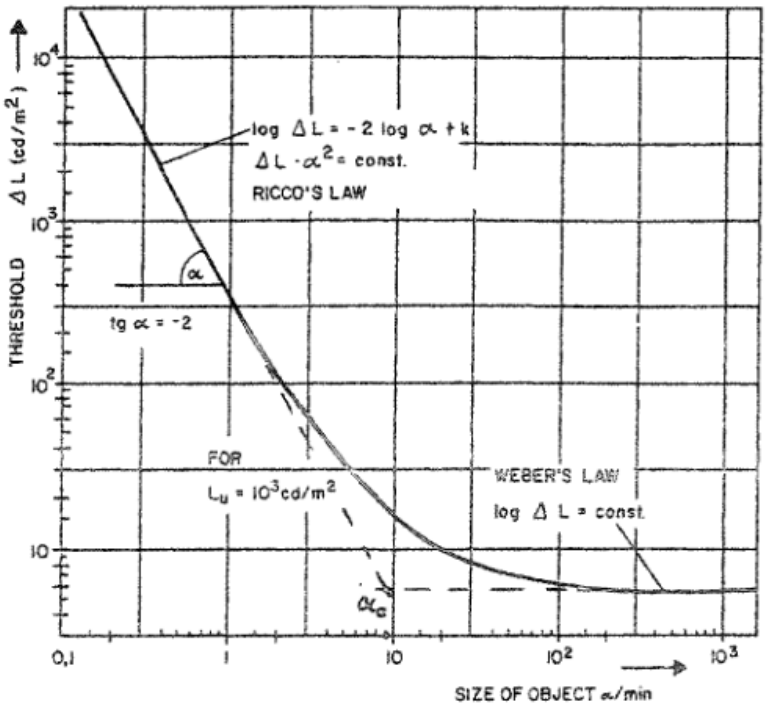

Figure 12. Visibility threshold ΔL_{th} as a function of object size α, with both Ricco's and Weber's law represented. Adapted from Adrian (1989).

The part of the model that follows Ricco's law is applicable to small targets. Originating from astrology, Ricco's law states that there is a linear relationship between object size and the required luminance threshold. This is easy to illustrate with an example from astrology: when observing stars, object sizes (i.e., the signal, a star) on our retina are small, while the background (i.e., noise, the surrounding sky) is respectively large. A small change in object size highly influences the visibility of our object, as the signal-to-noise ratio improves significantly. The part of the model covered by Ricco's law is given by the following equation (Adrian, 1989).

$$log(\Delta L) = -2\log(\alpha) + k\,|_{\alpha \to 0} \tag{6}$$

For larger object sizes, on the right side of Figure 12, the relationship between the visibility threshold and object size follows Weber's law: the threshold is no longer dependent on object size. Using a signal-to-noise perspective, this makes intuitive sense. When the object of interest covers a huge part of the retina (i.e., the signal), a small increase or decrease in object size (and the corresponding decrease or increase of the background/noise), would not make a difference when it comes to object visibility. The part of the model following Weber's law is given by the following equation (Adrian, 1989).

$$\log(\Delta L) = const.\,|_{\alpha \to \infty} \tag{7}$$

From this, it follows that in the part of the model respecting Weber's law, the visibility threshold is only dependent on the background luminance. This leads to the more general expression of Weber's law in the field of perception, namely that the size of a difference threshold is proportional to the size of the initial stimulus.

From Weber's law, another common law within psychophysics can be derived: Steven's power law (Stevens, 1960). This law describes that the perceived intensity of a stimulus (S) can be expressed as a power function of the physical intensity of a stimulus (I). This law can be seen in the equation below, which also includes the power law index that indicated the strength of the relationship (n) and a scaling constant (c).

$$S = c \cdot I^n \tag{8}$$

The final part of the rightmost factor in Equation 2 that needs to be highlighted is k, which is a constant based on the type of psychometric experiment that is performed. Given the two auxiliary functions, it was found that k should be around 2.6 to fit the data on which the model was based. Recently, Spieringhs et al. (2021) also assessed this factor, and they found that 2.55 was more optimal for their data. Nevertheless, they found a k in accordance with the original value.

The next factor to be considered is the age factor AF. As will be explained later, visual functioning declines with age, resulting in higher visibility thresholds for elderly. Adrian's (1989) model accounts for this by using the following factors.

$$AF = \frac{(\text{age} - 56.6)^2}{116.3} + 1.43 \quad \text{for } 64 \text{ years} < \text{age} < 75 \text{ years} \tag{9}$$

$$AF = \frac{(\text{age} - 19)^2}{2160} + 0.99 \quad \text{for } 23 \text{ years} < \text{age} \leq 64 \text{ years} \tag{10}$$

$$AF = 1 \quad \text{for age} \leq 23 \text{ years} \tag{11}$$

Adrian (1989) also realized that his model was not generalizable for all exposure times (the amount of time you can observe the target), as the data used resulted from experiments with 2 seconds or unlimited exposure time. It makes intuitive sense that the shorter the exposure time, the higher the contrast has to be for people to perceive the target. Therefore, he introduced the exposure time factor EF in his model, where t is the observation time in seconds.

$$EF = \frac{p(\alpha, L_b) + t}{t} \tag{12}$$

In this factor, p depends on target size α and luminance L_b according to the following equation (for target sizes smaller than 60'),

$$p(\alpha, L_b) = \frac{\sqrt{p(\alpha)^2 + p(L_b)^2}}{2.1} \tag{13}$$

in which,

$$p(\alpha) = 0.36 - 0.0972 \cdot \frac{(\log(\alpha) + 0.523)^2}{(\log(\alpha) + 0.523)^2 - 2.513(\log(\alpha) + 0.523) + 2.7895} \tag{14}$$

and,

$$p(L_b) = 0.355 - 0.1217 \cdot \frac{(\log(L_b) + 6)^2}{(\log(L_b) + 6)^2 - 10.4(\log(L_b) + 6) + 52.28} \tag{15}$$

Finally, Adrian (1989) considers a contrast polarity factor PF. In the data he based his model on, experiments considered positive contrasts: the target has a higher luminance than its background. Since for our purposes, we also work with positive contrasts, $PF = 1$ should be used. Nevertheless, for the sake of completeness, the PF for negative contrasts (the target has a lower luminance than its background) can be calculated with the following equations. $\Delta L_{pos,t=2}$ represents the value for an exposure time of 2 seconds.

$$PF = 1 - \frac{m \cdot \alpha^{-\beta}}{2.4 \cdot \Delta L_{pos,t=2}} \tag{16}$$

in which,

$$m = 10^{-10^{-(0.125(\log L_b + 1)^2 + 0.0245)}} \quad \text{for } L_b \geq 0.1 \frac{cd}{m^2} \tag{17}$$

$$m = 10^{-10^{-(0.075(\log L_b + 1)^2 + 0.0245)}} \quad \text{for } L_b > 0.004 \frac{cd}{m^2} \tag{18}$$

and,

$$\beta = 0.06 \cdot {L_b}^{-0.1488} \quad \text{for } all\ L_b \tag{19}$$

Not part of Adrian's (1989) base model, but nevertheless discussed in his paper, is the effect of disability glare on the predicted contrast threshold. To take this into account, one should add veiling luminance to the background luminance. Details of this will be covered in the section "*Modeling straylight*".

Image-based models. Since Adrian's model is based on uniform targets seen against uniform backgrounds, its ecological validity in complex visual scenes might be questioned. Therefore, a new branch of contrast models emerged from the field of computer vision. These models do not require any assumptions about the luminance of the target and background in a scene, but instead, use edge and contour detection algorithms to identify objects. In turn, the local contrast along these edges is calculated (Hautière & Dumont, 2007). Note that these models do not directly predict a luminance difference threshold, but rather use the model value as a generalized measure of contrast. Two image-based models will be discussed: a simple difference of Gaussians (DoG) model by Tadmor and Tolhurst (2000), and a more advanced DoG model by Joulan et al. (2011), which includes multiple DoG at different spatial scales to simulate a human contrast sensitivity function.

The Tadmor and Tolhurst (2000) model defines the response of ganglion cells and LGN neurons as a subtraction of the output of the surround receptive field $R_s(x,y)$ from that of the center receptive field $R_c(x,y)$, as shown in Equations 20 - 22. The spatial sensitivity of both center and surround receptive fields are modeled by a 2-dimensional circular-symmetric Gaussian G with a peak amplitude of 1 (Spieringhs et al., 2021; Tadmor & Tolhurst, 2000). For the surround Gaussian, there is a scaling factor of $0.85\left(\frac{r_c}{r_s}\right)^2$ compared to the center Gaussian, which represents the lower sensitivity of the surround receptive field that has been found in previous research (Tadmor & Tolhurst, 2000).

$$DoG(x,y) = R_c(x,y) - R_s(x,y) \tag{20}$$

$$R_c(x,y) = \sum_{i=x=3r_c}^{x+3r_c} \sum_{j=y=3r_c}^{y+3r_c} G(i-x, j-y, r_c) \cdot L(i,j) \tag{21}$$

$$R_s(x,y) = \sum_{i=x=3s}^{x+3r_s} \sum_{j=y=3r_s}^{y+3r_s} 0.85\left(\frac{r_c}{r_s}\right)^2 \cdot G(i-x, j-y, r_s) \cdot L(i,j) \tag{22}$$

R_c = output of the center component of the receptive field
R_s = output of the surround component of the receptive field
r_c = radius of the center Gaussian
r_s = radius of the surround Gaussian
(x,y) = mid-point of a receptive field center
$L(i,j)$ = luminance at the pixel location i,j
$G(i-x, j-y, r)$ = bivariate Gaussian centered at x,y and with radius r

Tadmor and Tolhurst (2000) then highlight that this simple DoG model assumes that the response of ganglion cells and neurons only depends on local luminance difference between center and surround. However, in reality this is not the case, as the response of these cells is also influenced by light adaptation. Since light adaptation is dependent on the mean luminance in a scene (Vissenberg et al., 2021), this model must be normalized through division by the local mean luminance (Tadmor & Tolhurst, 2000). Equations 23 - 25 show three possible normalization divisions to make the DoG model dependent on contrast instead of absolute luminances. Tadmor and Tolhurst (2000) proposed three of them, as it is not clear what region of the receptive field is used to evaluate mean luminance in a scene (i.e., the center, surround, or both).

$$Contrast\ output(x,y) = \frac{R_c(x,y) - R_s(x,y)}{R_c(x,y)} \quad \text{for center-only adaptation} \tag{23}$$

$$Contrast\ output(x,y) = \frac{R_c(x,y) - R_s(x,y)}{R_s(x,y)} \quad \text{for surround-only adaptation} \tag{24}$$

$$Contrast\ output(x,y) = \frac{R_c(x,y) - R_s(x,y)}{R_c(x,y) + R_s(x,y)} \quad \text{for center + surround adaptation} \tag{25}$$

Later, Spieringhs et al. (2021) proposed modifications to this model in order to obtain the global DoG value for a visual scene (i.e., an input picture) instead of the local DoG values per pixel. In order to achieve this, all local DoG values over the number of pixels N_p were summed according to Equation 26.

$$C_{DoG} = \sum_{p=1}^{N_p} |DoG(x,y)| \tag{26}$$

Individual DoG values need to be substituted by their absolute values to avoid positive and negative DoG pixel values to cancel each other out, and as such include the effects of both ON-center and OFF-center receptive fields. Also, the previously introduced weighting factor of $0.85\left(\frac{r_c}{r_s}\right)^2$ was replaced by a weighting factor of $\left(\frac{r_c}{r_s}\right)^2$, which ensured that uniform luminance regions from the edge of the surround receptive field did not influence C_{DoG}, rendering the number of background pixels in C_{DoG} much lower. As the last modification, the radius of the center and surround Gaussians were set to 1 and 2 pixels respectively to represent the angular resolution of the fovea (Spieringhs et al., 2021).

When Joulan and colleagues (2011) prosed their model, they emphasized that previous models did not consider that our visual system contains ganglion cells and visual neurons with varying receptive field sizes, allowing us to perceive information at different spatial scales. Therefore, based on the research by Barten (1999), Joulan et al. (2011) included the human contrast sensitivity function in their model. They designed a set of spatial filters that represents our visual system (see Table 1). This set of spatial filters is based on Barten's contrast sensitivity function. Given any contrast sensitivity function, one can compute a fitting set of DoG filters which can be used in further analysis of the visual scene (Joulan et al., 2012; Joulan, Hautiere, et al., 2011). Additionally, their model also takes into account visual adaptation.

Table 1

Characteristics of the DoG filters, adapted from Joulan et al. (2011).

	DoG 1	DoG 2	DoG 3	DoG 4	DoG 5	DoG 6
Spatial frequency (cpd)	2.90	7.70	1.00	0.40	1.50	0.10
Standard deviation center σ^+ (cpd)	0.25	0.10	0.74	1.85	0.49	7.41
Weighing factor ω	393.20	169.26	134.46	45.83	22.98	17.21

Their model is based on two algorithms. The first one, presented below, considers the visual adaptation. A luminance image I_0 with normalized a gain factor $\frac{1}{L_a}$ is used as input (Joulan, Hautière, et al., 2011).

$$I_1 = I_0 \frac{1}{L_a} \tag{27}$$

$\frac{1}{L_a}$ = gain factor (the inverse of the adaptation luminance)
I_0= input luminance image
L_a= adaptation luminance

In the next step, this adaptation-corrected luminance image I_1 is used as input to mimic a given contrast sensitivity function as a weighted sum of DoG $(SDoG)$.

$$SDoG(I_1) = \sum_k \omega_k \left[G_{\sigma_k^+} - G_{\sigma_k^-} \right] (I_1) \tag{28}$$

ω_k= weight of the DoG for filter k
G_σ= the normalized Gaussian with standard deviation σ_k^+ for the center and σ_k^- for the surround for filter k. The standard deviation for the center is computed from Barten (1999) and that for the surround is given by $\sigma_k^- = \lambda \sigma_k^+$ with $\lambda = 3$ (Joulan, Hautière, et al., 2011).

Again, like with the Tadmor and Tolhurst (2000) model, Spieringhs et al. (2021) suggest a slight modification of the model to account for a global $SDoG$ (C_{SDoG}) over the entire visual scene. Like before, this is achieved by summing the individual local $SDoG$ of each pixel.

$$C_{SDoG} = \sum_{p=1}^{N_p} DoG(x, y) \tag{29}$$

Glare perception

The second aspect of visual perception that deserves a more detailed description is the perception of glare, and more specifically, the effect of glare on contrast perception. Everyone has experienced glare: it is the accumulation of too much light in the eye, rendering you annoyed or unable to perform your visual tasks. In the literature, two main types of glare are discussed: disability glare and discomfort glare. As we will discover in this section, disability glare is rooted in the physiology of the eye, while discomfort glare is a less well-explained psychological phenomenon (Donners et al., 2015). In our context of driving at night, disability glare is more important, as we want to investigate the impact of glare on visual performance.

Disability glare

Starting with the more defined type of glare, disability glare is associated with reduced visual performance because of scattered light coming from a bright source (van den Berg et al., 2009). This means, when people experience disability glare, they are less able to perform tasks that require vision, for example, driving. Disability glare is caused by light scattering at the cornea, the lens, and the fundus, and by the transparency properties of the iris (Franssen & Coppens, 2007), which is visualized in Figure 13 by van Bommel (2015).

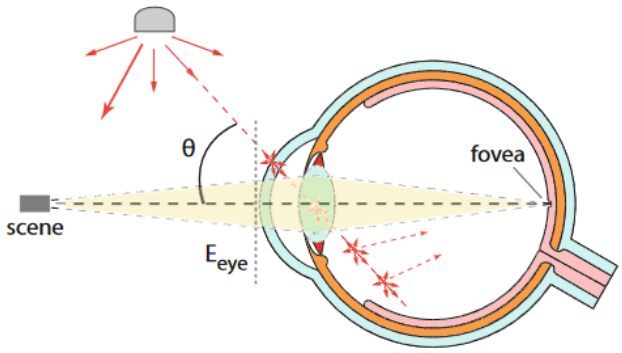

Figure 13. Scattering of light in the eye. Adapted from van Bommel (2015).

As a result of this scattering, extra light enters the retina around the area that is directly illuminated according to a point-spread function (Figure 14). This function has a sharp peak at the center of illumination,

but also has a significant amplitude around this center (Franssen & Coppens, 2007). This scattered light around the center of vision (≥ 1.3°) is called straylight, and results in distorted images on the retina (van den Berg et al., 2009). Put in other words, a point light-source does not hit the retina as an equally large point, but it spreads out across the retina (van den Berg et al., 2010). Due to straylight people experience a so-called veiling luminance (a luminance superimposed on the entire retina), which results in loss of retinal image contrast (Aslam et al., 2007). A clear example of this is provided in Figure 15 by Löfving et al. (2015), in which we see how contrast in the image reduces as a result of straylight. This is especially clear when you look at the white road markings.

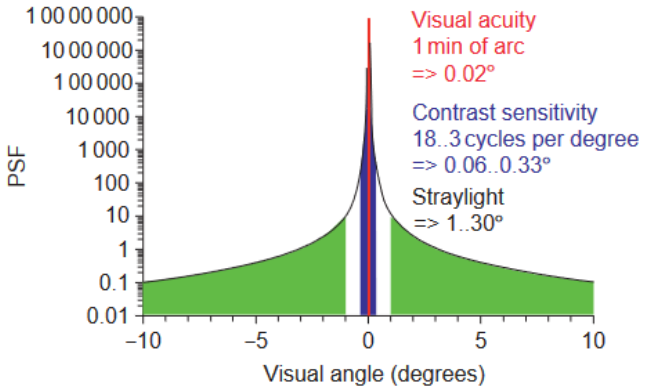

Figure 14. Point-spread function of the human eye according to the CIE in 1999. Adapted from van den Berg et al. (2010).

Figure 15. An example of lowering of contrast perception due to a veiling luminance caused by straylight, adapted from Löfving et al. (2015), and slightly modified by the author.

The amount of straylight a healthy population experiences is dependent on multiple factors. First, there is the age of the observer, where older observers experience more straylight. Second, pigmentation of

the iris, where more pigmentation (darker eyes) leads to less straylight. This is caused by the fact that different types of pigmentation cause variations in the transmission of light (van den Berg et al., 1991). Third, the angle of the glare source with respect to the eye, where larger angles result in less straylight (Franssen & Coppens, 2007). Fourth, the wavelength of the light, the effects of which are highly dependent on age, pigmentation, and angle of incidence. For example, van den Berg and colleagues (1991) found that for light-pigmented eyes, long-wavelength light (red) resulted in more straylight than medium-wavelength light (green). Finally, pupil size is a factor, where smaller pupil sizes in combination with larger light angles result in more straylight (Franssen et al., 2007).

Besides these factors that occur in healthy eyes, there are also other causes of increased straylight perception, such as the development of cataracts, corneal disturbances, refractive surgery, and wearing contact lenses or dirty glasses (Franssen & Coppens, 2007).

Modeling straylight

The reduction of contrast as a result of straylight can be modeled by using an equation similar to Equation 1, in which a veiling luminance L_v $[\frac{cd}{m^2}]$ is added to both the object L_o $[\frac{cd}{m^2}]$ and background luminance L_b $[\frac{cd}{m^2}]$. C_0 represents the contrast of the object in absence of glare. The result is the so-called effective luminance contrast in presence of glare C_{eff} (Davoudian et al., 2014).

$$C_{eff} = \frac{|(L_o + L_v) - (L_b + L_v)|}{(L_b + L_v)} = C_0 \left(\frac{L_b}{L_b + L_v}\right) \tag{30}$$

An approximation of the effects of straylight on the retina for an individual, the veiling luminance, can be assessed using the previously discussed factors of influence: age of the observer A, the illuminance on the eye E_{eye} $[lx]$, and the angle between viewing direction and direction of light incidence θ [°] (Davoudian et al., 2014; NEN 13201-3, 2016):

$$L_v = 9.86 \cdot \left[1 + \left(\frac{A}{66.4}\right)^4\right] \cdot \frac{E_{eye}}{\theta^2} \qquad \text{for } 1.5° < \theta \leq 60° \tag{31}$$

and

$$L_v = E_{eye} \left(\frac{10}{\theta^3} + \left[\frac{5}{\theta^2}\right] \cdot \left[1 + \left(\frac{A}{62.5}\right)^4\right]\right) \quad \text{for } 0.1° < \theta \leq 1.5° \tag{32}$$

As mentioned earlier, straylight on the retina can not only be characterized by its resulting veiling luminance, but also by a point-spread function PSF $[sr^{-1}]$. The CIE (Vos & van den Berg, 1999), provides

the following equation for their Standard Glare Observer that besides age A, glare angle θ [°], also includes a pigmentation factor p in which $p = 0$ represents very dark eyes, $p = 0.5$ brown eyes, and $p = 1.0$ blue-green eyes (Franssen & Coppens, 2007).

$$
\begin{aligned}
PSF = \left[L_v/E_{eye}\right]_{total} \\
&= [1 - 0.08 \cdot (A/70)^4] \cdot \left[\frac{9.2 \cdot 10^6}{[1 + (\theta/0.0046)^2]^{1.5}} + \frac{1.5 \cdot 10^5}{[1 + (\theta/0.045)^2]^{1.5}}\right] \\
&+ [1 + 1.6 \cdot (A/70)\text{^}4] \\
&\cdot \left\{\left[\frac{400}{1 + (\theta/0.1)^2} + 3 \cdot 10^{-8} \cdot \theta^2\right] + p \cdot \left[\frac{1300}{[1 + (\theta/0.1)^2]^{1.5}} + \frac{0.8}{[1 + (\theta/0.1)^2]^{0.5}}\right]\right\} \\
&+ 2.5 \cdot 10^{-3} \cdot p
\end{aligned}
\tag{33}
$$

Multiplying both sides of Equation 33 by E_{eye} provides you with a complete equation for L_v. More simplified and practical variations were presented in Equations 30 and 31.

As highlighted before, glare caused by straylight reduces the visibility of objects. The threshold increment is a measure regarding the loss of visual performance due to glare (van Bommel, 2015), and is defined by the NEN 13201-2 (2016) as "*the percentage increase of contrast of an object that is needed to make it stay at threshold visibility in presence of disability glare generated by luminaires of a road lighting installation*" (p. 6). To get a better feeling for this quantification, imagine driving in the dark. About 80 meters ahead, you are barely able to perceive a person crossing the road, this person is just on the threshold of your visibility. Now imagine yourself in the same situation, but you are experiencing disability glare from an inadequately installed traffic light. It is not hard to imagine that in this situation, the person that was first on the threshold of your visibility now becomes unperceivable. To make this person perceivable again, the contrast between the person and their background would have to increase. This is exactly what the threshold increment quantifies. The threshold increment TI [%] is dependent on the veiling luminance L_v $[\frac{cd}{m^2}]$ and an average background luminance L_{av} $[\frac{cd}{m^2}]$, and is approximated by the following equation (NEN 13201-3, 2016).

$$
TI = 65 \cdot \frac{L_v}{{L_{av}}^{0.8}} \quad \text{for } 0.05\frac{cd}{m^2} < L_{av} \leq 5\ \frac{cd}{m^2}
\tag{34}
$$

For our case, that of straylight perception while driving a motorized vehicle, there exists a recommended TI value. According to NEN 13201-1 (2016) and NEN 13201-2 (2016), the maximum TI for lighting case M4 (which is commonly used in road light design) is 15%. From this, and given a certain background luminance, one can calculate the maximum allowed amount of L_v using Equation 34.

Disability glare in Adrian's contrast model. The earlier introduced contrast model by Adrian (1989) can be extended by considering disability glare. He highlights the fact that disability glare will reduce contrasts, and models this in a similar way as in Equation 30, by adding a veiling luminance L_v to the already existing background luminance in all factors in the model.

$$L_v = k \sum_{i=1}^{n} \frac{E_{Gl_i}}{\theta_i^2} \tag{35}$$

E_{Gl_i}= illumination at the eye from glare source I $[lx]$
θ_i = glare angle between the center of the glare source and the fixation line [°] (valid for angles between 1.5° and 30°)
k = an age-dependent constant according to the following equation

$$k = (0.0752 \times \text{age} - 1.883)^2 + 9.2 \quad \text{for } 25 \text{ years} < \text{age} < 80 \text{ years} \tag{36}$$

Measuring straylight

When quantifying the amount of straylight in an eye, one uses the straylight parameter s. This parameter represents the ratio between scattered light (unwanted light that causes contrast reduction) and non-scattered light (the light required for accurate vision). It is, however, more convenient to use $\log(s)$, in which a higher $\log(s)$ indicates more straylight (Franssen & Coppens, 2007).

Recently, tools have become available to accurately measure straylight in the eye for each individual, for example, the C-Quant retinal straylight meter, leaving us less dependent on the approximations presented earlier (Aslam et al., 2007; van Bommel, 2015). These measurement tools use the compensation comparison method, which is a 2 alternative forced choice (2AFC) psychometric paradigm. As Franssen and Coppens (2007) explain, in this paradigm participants look with one eye at an arrangement of circles that can light up (Figure 16). In the middle, two test fields are located that both flicker with different properties. The flicker of one field consists of only straylight, while the flicker of the other field consists of straylight and compensation light that flickers in counterphase with the straylight. It is randomly chosen which of the two test-field contains only straylight, and which also contains the compensation light. The task for the participants is then to determine in which of the two test fields the flicker appears stronger. During the trials, the amount of compensation light in the test field varies, and based on this a psychometric curve is fit through the participant's responses. From this curve, one reads the straylight parameter s.

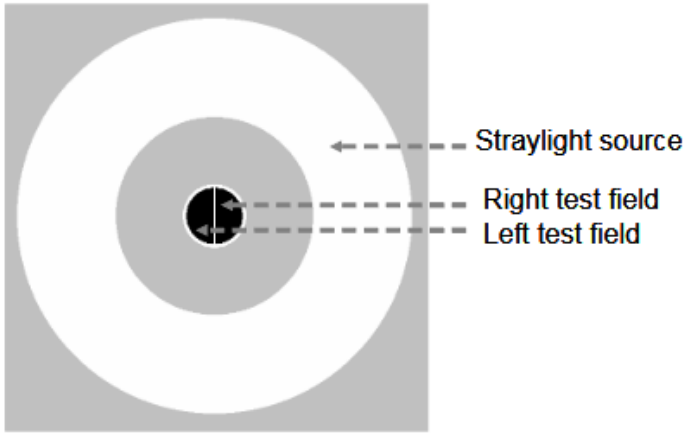

Figure 16. Stimulus layout of the compensation comparison method paradigm. Adapted from Franssen & Coppens (2007).

Discomfort glare

The other major type of glare, discomfort glare, is less strictly defined. Definitions include aspects like experiencing discomfort without impaired vision, experiencing irritating or distracting effects, and experiencing the urge to look away (Pierson et al., 2017, 2018). These things might all occur in disability glare as well, but there is a crucial difference between the two. Discomfort glare does not necessarily negatively interfere with a visual task, and in cases that it does interfere, people may not notice their task performance is affected at all (Osterhaus, 2005).

The specific mechanisms of our visual system that causes discomfort glare are still unknown, but research shows that experiencing discomfort glare coincides with uncomfortable contractions of the iris, lens, and eye muscles (van Bommel, 2015). This lack of physiological basis did not stop scientists from developing discomfort glare prediction models. Four aspects are commonly used as variables in these models: the luminance of the glare source, the adaptation level, the solid angle of the glare source, and the position index (Pierson et al., 2018). The most commonly used discomfort glare method for the evaluation of indoor spaces is the Unified Glare Rating (CIE, 1995).

Recent work by Vissenberg et al. (2021) provides an alternative model of discomfort glare, one that is rooted in the human visual system instead of rooted in practice (like the UGR). In their work, they suggest that the main reason we experience certain types of glare as discomfort, is the high metabolic demand by overstimulation of the visual neurons. To understand this, we must introduce the concept of adaptation, which is defined by Clifford et al. (2007) as "*the processes by which the visual system alters its operating properties in response to changes in the environment*" (p. 1). One can notice adaptation when our system shifts from photopic (i.e., light) to scotopic (i.e., dark) vision; it takes a while for our visual system to see properly in the dark. The current adaptation level of our visual system is called its adaptation state, which is dependent on ambient light conditions, the glare source, and the light history of a person

(Vissenberg et al., 2021). The overstimulation of visual neurons that causes discomfort glare is mainly caused by *misadaptation*: the difference between our current adaptation state and the local retinal illuminance. This model is promising, as it correlates well with various other glare models.

Aging and the visual system

As we age, our visual system ages with us, negatively impacting our vision in general. Since the target group of this work is elderly, it is worthwhile to focus on several changes that happen in their visual systems, which affect, among a range of other things, their contrast and glare perception.

First, elderly experience a loss of flexibility in the lens, leading to a reduced range of accommodation (CIE, 2017). In younger people, the lens can thicken to change its focal length, allowing us to focus on objects at different distances. This capability deteriorates with age, and according to Mather (2016), there is almost no accommodation capability left when most people are in their fifties. This makes it difficult for old people to focus on nearby objects, rendering them far-sighted.

Second, besides losing flexibility, the eye lens of elderly also yellows due to the accumulation of yellow pigment over our lifespan (CIE, 2017). Yellowing of the lens influences its spectral transmittance, resulting in short wavelengths (blue) getting absorbed in the lens, thus not entering the eye. This results in changed color vision and lower illuminance on the retina, which is especially detrimental in a world with screens and cool white artificial light, which contains a lot of short wavelengths (van Bommel, 2015).

Third, the older you get, the less mobile your pupil becomes. As a result, the pupils of elderly remain relatively small in dim light situations (Mather, 2016). At the age of 65, your maximum pupil diameter has reduced to 55% of the maximum diameter of a 25-year-old (van Bommel, 2015). This reduced mobility results in decreased retinal illuminance, reducing the clarity of your vision. Combining a reduced pupil size and yellowing of the lens, the retinal illumination of a 65-year-old can be less than 30% of the available light (van Bommel, 2015).

Fourth, proteins in the lens degrade with age, leading to clouding of the lens (CIE, 2017). As a result of this, intraocular light scattering increases. This increased scattering results in reduced spatial contrast sensitivity and increased disability glare (van den Berg et al., 2010). Figure 17 shows the expected straylight parameter values $\log(s)$, where higher values indicate more expected straylight at the retina.

Fifth, the density of photoreceptors and ganglion cells in the retina reduces with age, which reduces central vision and spatial contrast sensitivity (CIE, 2017). One of the causes is the degeneration of the pigment epithelium, which is responsible for the nourishing and regeneration of photoreceptors (Mather, 2016).

Sixth, the combination of reduced pupil diameter and clouding of the lens leads to an increase in the scotopic vision threshold (CIE, 2017). At the same time, rhodopsin regeneration is reduced (see previous

paragraph), resulting in a slower dark adaptation. The older you become, the slower your visual system switches to dark-vision. It is therefore crucial to not expose elderly to bright lights in dark environments, as this depletes rhodopsin that is needed for dark-vision (CIE, 2017).

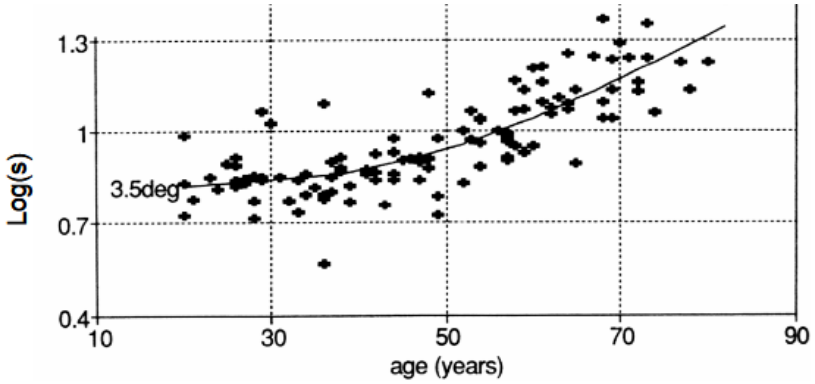

Figure 17. Expected straylight values as a function of age in a healthy population, adapted from Franssen & Coppens (2007).

A healthy population will experience all of the previously mentioned effects of age on their vision. In addition to these effects, aging people also run the risk of contracting conditions that can lead to visual impairments. The most common conditions are cataracts, refractive errors, glaucoma, and macular degeneration (CIE, 2017). Especially cataracts and corrected refractive errors may lead to increased intraocular scattering (van den Berg et al., 2010).

A simple solution might be to provide more light to accommodate the characteristic of elderly visual systems. However, with the increase of light in an environment also the risk of intraocular light scattering and glare increases, which might result in a worse perception of the environment than before this extra light was introduced (van Bommel, 2015). Therefore, designing light for an elderly population is a tricky balancing act.

Method

Research design

This experiment has a 3x3x2 within-subject design. Independent variables are the angular size of the road mark arrow (20.3, 9.5, and 5.5 arcmin), the road luminance (0.25, 0.66, and 0.99 cd/m^2), and the presence or absence of glare (12.6 lx and 0 lx). The levels for the road luminance and arrow sizes are similar to those in Spieringhs et al. (2021), with the exclusion of their 3.6 arcmin angular size, since it is likely that the visual systems of our elderly sample are not sensitive enough to detect this smallest arrow size. The angular sizes of the road mark arrow were chosen to represent different distances from the observer to the arrow: 40, 60, and 80 meters (Spieringhs et al. (2021).

The dependent variable consists of judgments that participants had to make regarding the direction of the road mark arrow of different luminances (varying between 0.25 and 1.24 cd/m^2, depending on the specific angular size of the arrow and road luminance). The exact arrow luminances were determined by the QUEST+ procedure, which is further described in the section below. The arrow presented during the trials was either pointing to the left or pointing to the right, which was randomly varied across all trials. In a two-alternative forced choice paradigm, participants had to choose the direction of the arrow within 3 seconds, and their responses were recorded as being either correct or incorrect.

Psychophysical measurement procedure: QUEST+

In this experiment, we want to investigate contrast perception for different conditions and determine the just noticeable difference (i.e., the luminance difference threshold) of our sample. This is done by fitting a psychometric curve through the data from our 2AFC experiment. This curve will, on one axis run from '50% correct judgments (randomly guessing the direction of the arrow)' to '100% judgments (always perceiving the arrow direction)', making 75% correct judgments our visibility threshold (Figure 18).

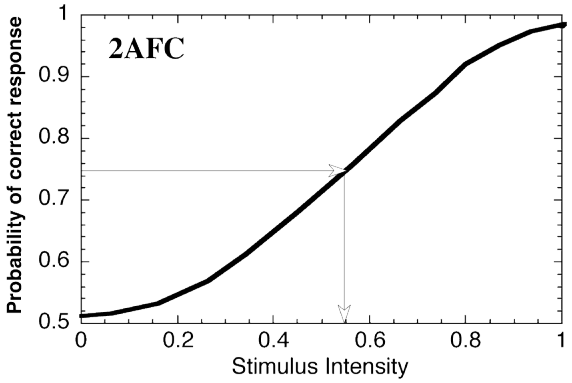

Figure 18. Example of a psychometric curve in a 2AFC experiment, adapted from RIT (n.d.)

Traditional psychophysical experiments use the method of limits, adjustment, or constraint stimuli to assess this threshold. Here, however, we used the adaptive QUEST+ method (Watson, 2017). In this procedure, participants are exposed to trials of increasing difficulty (in our case, lower contrast between the road and arrow). As soon as a mistake in judgment is made, following trials will be around this level of difficulty, thereby gaining more detailed information on the range of the visibility threshold compared to non-adaptive methods.

In 1983, Watson and Pelli presented their QUEST procedure, which used two types of prior knowledge to improve psychometric procedures: data from previous trials and existing knowledge regarding the perceptual threshold under the study's particular conditions (Watson & Pelli, 1983). Using Bayesian maximum likelihood estimates after each trial, this procedure is more efficient in finding the threshold value. Later, Watson (2017) presented an improved procedure called QUEST+, which improved the old procedure, making it more applicable in different contexts. One of the relevant improvements is that QUEST+ can estimate more than one of the psychometric function parameters at the same time.

For a 2AFC experiment, the proportion of correct trials $\psi(C)$, as represented by a psychometric function, is described as follows (Jones, 2018):

$$\psi(C) = \gamma + (1 - \lambda - \gamma)\phi(x; \mu, \sigma) \tag{37}$$

In this equation, ϕ is a cumulative Gaussian function, x represents the stimulus values (arrow luminances), and the four earlier discussed parameters of the psychometric function return: threshold μ, slope σ, lapse rate λ, and guess rate γ (Figure 19). The guess rate γ is fixed at 0.5, as this is the probability of a participant correctly guessing the direction of the arrow. Lapse rate λ, that is the rate of incorrect responses to correctly perceived stimuli due to a variety of reasons (e.g. inattention, finger error, fatigue), is set at 0.02, which is broadly applicable in psychometric research (Jones, 2018).

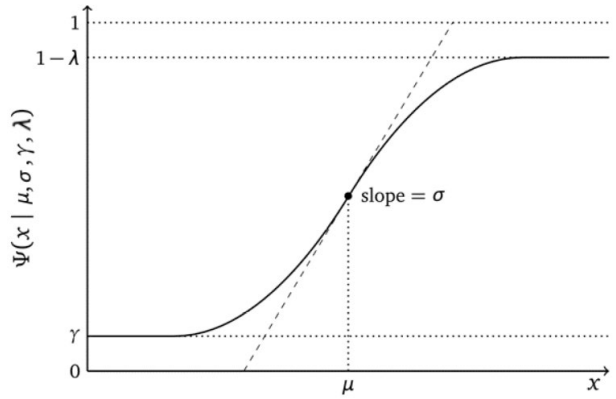

Figure 19. Parameters that describe a psychometric function. Adapted from ADOpy developers (2020), with symbols altered by the author.

As explained, one of the advantages of using the QUEST+ procedure is that it can very efficiently estimate multiple parameters of the psychometric function at once. For this experiment, both the slope σ and threshold μ are free parameters. For each of these parameters, a set of hypotheses is used as input in the procedure, after which QUEST+ figures out which has the maximum likelihood of being the actual value (Watson, 2017). For the slope σ, there are three possible values in each of the 3 (road luminance) x 3 (simulated arrow distance) conditions. These possible slopes are based on previous work by Spieringhs et al. (2021), making a comparison with this work possible. The slope hypotheses for each condition are presented in Table 2.

Table 2

Possible slope σ values for each of the conditions.

Arrow size (arcmin) *[simulated distance from observer]*	Road luminance (cd/m^2)	Possible slope σ values		
20.3 [*40m*]	0.25	0.0142	0.0177	0.0212
9.5 [*60m*]	0.25	0.0156	0.0195	0.0235
5.5 [*80m*]	0.25	0.0321	0.0401	0.0481
20.3 [*40m*]	0.66	0.0295	0.0369	0.0442
9.5 [*60m*]	0.66	0.0326	0.0407	0.0489
5.5 [*80m*]	0.66	0.0654	0.0817	0.0981
20.3 [*40m*]	0.99	0.0485	0.0606	0.0727
9.5 [*60m*]	0.99	0.0529	0.0662	0.0794
5.5 [*80m*]	0.99	0.0566	0.0707	0.0849

For the threshold μ, there are different hypotheses based only on the specific background luminance (3 levels), without distinguishing between arrow sizes. For each background luminance, a lower and an upper bound for the possible threshold was set. Within this range, 20 uniformly spaced linearly-distributed possible values were extracted and used as hypotheses. These ranges were set similarly to those in Vesters (2022), as he investigated the same target demographic. The luminance ranges are presented in Table 3, in which the corresponding RGB (R=G=B) values used in the experiment code to achieve the corresponding luminances are provided. The RGB-luminance relationship for this specific experimental setup was found by Spieringhs et al. (2021) and is presented below. Note that, since R=G=B, only grayscales are involved, and a single channel is used as input for this function.

$$L = 0.0006363 \cdot \mathrm{RGB}^2 - 0.1301 \cdot \mathrm{RGB} + 6.782 \tag{38}$$

Table 3

Arrow luminance ranges for each road luminance level, with corresponding RGB (R=G=B) values.

Road luminance (cd/m^2)	Arrow luminance minimum (cd/m^2)	Arrow luminance maximum (cd/m^2)	RGB minimum	RGB maximum
0.25	0.252	0.433	116	124
0.25	0.658	0.992	131	139
0.25	0.992	1.407	139	147

For each of the 9 conditions, a separate QUEST+ model was initialized, using the corresponding fixed and free parameters for each condition. Then, after participants completed a trial within a certain condition, the posterior probability of the most likely free parameters was updated. Using Bayes' theorem, the posterior probability can be written as the product of the prior density function and the likelihood of the data (Watson, 2017):

$$P'_k(s|X_k, r_k) = P(s) \cdot p(r_k|X_k, s) = P(s) \cdot \prod_k p(r_k|x_k, s) \tag{39}$$

$P'_k(s|X_k, r_k)$ = posterior probability density function of the parameters s after k trials
s = the set of psychometric function parameters
$P(s)$ = prior probability density function of the parameters
$X_k = \{x_1, x_2, \dots, x_k\}$ = the complete set of stimulus values
$r_k = \{r_1, r_2, \dots, r_k\}$ = the sequence of participant responses (the data)
$p(r_k|x_k, s)$ = probability of the data

Since this research added a new component, namely the glare source, the work of Vesters (2022) was not used to infer priors for the two free parameters, resulting in (default) uniform priors being used in all QUEST+ models.

Two different stopping criteria were included in this procedure. The first one is based on the maximum number of trials participants could be exposed to. This was set at 200, which was required to keep the experiment within the allocated time limit of one hour. The second criterion is based on the principle of entropy. After each trial within a condition, the negative Shannon entropy was calculated for all hypotheses regarding the slope and threshold, indicating how well each hypothesis fits the data (Jones, 2018). After trial and error, an entropy of 3 was used as a cut-off point, as this would provide sufficient information about the threshold value.

The used Matlab code to run this procedure is made by Jones (2018), and has been changed by Vesters (2022) and the author to fit the current experimental paradigm; it can be found in Appendix A1.

Participants and sample size justification

Using an a-priori power analysis, the ideal sample size for this experiment was found to be 26. The expected effect size for this analysis was based on a similar study on a younger demographic (Spieringhs et al., 2021) and a similar study using the same demographic of elderly (Vesters, 2022). These studies had sample sizes of 18 and 24, respectively. The first study found effect sizes of $\eta^2 = 0.89$ for the road mark arrow size, and $\eta^2 = 0.7$ for surface luminance. The second study found similar effect sizes, namely $\eta^2 = 0.75$ for arrow size and $\eta^2 = 0.79$ for surface luminance.

Based on these effect sizes, G*Power 3 (Faul et al., 2007) was used to conduct an a-priori power analysis using an X^2 Goodness-of-fit test (since a likelihood ratio test will be performed), an effect size of 0.75 (matching the lowest found effect size in Vesters (2022)), an alpha of 0.05, power of 0.9, and 3 degrees of freedom. This results in a required sample size of 26 participants, which is comparable to the previous study that investigated a similar demographic of elderly (Vesters, 2022).

Participants were recruited via the author's and supervisors' personal networks, or randomly selected from the JSF Participant Database, which is part of the Human-Technology Interaction group at Eindhoven University of Technology. The inclusion criteria for this experiment were an age between 63 and 80, and having normal or corrected-to-normal vision. In total, 18 participants (5 female, 13 male) completed the experiment, of which detailed demographic information can be found in Table 4. Unfortunately, due to time constraints and difficulties in finding people of the right demographic, this was lower than the desired number of participants. Nevertheless, the work of Spierhings et al. (2023) [Unpublished manuscript], to which the results of this work will be compared, also had a sample size of 18. So, even though the desired statistical power cannot be achieved, a fair comparison with this work is still possible.

The experiment took about 60 minutes, and all participants were compensated for their time by receiving 10 euros if they completed the complete experiment, or 2 euros if they did not pass the visual acuity test. Furthermore, participants from outside the institution (TU/e) were compensated an extra 2 euros for their travel time.

Table 4

Detailed demographic information of the sample of elderly.

Demographic	**Mean *(SD)***	**Range**
Age (years)	70.2 *(4.3)*	63 - 79
Visual acuity	0.94 *(0.29)*	0.5 - 1.5
Straylight parameter (log(s))	1.28 *(0.20)*	1.0 - 1.9
Pigmentation factor	0.94 *(0.13)*	0.5 - 1.0
Road-usage (hours per week)	2.7 *(2.8)*	0 - 11

Materials

Setup and display characteristics. The experiment took place in the General Purpose Lab 2B of the Human-Technology Interaction group at Eindhoven University of Technology. The setup consisted of a table, chair, chinrest, keyboard, a glare source, and a big TV display (Figure 20). The display was a 65-inch Samsung QE65Q90, with a 4k resolution (3840 x 2160 pixels) and a refresh rate of 120 Hz. The screen was centered and perpendicularly aligned to the participant's eyes, at a distance of 108 cm. In this configuration, the participant's field of view that was covered by the screen was 42° vertically and 68° horizontally. The position of the chinrest and the screen assured that the road mark arrows on the screen were perceived at the simulated distances explained before.

In the first experiment from this line of research, Spieringhs et al. (2021) performed a detailed calibration of the display screen. They explained that first of all, the maximum luminance value of the screen was lowered to 33.19 cd/m^2 to ensure sufficiently high resolution at low luminance levels. Second, spectral radiance measurements were performed on the stimulus area (the place on the screen on which the road arrow was displayed, a square of 150x150 pixels), which resulted in a look-up table that could convert RGB-values to luminance values. Third, they checked the stability of the display over time and found this to be very high, finding standard deviations of the luminance between 0.0007 and 0.002 cd/m^2, which is orders of magnitudes away from the mean luminance measured (1.55 cd/m^2). For more details regarding this calibration and measurement procedure, the reader is referred to Spieringhs et al. (2021).

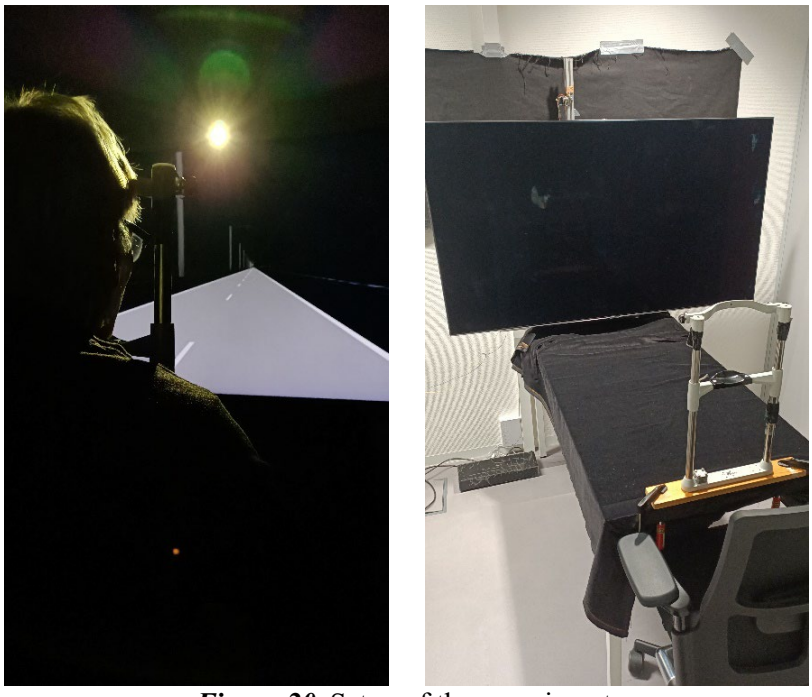

Figure 20. Setup of the experiment.

Glare source characteristics and calibration. To simulate glare in the driving simulation, a white LED was used. This LED was placed on top of the display and aimed at the eyes of the participants. The angle between the glare source and the point of focus of the participant was dependent on the arrow size, as for each arrow size the location of the arrow on the road was slightly different. For arrow sizes of 20.3, 9.5, and 5.5 arcmin, the glare angles correspond to 22.39, 21.58, and 21.38 degrees respectively.

Using a Keithley 2425 100W SourceMeter, the voltage and current were set at 21 V and 32 mA respectively. With help of the JETI Spectroradiometer Specbos 1211-2, and the accompanying JETI LiMeS 4.9.1 software, the glare source was characterized (JETI, 2022). Results showed that at the 21 V / 32 mA settings, the CCT was 5009 K and the desired illuminance of 12.6 lux at eye level was achieved. The relation between current and illuminance can be found left in Figure 21, which shows that in the 10-60 mA range, there is a near-perfect linear relation between illuminance and current. To deal with potential fluctuations over time (e.g., due to the warm-up of the LED), the illuminance was also measured over time, as shown right in Figure 21. This shows that after two minutes, the output of the LED is stable within a range of 0.2 lux.

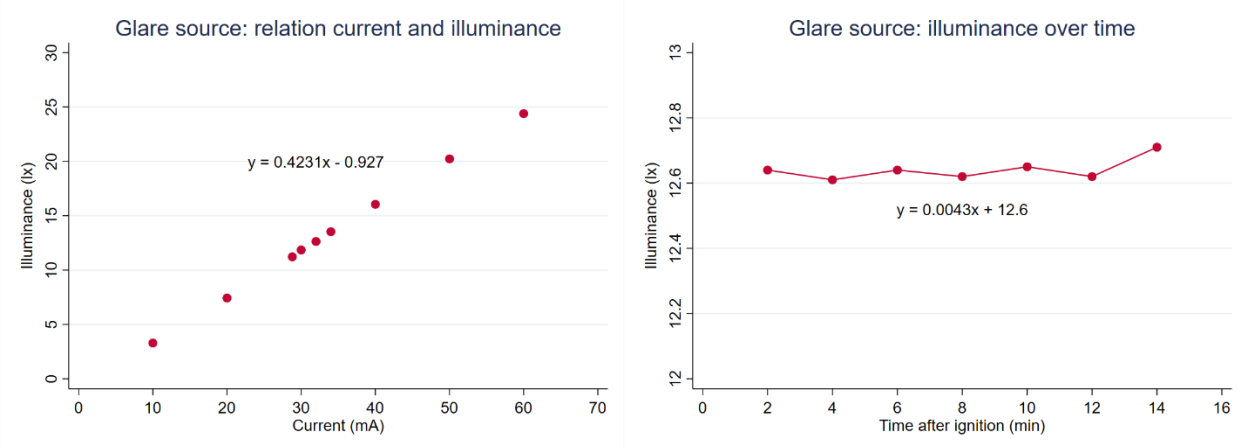

Figure 21. Glare source characteristics. Left: relation between current and illuminance of the glare source. Right illuminance at eye level caused by the glare source over time.

Testing equipment. Before participants started the experimental procedure, their visual acuity, color vision, and levels of retinal straylight were measured. Visual acuity was measured using a Landolt C chart from TNO (n.d.), as presented in Figure 22. The used version of the chart required participants to stand five meters away from the chart. For participants to perceive the smallest arrow size in the experiment (5.5 arcminutes), their visual acuity should be at least 1/5.5. However, participants with worse visual acuity were not excluded, as their data for the bigger arrows was still useful. Color vision was measured with the Ishihara test. Potential abnormalities were noted, but there were no requirements regarding color vision for participation in the experiment. Retinal straylight was measured using the Oculus C-Quant, on E-moderate

settings, as the stimuli in these settings are centered around the most likely range of values of the straylight parameter the target demographic would achieve (Franssen & Coppens, 2007).

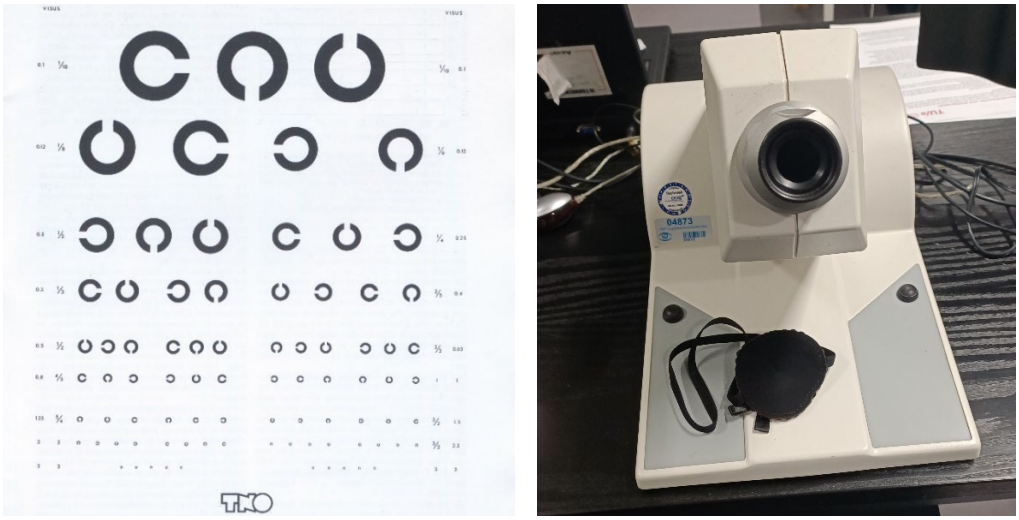

Figure 22. Left: the Landolt C visual acuity chart (TNO, n.d.). Right: the Oculus C-Quant.

Questionnaire. A questionnaire was administered, consisting of several items that will serve as control variables. These questions regarded their eye-health (e.g., "Have you undergone any eye surgery?"), alertness (e.g., "How alert do you feel at this moment"), and traffic participation (e.g., "Do you have a driver's license"). For the questions regarding alertness, validated measures like the Karolinska Sleepiness Scale (Shahid et al., 2011) and the Consensus Sleep Diary (Carney et al., 2012) were used. The complete questionnaire can be found in Appendix B.

Road scenes. This experiment used the same road renderings as in Spieringhs et al. (2021). As they have explained, multiple layers of the scene (sky, grass, road surfaces, middle road markings, a road marking arrow, etc.) were all individually rendered in Mitsuba. These individual layers were needed to be able to adjust the RGB values of all elements in Matlab. Then, using Blender, the camera option was used to capture a specific road scene. This scene captured the point of view of a person driving on the road: 1.5 m above the road, 1.3 m to the right of the middle road markings, and 1 degree below the horizontal (NEN 13201-2, 2016; Spieringhs et al., 2021). Besides this, the characteristics of the human eye were approximated by using a focal length of 16.7 mm and a sensor size of 22.3 mm (Spieringhs et al., 2021).

Using guidelines from the Dutch Ministry of Infrastructure (Ministerie van Infrastructuur en Waterstaat, 2019; Ministerie van Verkeer en Waterstaat, 1991), Spieringhs et al. (2021) created highway scenes that represent a 7 m wide road split into two lanes of 3.5 m wide. The scenes include an arrow that is 7.5 m wide and 1.05 m long, left and right continuous road markings of 15 cm wide, and middle road

markings that are 10 cm wide and 3 m long spaced out every 9 m. The final elements of the scene are lamp poles of 18 m high, spaced out every 90 m, and trees placed every 25 m. An example rendering can be found in Figure 23.

Figure 23. A rendering of a highway scene in Mitsuba. Adapted from Spieringhs et al. (2021).

Procedure

Upon entering the lab, participants were invited to read and sign the informed consent form (Appendix C). After that, a short questionnaire was administered, consisting of questions regarding their eye-health, traffic participation, and alertness. Furthermore, three visual tests were conducted: an Ishihara colorblindness test, a visual acuity test, and the straylight measurement using the Oculus C-Quant. For the straylight measurement, there was a practice round, as participants were most likely unfamiliar with this test. After this, straylight was measured at both eyes separately.

Next, the experiment started. Participants were seated in front of the screen, resting their chin on the chinrest. They were explained the procedure, including the instruction to not directly look into the glare source, and a couple of test trials were done to ensure they understood the task. Participants were explicitly instructed to answer as quickly and accurately as possible, even in cases they were not 100% sure of the arrows' direction. Some control trials were added, in which a road scene without any arrow was displayed.

During the task, a road scene was presented for three seconds, and the participants had to indicate whether the arrow on the road pointed to the left or the right. Then, a three-second gray screen was displayed, after which the next scene was presented. The participant's response was compared to the actual direction of the arrow and a correct (i.e., 1) or incorrect (i.e., 0) was recorded. When the participant took

too long to respond, a randomly correct of incorrect was registered, mimicking a random guess. This repeated until the QUEST+ stopping criteria were met. This experimental phase took between 20 and 25 minutes, depending on how quickly the algorithm could conclude the participant's visibility threshold. Then, the experiment was repeated for the second glare condition (with or without glare, depending on which was the first one). The order of the glare conditions was reversed after every participant.

After this procedure, participants were debriefed, and there was an opportunity to ask any questions regarding the experiment. To conclude, participants were thanked and compensated for their participation.

Data Analysis

General Analysis. As a first step, the data from the QUEST+ procedure was used as an input to fit psychometric curves. In total, 18 curves were fit for each participant, corresponding to the 3 (road luminance) by 3 (arrow size) by 2 (glare) conditions. While the QUEST+ also fitted psychometric curves, these were not used to determine the luminance difference threshold because the values for the slope are restricted (see Table 2). Instead, psychometric curves were fitted through the data using the *psignifit (v.4)* Matlab package. This package was developed by Schütt et al., (2016), and its specific implementation as made by the author and project supervisor can be found in Appendix A2. From these psychometric curves, the luminance difference value at the 75% correct-response point was used as the threshold value.

Then, using code from Spieringhs et al. (2021), the Adrian model was used to predict luminance difference threshold values. The original model (without a factor for glare) was used to predict the threshold for our conditions without glare, while a model that was adapted by the author to include Adrian's glare factor (Equation 35) was used on our data with glare. The Matlab code for this can be found in Appendix A3.

To conclude, using code from Spieringhs et al. (2021), the image-based models were given an input image of the arrow and the road surface directly surrounding it (150x150 pixels). The output was, for each of the 18 conditions, a sum of the DoG values for each pixel. Just like with the Adrian model, the author made adjustments to the original code to include a factor of glare. In both image-based models, this was done by superimposing a veiling luminance as calculated with the CIE point-spread function (Equation 33) on the full input image. For the simple DoG model of Tadmor & Tolhurst (2000), this meant adding this veiling luminance to the luminance presented in Equations 20 - 22, while for the complex DoG model of Joulan, Hautiere, et al. (2011) this meant adding this same luminance to the luminance in Equation 27. The corresponding Matlab codes can be found in Appendix A4 and Appendix A5, respectively.

Outlier detection & assumption checking. Before analysis, the measured luminance difference thresholds were checked for outliers using absolute z-scores > 3 as a cut-off point. This check

resulted in three outliers, all from the same participant (id 31). This participant showed an average luminance difference threshold across all conditions (0.34 cd/m^2) that was more than twice as large compared to the rest of the sample (0.16 cd/m^2). There are two possible explanations for this deviation. First, the participant had a lazy eye, resulting in exotropia and difficulties focusing on the screen. Second, during the visual acuity test, this participant indicated having trouble with differentiating left vs. right, which was a crucial aspect of the experiment. Unless indicated otherwise, this participant's data is included in the analysis.

To conduct a proper repeated measures ANOVA, assumptions of normality, homogeneity of variance, and sphericity were checked. By conducting Shapiro-Wilk tests and Skewness & Kurtosis tests on both the measured thresholds within each condition and the residuals, normality was rejected. Since, in most conditions, data was skewed, homogeneity of variances was tested using a Levene's test centered at the median (Brown & Forsythe, 1974), which showed that this assumption was met ($F(17, 306) = 1.23$, $p = 0.24$). Sphericity was rejected using Mauchly's test. Because of this, and unless stated otherwise, comparisons of mean thresholds between conditions will be made on the observed means instead of the predicted ones. Additionally, Greenhouse-Geisser corrected p-values will be reported for main or interaction effects in repeated measures ANOVAs.

Control variables and order effects. Several control variables that could potentially influence the participants' performance were measured. In a mixed ANOVA (within factors were road luminance, arow size, and glare; between factors were the control variables), their effects on the threshold were investigated. Of the three control variables sleep quality ($F(1, 323) = 0.01$, $p = 0.92$), alertness ($F(1, 323) = 0.18$, $p = 0.67$), and average weekly time spent driving ($F(1, 323) = 0.01$, $p = 0.93$)), none had a significant effect on the measured thresholds in both the with and without glare conditions.

The order of the with- or without-glare condition was alternated between each participant to prevent learning or fatigue effects. The effect of condition order was tested in a similar way as the effect of control variables, and no statistically significant differences were found ($F(1, 323) = 2.17$, $p = 0.15$).

Results

In this section, the results of the experiment are described. The section "*Effects of glare in an elderly population*" presents findings related to the first sub-research question about the influence of glare on the luminance difference threshold in an elderly sample, while the section "*Effects of age under glare conditions*" focusses on the second sub-question about the effects of age on the luminance difference threshold. In addition to the remaining sections, which focus on the Adrian and DoG models, these will answer our main question regarding the influence of glare on luminance threshold and how to model this.

Experiment descriptives

On average participants received 192.5 trials for both the conditions with and without being exposed to glare, which is close to the maximum amount of 200 trials that was set as a stopping condition. This corresponds to 21.4 trials for each of the nine conditions. Across all conditions, 49% of the presented arrows pointed to the left, and 51% to the right. The average participant gave a left-response 45% of the time, and a right-response 46%. This means that in 9% of the trials, participants responded too late (i.e., reaction times larger than 3 s), and the QUEST+ procedure randomly selected a response to mimic guessing behavior. Participants responded correctly to the direction of the arrow in 78% of the trials.

Based on the proportion of correct responses in each condition, psychometric curves were fit through the QUEST+ data using the *psignifit (v.4)* Matlab package. There were a total of 18 curves for each participant, one for each of the conditions (i.e., 3 road luminance X 3 arrow size X glare/no glare). Since this experiment was 2AFC, and a guessing behavior was mimicked for nonresponses, the luminance difference threshold was set at the 75%-correct point within each condition. Examples of this can be found in Figure 24, in which the size of the blue dots indicates the number of trials the QUEST+ procedure provided to the participant at that specific stimulus level. It is fair to highlight that using this fully automated and adaptive psychometric method, not all data was perfectly fit to be described by a psychometric curve (Figure 24 on the right). Psychometric curves could describe most of the data acceptably (average R^2 = 0.67).

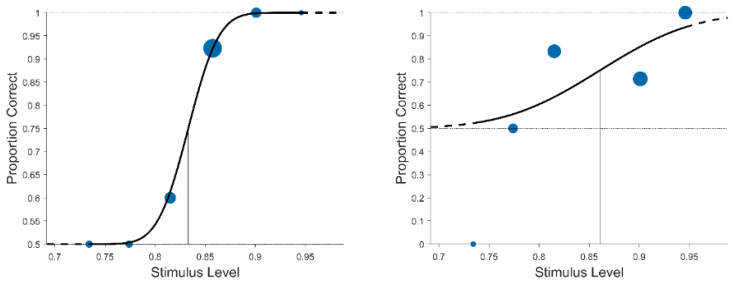

Figure 24. Two examples of psychometric curves fit through the data. Left: participant 19 with glare, road luminance of 0.66 cd/m^2, arrow size of 9.5 arcmin. Right: participant 29 with glare, road luminance of 0.66 cm/m^2, arrow size of 5.5 arcmin.

Effects of road luminance and arrow size

Two trends can be observed in both the with and without glare conditions, as seen in Figure 25. The higher the road luminance, the higher the luminance difference threshold. Furthermore, the larger the arrow size, the lower the road luminance difference threshold. These effects were statistically investigated using factorial repeated measures ANOVAs. They revealed that in the conditions with glare, there was a main effect of road luminance ($F(2,15)= 54.37$, $p < .001$, $\eta^2_{partial} = .76$), a main effect of arrow size ($F(2,15)= 84.42$, $p < .001$, $\eta^2_{partial} = .83$), and an interaction effect of road luminance and arrow size ($F(4,9)= 11.43$, $p < .001$, $\eta^2_{partial} = .40$). In the conditions without glare, there was also a main effect of road luminance ($F(2,15)= 54.42$, $p < .001$, $\eta^2_{partial} = .76$), arrow size ($F(2,15)= 85.21$, $p < .001$, $\eta^2_{partial} = .83$), and an interaction effect of the two ($F(4,9)= 5.86$, $p <.001$, $\eta^2_{partial} = .26$). The main effects are of similar size in the conditions with and without glare, while the interaction effect is weaker in the condition without glare.

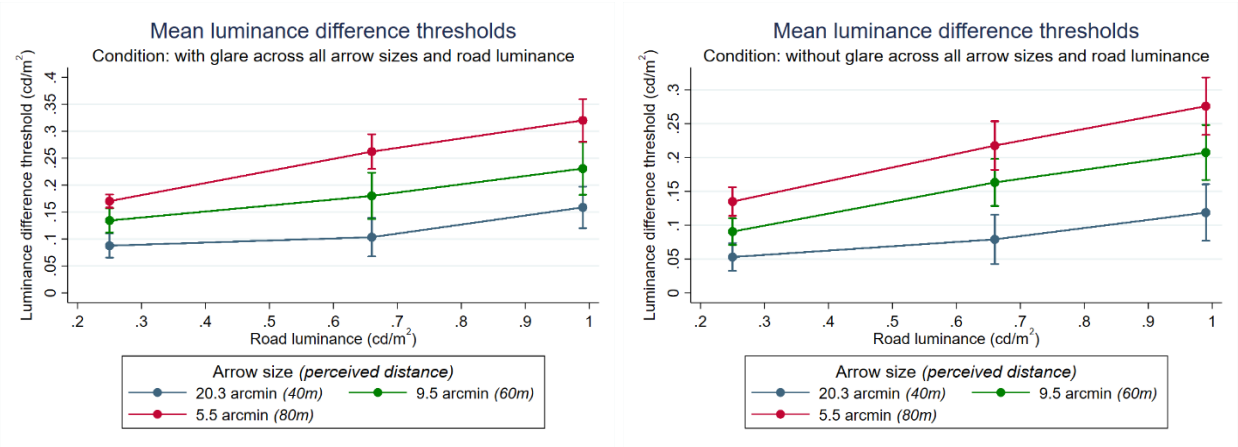

Figure 25. The effects of road luminance and arrow size on the observed mean luminance difference thresholds in conditions with (left) and without (right) glare.

Comparing the mean thresholds across road luminance and arrow size separately, significant differences are found between each comparison. Contrasts are found in Table 5 below, including Bonferroni-corrected *p*-values.

Table 5

Differences between observed means across road luminance and arrow size, for with and without glare conditions.

Contrast	Threshold difference with glare	Threshold difference without glare
Road luminance		
0.66 – 0.25 cd/m^2	0.182 – 0.131 = 0.051, p = .015	0.153 – 0.093 = 0.060, p = .002
0.99 – 0.25 cd/m^2	0.237 – 0.131 = 0.106, p < .001	0.201 – 0.093 = 0.108, p < .001
0.99 – 0.66 cd/m^2	0.237 – 0.182 = 0.055, p = .008	0.201 – 0.153 = 0.047, p = .020
Arrow size		
9.5 – 20.3 arcmin	0.182 – 0.117 = 0.065, p < .001	0.154 – 0.084 = 0.070, p < .001
5.5 – 20.3 arcmin	0.251 – 0.117 = 0.134, p < .001	0.209 – 0.084 = 0.125, p < .001
5.5 – 9.5 arcmin	0.251 – 0.182 = 0.069, p < .001	0.209 – 0.154 = 0.055, p = .003

Effects of glare in an elderly population

Focusing on the first sub-research question, a comparison of the paired thresholds for each participant in their conditions with and without glare is presented in Figure 26. It was found that in 77% of the cases, the luminance difference threshold under conditions of glare is higher than the threshold without glare. The green dots indicate the data from participant 31, which has been described earlier to be an outlier in several conditions.

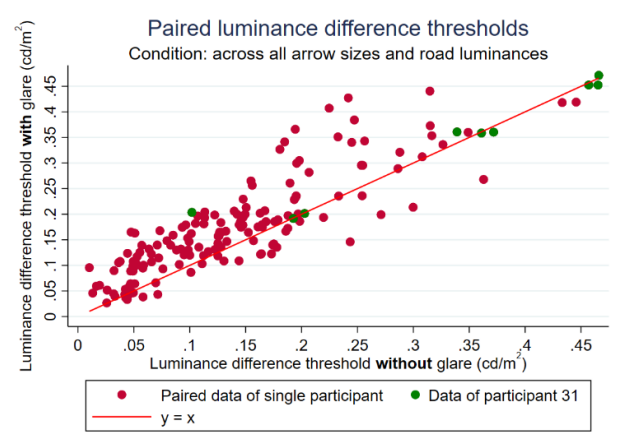

Figure 26. Paired luminance threshold difference data for each participant with and without being exposed to glare, each dot indicating one of the nine conditions.

A repeated measures ANOVA showed a main effect of glare ($F(1,16)$= 34.12, p < .001, $\eta^2_{partial}$ = .66), while the interaction effects of glare, road luminance, and arrow size were not significant. Also, the three-way interaction between these factors was not significant. Figure 27 shows the mean differences in thresholds between conditions with and without glare for each road luminance and arrow size condition. While there was a significant main effect of glare, and the mean thresholds with glare are higher, pairwise

comparisons using Bonferroni-corrected *p*-values show that only two means are statistically different (Table 6). Only for the lowest background luminance, glare has a statistically significant influence on the luminance threshold.

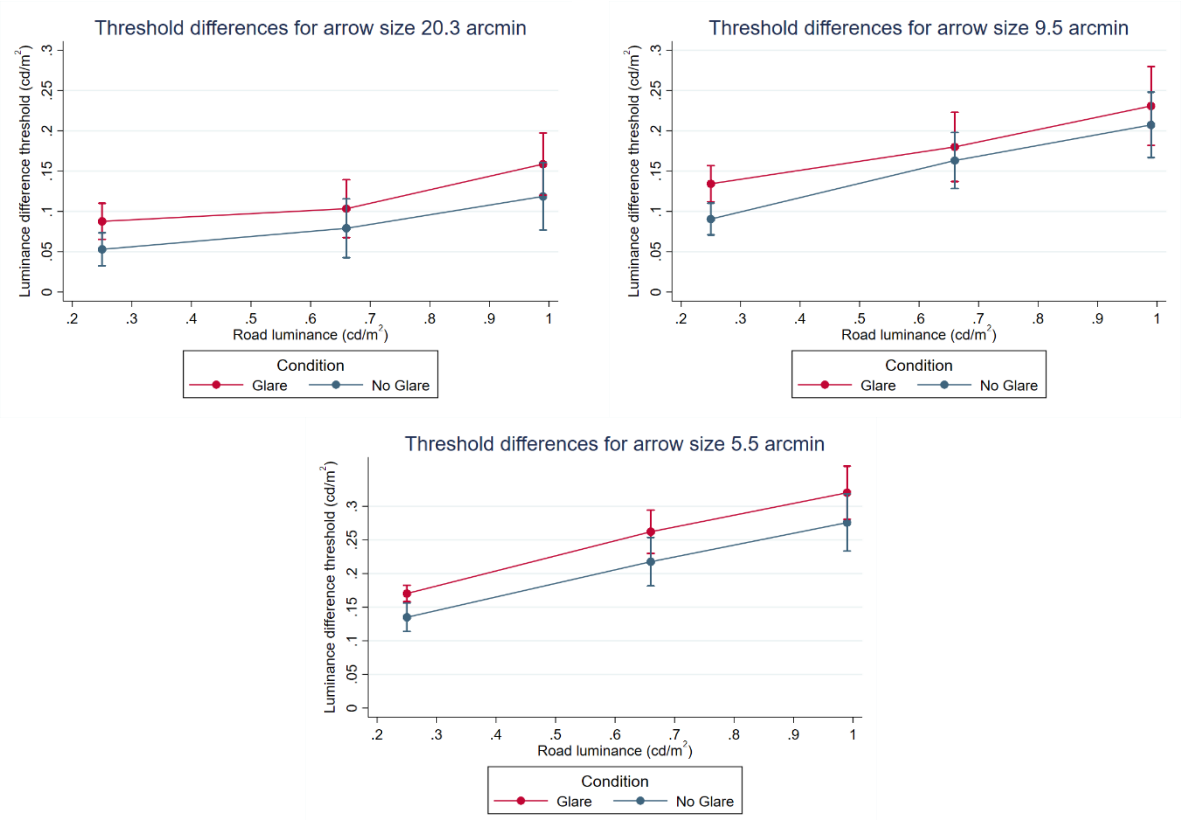

Figure 27. Comparisons of luminance difference thresholds in conditions with and without glare.

Table 6

Observed mean threshold differences with minus without glare, across all conditions.

	0.25	**0.66**	**0.99**
20.3	0.087 – 0.053 = 0.034, *p* = .096	0.103 – 0.079 = 0.024, *p* = .999	0.159 – 0.119 = 0.040, *p* = .531
9.5	0.134 – 0.091 = 0.043, *p* = .021	0.180 – 0.163 = 0.017, *p* = .999	0.231 – 0.207 = 0.024, *p* = .999
5.5	0.170 – 0.135 = 0.035, *p* = .024	0.262 – 0.218 = 0.044, *p* = .237	0.320 – 0.276 = 0.044, *p* = .429

Given the found main effect of glare, this factor is worthy of further investigation. Each participant's sensitivity to glare was measured separately in both eyes. For this analysis, the average of these two straylight parameters (log(s)) will be used and referred to simply as log(s). The relation between age and log(s) is shown in Figure 28, and indicates that sensitivity for glare increases with age. Participants with visual impairments are highlighted in blue, with a label for their corresponding impairment.

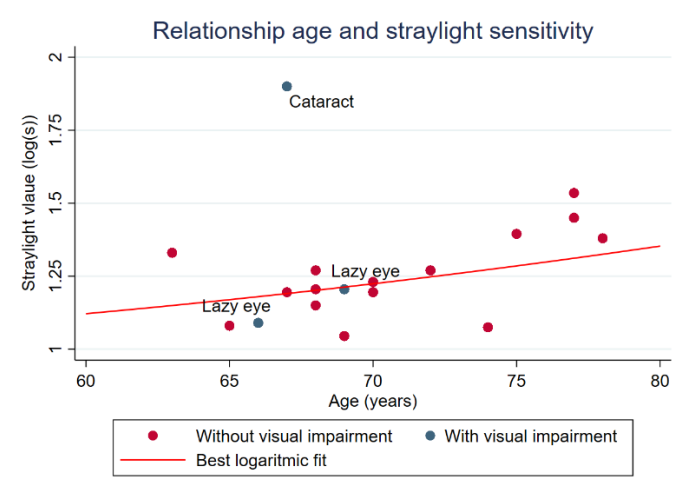

Figure 28. Relation between age and the average straylight parameter of both eyes.

A logarithmic function in the form of $\beta + \log\left(1 + \left(\frac{\text{age}}{65}\right)^4\right)$ was fitted through the data (excluding the participant with cataract) where β was a fitting parameter. This form was chosen after work by van den Berg et al. (2007), who stated that this function accurately describes the relationship between age and the straylight parameter (log(s)). The resulting model with an R^2 of .34 is presented below.

$$\log(s) = 0.95 + \log\left(1 + \left(\frac{\text{age}}{65}\right)^4\right) \tag{40}$$

Lastly, there is a statistically significant positive correlation between the straylight parameter and the measured thresholds ($r = 0.21$, $p < .001$), indicating that the more sensitive a person is to straylight, the higher the luminance difference thresholds are.

Effects of age under glare conditions

Next, the focus will be on the second sub-research question, comparing the effect of glare on an old and young sample. For this comparison, data from Spieringhs et al. (2023) [Unpublished manuscript] was used. This study investigated, using a similar experimental paradigm, the luminance contrast difference thresholds in a younger population. One difference between the methods used is the exposure time of the road scenes, which was 2 seconds in the younger sample compared to 3 seconds in the old same. Another difference is that Spieringhs et al. (2023) [Unpublished manuscript] used a predetermined set of arrow luminances, while the adaptive QUEST+ method was used in this study.

The average age of the participants in the Spieringhs et al. (2023) [Unpublished manuscript] study was 28.4 years ($SD = 3.7$), compared to the average of 70.2 years in this study ($SD = 4.3$). Figure 29 shows

the mean differences in thresholds across all conditions, comparing the young and old samples. In every condition, mean thresholds are higher for the older population. Table 7 shows the pairwise comparisons with Bonferroni-corrected *p*-values. This indicates that the difference in means is statistically significant in seven of nine conditions. Pooling data from both studies, a significant positive correlation between age and luminance difference threshold under glare conditions was also found ($r = .45$, $p < .001$).

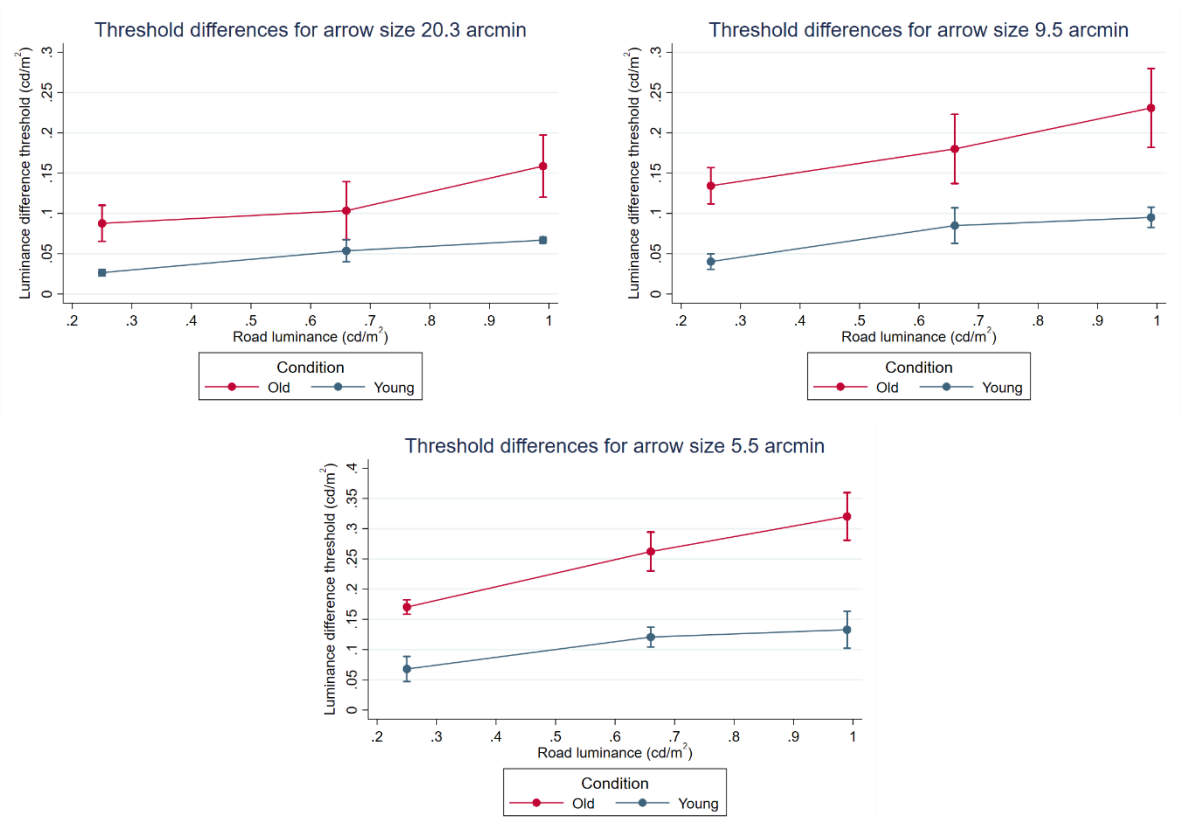

Figure 29. Comparisons of luminance difference thresholds in an old and young sample.

Table 7

Observed mean threshold differences with old minus young, across all conditions.

	0.25	**0.66**	**0.99**
20.3	0.087 – 0.027 = 0.060, $p = .018$	0.103 – 0.054 = 0.049, $p = .417$	0.159 – 0.067 = 0.092, $p = .045$
9.5	0.134 – 0.040 = 0.094, $p < .001$	0.180 – 0.085 = 0.095, $p = .069$	0.231 – 0.095 = 0.136, $p = .015$
5.5	0.170 – 0.068 = 0.102, $p < .001$	0.262 – 0.121 = 0.141, $p < .001$	0.320 – 0.133 = 0.187, $p < .001$

Applicability of Adrian's models

The luminance difference threshold predictions made by two variations of Adrian's 1989 model were investigated. Both the predictions made by the classic model without glare, and the classic model with Adrian's glare correction (Equation 35), were compared to the measured thresholds.

To assess the fit of Adrian's models, the data of some participants were left out from the analyses in this section. Since the original model did not include a factor for visual disabilities like cataracts, lazy eyes, and exotropia, three participants (id: 18, 27, 31) with these visual impairments were excluded.

Figure 30 presents the fit between the predicted thresholds by Adrian's models and the measured thresholds. Blue dots indicate the data of the excluded participants. A linear prediction is fitted through the included data, indicated with red dots. The predicted thresholds by both Adrian's model without the glare factor ($R^2 = 0.51$) and Adrian's model with the glare factor ($R^2 = 0.49$) had moderate, but comparable linear fits with the measured threshold.

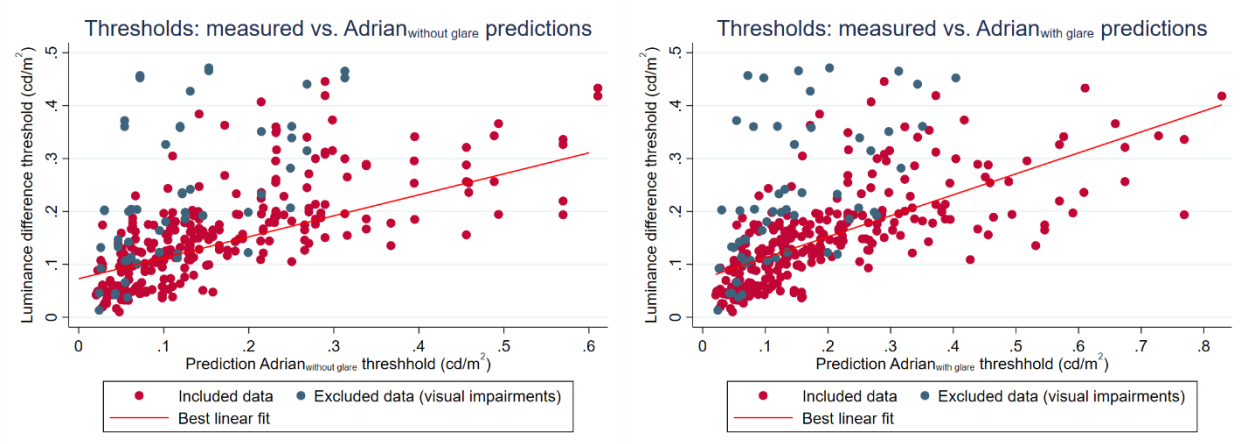

Figure 30. Left: prediction $\text{Adrian}_{\text{without glare}}$ thresholds vs. measured thresholds. Right: prediction $\text{Adrian}_{\text{with glare}}$ thresholds vs. measured thresholds

To assess the performance of Adrian models within each condition, means and 95% confidence intervals of the Adrian predictions were calculated across the nine road luminance and arrow size conditions. These were compared with the measured thresholds and can be found in Figure 31. In this figure, we find that across road luminances, the same trend appears: the Adrian models make better predictions when the arrow size is 20.3 or 9.5 arcmin, and overestimate the threshold for the smallest arrow size of 5.5 arcmin.

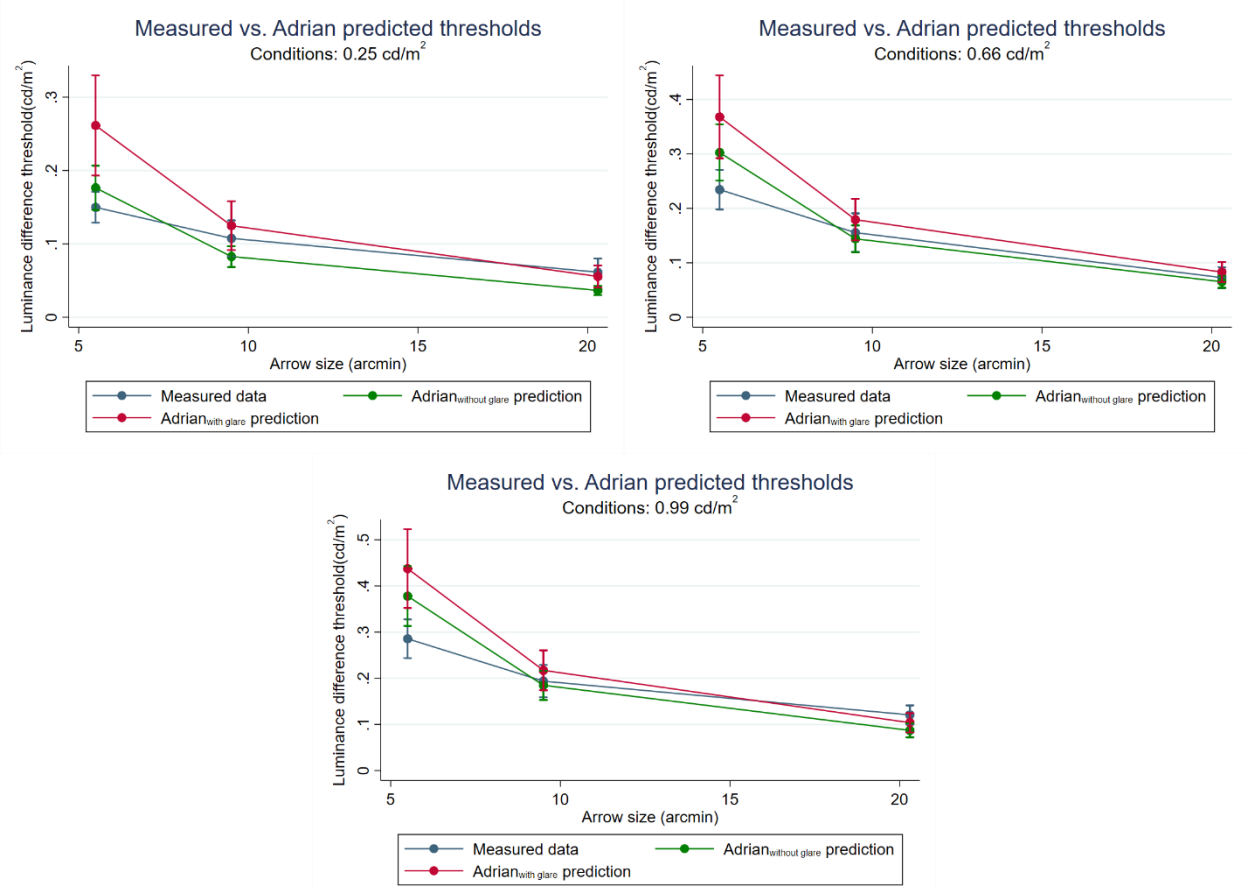

Figure 31. Pairwise comparisons of measured vs. Adrian-predicted luminance difference thresholds.

Table 8 presents the differences between measured thresholds and the ones predicted by Adrian's model *without* glare factor, as well as the results of one-sample t-tests using Bonferroni-corrected *p*-values. These numbers do partly confirm the earlier observed trend. Indeed, for the smallest arrow size the model is overestimating the threshold significantly, but there is also significant underestimation for two of three conditions with the largest arrow size. Similarly, Table 9 presents the differences between the measured threshold and the prediction threshold by Adrian's model *with* the glare factor. For this model, there again is a significant overestimation of the threshold for the smallest arrow size, but for all the other conditions there is no statistically significant difference between the predicted and measured threshold.

Table 8

Differences observed vs. Adrian$_{without\ glare}$ predicted thresholds, presented as 'observed minus predicted'.

	0.25	**0.66**	**0.99**
20.3	0.061 – 0.037 = 0.024, $p = .016$	0.073 – 0.065 = 0.008 $p = .999$	0.121 – 0.087 = 0.034, $p = .002$
9.5	0.108 – 0.083 = 0.025, $p = .160$	0.155 – 0.144 = 0.011, $p = .999$	0.194 – 0.185 = 0.009, $p = .999$
5.5	0.150 – 0.176 = -0.026, $p = .025$	0.234 – 0.303 = -0.069, $p < .001$	0.286 – 0.378 = -0.092, $p < .001$

Table 9

Differences observed vs. Adrian$_{with\ glare}$ predicted thresholds, presented as 'observed minus predicted'.

	0.25	**0.66**	**0.99**
20.3	0.061 – 0.056 = 0.005, p = .999	0.073 – 0.083 = -0.010 p = .999	0.121 – 0.104 = 0.017, p = .529
9.5	0.108 – 0.125 = -0.017, p = .999	0.155 – 0.179 = -0.024, p = .999	0.194 – 0.217 = -0.023, p = .999
5.5	0.150 – 0.261 = -0.111, p < .001	0.234 – 0.367 = -0.133, p < .001	0.286 – 0.427 = -0.141, p < .001

Applicability of the simple DoG model

Initially, two models were under investigation: the original Tadmor and Tolhurst (2000) model, and a modified model with the inclusion of a veiling luminance, calculated with the CIE Point-Spread Function (Equation 33), superimposed on the entire image (Equations 20 - 22). This process is visualized in Figure 32. As can be seen in this figure, both models produced the same DoG-filtered image, and as such had the same C_{DoG} threshold. Therefore, the models perform similar for our purposes, and for the remainder of the analyses in this chapter the original Tadmor and Tolhurst (2000) model will be used.

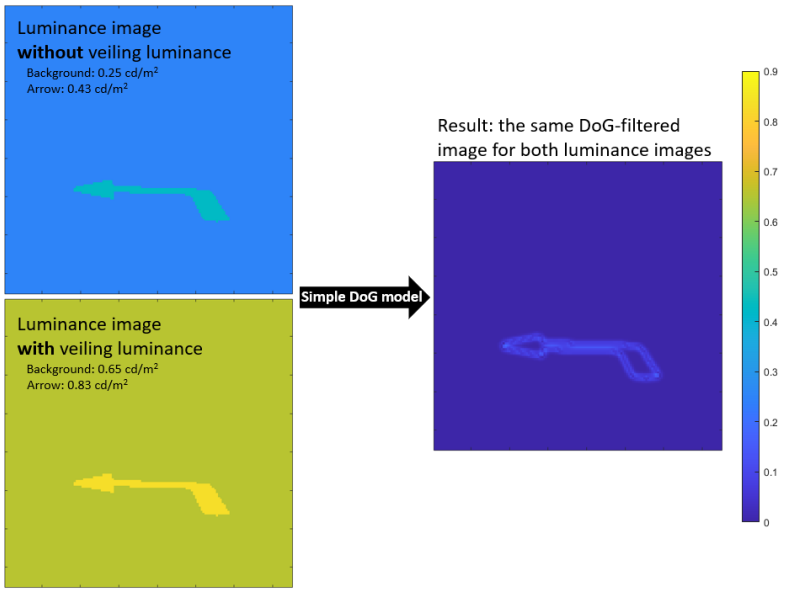

Figure 32. Visualization of the simple DoG model, showing the input without a veiling luminance across the entire image (top left), the input including a veiling luminance across the image (bottom left), and the resulting DoG -filtered image (right) which turned out to be the same for both models. Data of participant 32 is visualized, who experienced a veiling luminance of 0.40 cd/m^2.

Effects of road luminance and arrow size on C_{DoG} thresholds. Similar patterns emerge in both conditions with and without glare (Figure 33). While the C_{DoG} thresholds seems to clearly vary

between different road luminance conditions (a higher road luminance results in a higher C_{DoG} threshold), there seems almost no variance between different arrow size conditions. A repeated measured ANOVA confirmed this finding, showing a main effect of road luminance ($F(2,15) = 50.22$, $p < .001$, $\eta^2_{partial} = .88$) and not of arrow size ($F(2,15) = 0.33$, $p = .722$, $\eta^2_{partial} = .02$) in the condition with glare. The findings in the conditions without glare are similar: a main effect of road luminance ($F(2,15) = 47.73$, $p < .001$, $\eta^2_{partial} = .74$), and no main effect of arrow size ($F(2,15) = 0.83$, $p = .445$, $\eta^2_{partial} = .05$). There is, however, a difference found in the interaction effects: in the conditions with glare, there is a small but significant interaction effect of road luminance and arrow size ($F(4,9) = 3.89$, $p = .006$, $\eta^2_{partial} = .19$), while this was not found in the conditions without glare ($F(4,9) = 1.27$, $p = .290$, $\eta^2_{partial} = .07$).

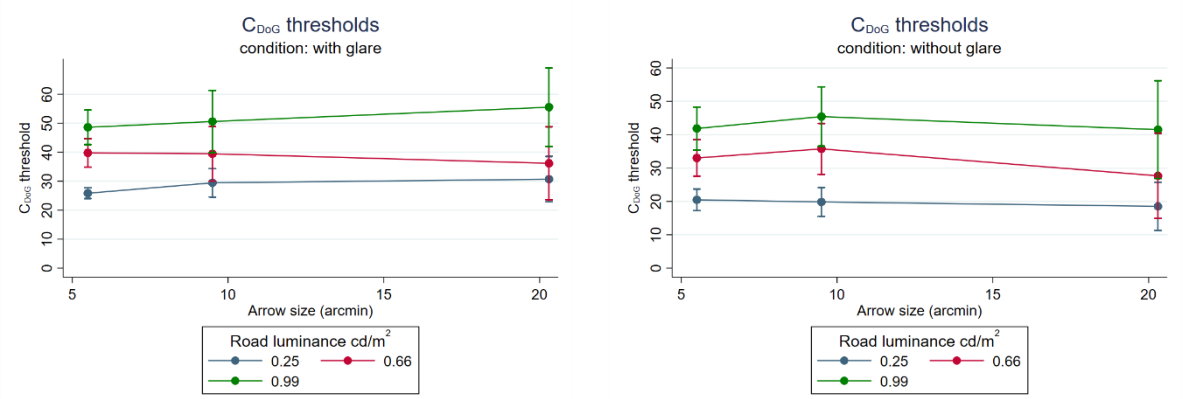

Figure 33. The effects of road luminance and arrow size on the mean C_{DoG} thresholds in conditions with (left) and without (right) glare.

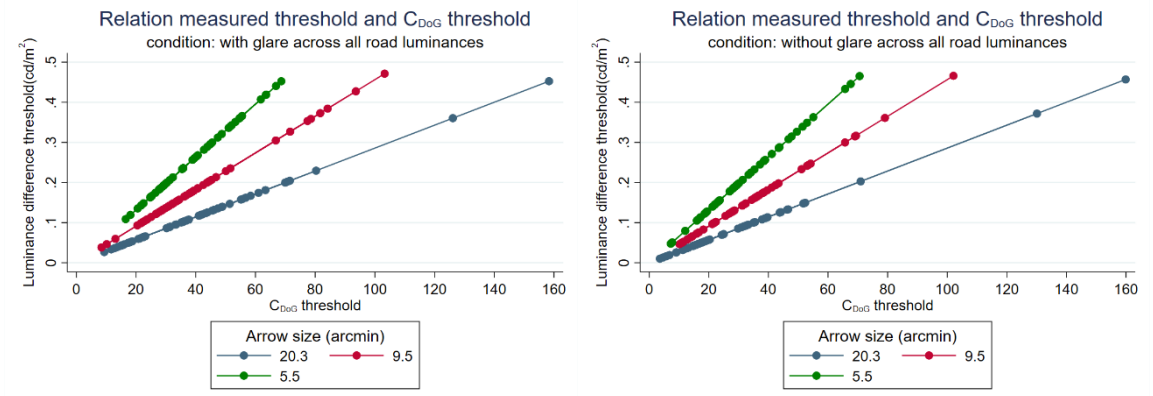

Figure 34. Relation between C_{DoG} thresholds and measured thresholds for different arrow sizes in conditions with (left) and without (right) glare.

Relationship C_{DoG} and measured threshold. Since there is no effect of arrow size on the C_{DoG} threshold between glare conditions, their relationship might be generalized. This is done in an attempt

to construct a simple formula to predict the luminance difference threshold from the C_{DoG} threshold. Figure 34 shows the relation between the measured and C_{DoG} thresholds, as a function of arrow size, in both the conditions with and without glare. Within the separate arrow size conditions, there are perfect linear relationships between the C_{DoG} threshold and the measured thresholds. Moreover, the slopes of the lines are similar for each arrow size, independent of glare. Finally, all lines have their intercept in origin. This gives us the following three linear relationships:

$$\begin{aligned} \Delta L_{threshold} &= 0.00286 \cdot C_{DoG\ threshold} && \text{for arrow size} = 20.3 \text{ arcmin} \\ \Delta L_{threshold} &= 0.00456 \cdot C_{DoG\ threshold} && \text{for arrow size} = 9.5 \text{ arcmin} \\ \Delta L_{threshold} &= 0.00659 \cdot C_{DoG\ threshold} && \text{for arrow size} = 5.5 \text{ arcmin} \end{aligned} \tag{41}$$

To further generalize this relationship, the three different slopes were plotted in Figure 35. Then, a power law function in the form of $\alpha \cdot \text{arrow size}^{\beta}$ was fitted, with the Greek letters indicating two fitting parameters. This power law form was chosen after Steven's power law ($R^2 > 0.99$), which is relevant here as there is a comparison between an absolute (arrow size) and a perceived (luminance difference threshold) change of stimuli.

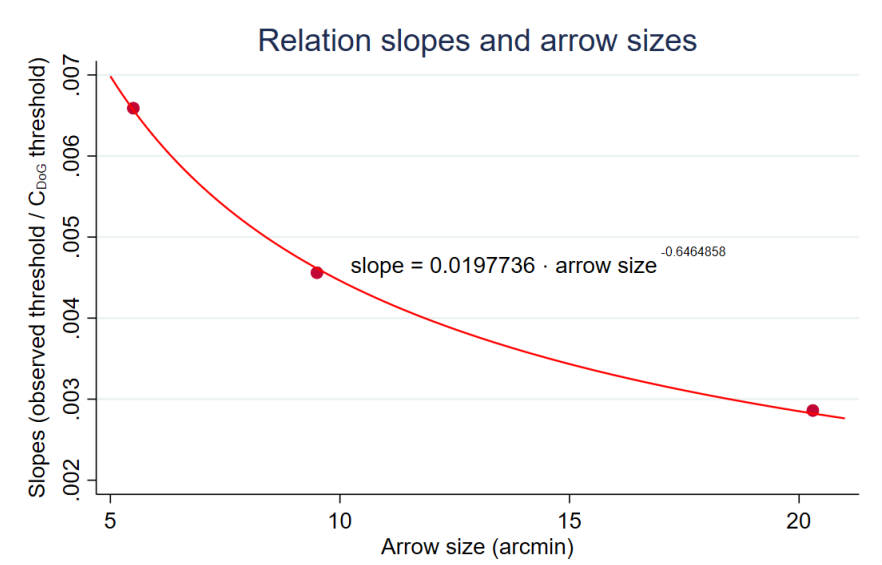

Figure 35. The relationship between slopes ($\frac{\text{Observed } \Delta L_{\text{threshold}}}{C_{\text{DoG threshold}}}$) and arrow sizes.

Using this relationship between the slope and arrow size, a generalized model for predicting the luminance difference threshold based on arrow size (in arcmin) and the C_{DoG} threshold was made, which is valid for conditions with and without glare:

$$\Delta L_{threshold} = (0.020 \cdot \text{arrow size}^{-0.0646}) \cdot C_{DoG\ threshold} \tag{42}$$

Relationship C_{DoG} in conditions with and without glare. Because there was no difference between the DoG-filtered images in conditions with and without a veiling luminance, the veiling luminance will be accounted for by a different approach. In this section, the focus will be on the paired data of each participant from the two glare conditions. As each participant was exposed to the same 3 x 3 x 2 (i.e., road luminance x arrow size x glare) conditions, a comparison of the C_{DoG} thresholds across glare conditions is possible. The analyses in this section also exclude the data of participants with visual impairments. The reason for this can be observed in Figure 36: when including this population, prediction models would be strongly overfitted, falsely making them seem more accurate than they are. This would, in the end, not allow for generalization to the average elderly population.

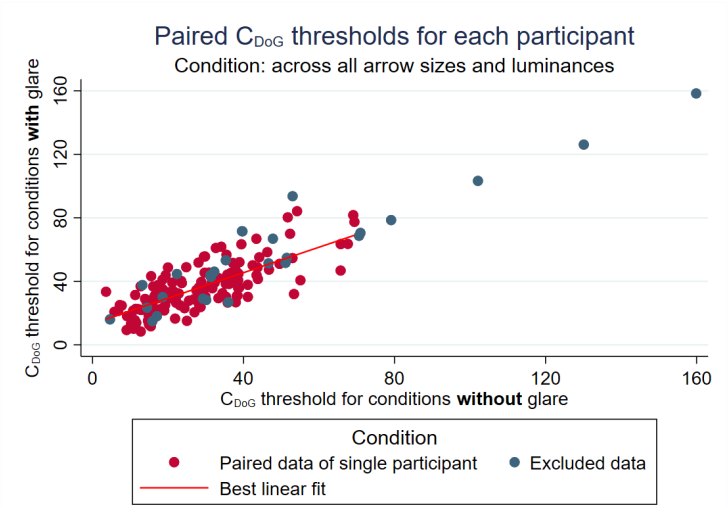

Figure 36. The relationship between the C_{DoG} thresholds with and without glare for each participant, across all conditions.

The best description of the relationship between the C_{DoG} thresholds with and without glare seems to be linear. Therefore, a linear model in which the slope is made dependent on the veiling luminance is fit on the data: $\alpha + (\text{veiling luminance} + \beta) \cdot C_{DoG\ threshold}$, where Greek letters represent fitting parameters. The best fit ($R^2 = 0.58$) is presented by the equation below, in which all fitting parameters have a significant influence on the outcome (all p-values < .05).

$$C_{DoG\ without\ glare\ threshold} = 4.690 + (\text{veiling luminance} + 0.195) \cdot C_{DoG\ with\ glare\ threshold} \quad (43)$$

Similarly, the $C_{DoG\ with\ glare\ threshold}$ can be expressed as a function of the and the $C_{DoG\ without\ glare\ threshold}$ ($R^2 = 0.56$). The veiling luminance is excluded here, as this is not present in the conditions without glare.

$$C_{DoG\ with\ glare\ threshold} = 13.384 + 0.802 \cdot C_{DoG\ without\ glare\ threshold} \tag{44}$$

Combining these two equations with Equation 42, a relation between the luminance difference threshold and the C_{DoG} thresholds can be modeled according to the equations below:

For conditions without glare ($R^2 = 0.96$):

$$\Delta L_{threshold} = \left(0.020 \cdot \text{arrow size}^{-0.0646}\right) \cdot \left(13.384 + 0.802 \cdot C_{DoG\ without\ glare\ threshold}\right) \tag{45}$$

For conditions with glare ($R^2 = 0.94$):

$$\Delta L_{threshold} = \left(0.020 \cdot \text{arrow size}^{-0.0646}\right) \cdot (4.690 + (\text{veiling luminance} + 0.195) \cdot C_{DoG\ with\ glare\ threshold}) \tag{46}$$

Applicability of the complex DoG model

Similar to the analysis of simple DoG models, two complex DoG models were used: the original Joulan et al. (2011) model, and a modified model with the inclusion of a veiling luminance, calculated with the CIE Point-Spread Function (Equation 33), superimposed on the entire image (Equation 27). Contrary to the simple DoG models presented earlier; these two variants of the model yielded different predictions (Figure 37). As such, the full attention in this section will be directed toward this modified Joulan model to investigate its usefulness for predicting the luminance contrast threshold.

Effects of road luminance and arrow size on C_{SDoG} thresholds. In the conditions with glare, there is a clear effect of arrow size: for larger arrows, the C_{SDoG} threshold increases (left in Figure 38). Within each arrow size condition, there does not seem to be an effect of road luminance, except for the largest arrow size of 20.3 arcmin. A repeated measured ANOVA found a main effect of road luminance ($F(2,15) = 11.32$, $p < .001$, $\eta^2_{partial} = .40$) and of arrow size ($F(2,15) = 14.78$, $p = < .001$, $\eta^2_{partial} = .47$) in the condition with glare. There also was an interaction effect between road luminance and arrow size ($F(4,9) = 5.82$, $p = < .001$, $\eta^2_{partial} = .25$). For the conditions without glare (right in Figure 38), something different occurs. While there is also an increase in the C_{SDoG} threshold as arrow sizes get larger, there seems to be a

more pronounced effect of road luminance: the larger the road luminance, the smaller the threshold. A repeated measured ANOVA found a main effect of road luminance ($F(2,15) = 35.72$, $p < .001$, $\eta^2_{partial} = .67$) and of arrow size ($F(2,15) = 3.84$, $p = .031$, $\eta^2_{partial} = .18$). In this case, there was no interaction effect between road luminance and arrow size ($F(4,9) = 1.60$, $p = .184$, $\eta^2_{partial} = .09$).

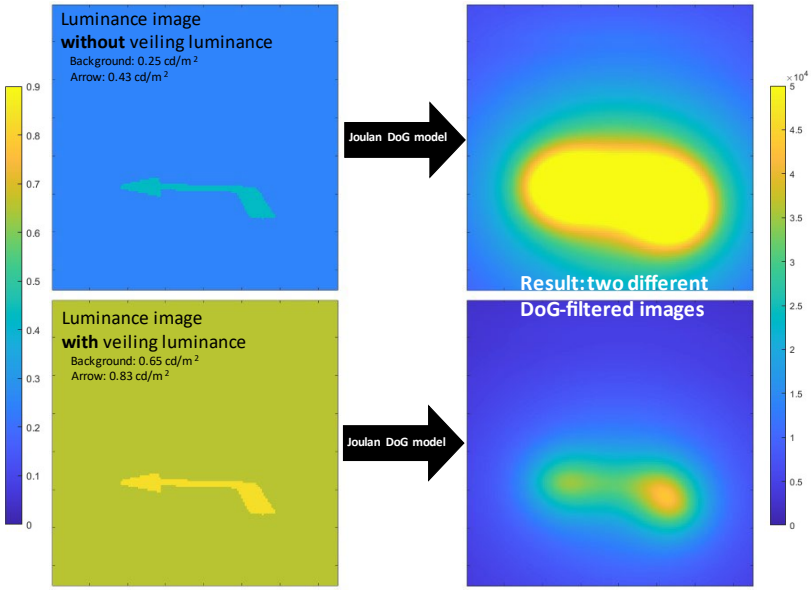

Figure 37. Visualization of the Joulan *DoG* model, showing the input without a veiling luminance across the entire image (top left), the input including a veiling luminance across the image (bottom left), and the resulting DoG-filtered image (right). Data of participant 32 is visualized, who experienced a veiling luminance of 0.40 cd/m2.

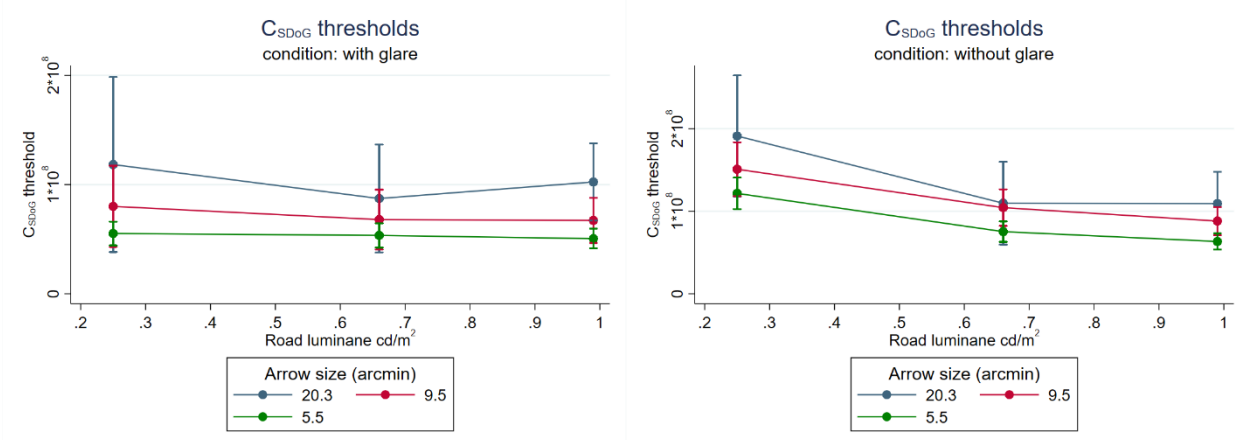

Figure 38. The effects of road luminance and arrow size on the mean C_{SDoG} thresholds in conditions with (left) and without (right) glare.

Relationship between measured and C_{SDoG} thresholds. Focusing on the modified C_{SDoG} model, we find interesting patterns when differentiating between all conditions. Looking at the data without glare (right in Figure 39), a similar pattern emerges like in the simple *DoG* model: perfect linear

relationships between predicted C_{SDoG} thresholds and measured luminance difference thresholds (average R^2 = 1.0). However, where in the simple DoG model there was only differentiation between the different arrow sizes, in this complex DoG model there is also a differentiation between different road luminances. The left side of Figure 39 shows the same relation, but now relates to the conditions with glare. Under conditions of glare, the linear relations between the measured luminance difference threshold and the C_{SDoG} threshold within each condition weaken (average R^2 = 0.94).

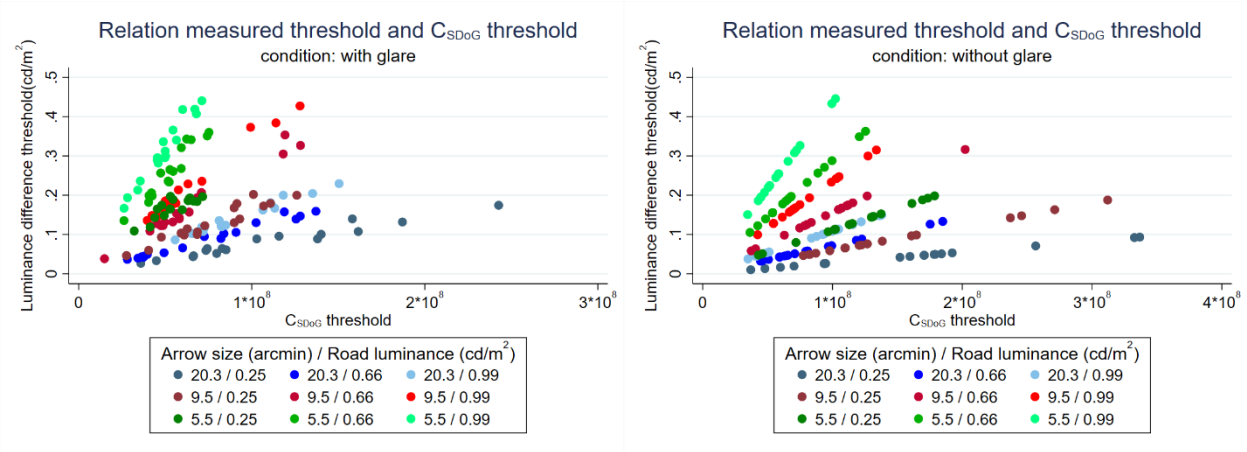

Figure 39. The relationship between the C_{SDoG} thresholds and measured luminance difference thresholds, for the data with (left) and without (right) a veiling luminance incorporated.

Using the same method as described in the paragraph on the simple DoG models, the relationship between the slopes of the lines in Figure 39 and their respective conditions were generalized in order to obtain simple formulas to calculate the luminance difference threshold from the C_{SDoG} threshold. Since the slope depends on both arrow size and road luminance, three different curves are fitted to account for all the conditions (Figure 40). These resulted in the equations presented in Equation Set 47 below.

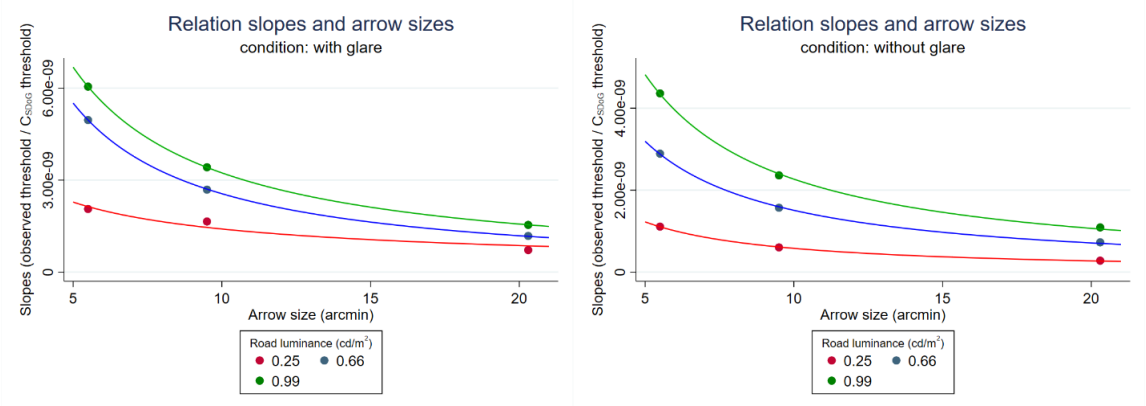

Figure 40. The relationship between slopes ($\frac{\text{Observed } \Delta L_{\text{threshold}}}{C_{\text{DoG threshold}}}$), arrow size, and road luminance, with the best power-relation fit on conditions with glare (left) and without glare (right).

Conditions with glare:	Conditions without glare:
for $0.25\frac{cm}{m^2}$	
$\Delta L_{threshold} = (7.04 \cdot 10^{-9} \cdot \text{arrow size}^{-.699}) \cdot C_{SDoG\ threshold}$	$\Delta L_{threshold} = (6.97 \cdot 10^{-9} \cdot \text{arrow size}^{-1.080}) \cdot C_{SDoG\ threshold}$
for $0.66\frac{cm}{m^2}$	
$\Delta L_{threshold} = (3.28 \cdot 10^{-8} \cdot \text{arrow size}^{-1.108}) \cdot C_{SDoG\ threshold}$	$\Delta L_{threshold} = (1.84 \cdot 10^{-8} \cdot \text{arrow size}^{-1.082}) \cdot C_{SDoG\ threshold}$
for $0.99\frac{cm}{m^2}$	
$\Delta L_{threshold} = (3.60 \cdot 10^{-8} \cdot \text{arrow size}^{-1.046}) \cdot C_{SDoG\ threshold}$	$\Delta L_{threshold} = (2.77 \cdot 10^{-8} \cdot \text{arrow size}^{-1.087}) \cdot C_{SDoG\ threshold}$

(47)

For each road luminance and arrow size condition, a more or less similar exponent of -1.08 is found. The only exception is the 0.25 cd/m^2 with glare condition, which has an exponent of -0.699. Nevertheless, the relation between $\Delta L_{threshold}$ and the conditions is further generalized by fixing the exponent at -1.08 and fitting a model that now includes the road luminance as a factor. Models in the form of $(\alpha \cdot \text{road luminance}) \cdot \text{arrow size}^{-1.08}$ are fit, again representing a power law form, with alpha as a fitting parameter. This results in the equation set below, with an R^2 of 0.98 and > 0.99, respectively.

For conditions with glare ($R^2 = 0.98$):

$$\Delta L_{threshold} = (4.20 \cdot 10^{-8} \cdot \text{road luminance} \cdot \text{arrow size}^{-1.08}) \cdot C_{SDoG\ threshold} \quad (48)$$

For conditions without glare ($R^2 > 0.99$):

$$\Delta L_{threshold} = (2.76 \cdot 10^{-8} \cdot \text{road luminance} \cdot \text{arrow size}^{-1.08}) \cdot C_{SDoG\ threshold} \quad (49)$$

Discussion

In this final chapter, the methods, results, and limitations of this experiment are discussed in detail, following the same order as in the '*Results*' chapter. For a short overview of the most important findings, the reader is referred to the '*Conclusion*' section.

Effects of road luminance and arrow size

In both the conditions with and without glare, significant differences in the luminance difference thresholds were found between all road luminance pairs and all arrow size pairs. The main effects of road luminance ($\eta^2_{partial}$ = .76) and arrow size ($\eta^2_{partial}$ = .83) were similar across glare conditions. These findings were not surprising, as similar effect sizes were found by Spieringhs et al. (2021). It turns out that for old and young populations, both factors have a comparable impact on the luminance difference threshold.

There was, however, a difference found in the size of the interaction effect of road luminance and arrow size. The interaction effect entails that for smaller arrow sizes, an increase in road luminance causes a larger increase in the threshold than for bigger arrow sizes. In the conditions with glare ($\eta^2_{partial}$ = .40), this effect size was larger than in the conditions without glare ($\eta^2_{partial}$ = .26). More research is required to explain this finding.

Effects of glare in an elderly population

To answer the first sub-research question, Figure 27 has revealed that for all conditions our elderly sample was exposed to, mean luminance difference thresholds are higher in the conditions with glare compared to conditions without glare, with a main effect of $\eta^2_{partial}$ = .66. This was to be expected given the characteristics of the aging visual system (e.g., degradation of the lens and the resulting increasing intraocular scattering). However, pair-wise comparisons have shown these differences are, with the exception of two out of nine conditions, never statistically significant. Glare only had a significant effect in two of the conditions with the lowest road luminance (0.25 cd/m^2). A possible explanation is the relative effect of glare in different road luminance conditions. The average veiling luminance participants experienced was 0.45 cd/m^2, which is almost twice as high as the lowest road luminance. In the conditions with a higher road luminance (0.66 and 0.99 cd/m^2), the relative size of the veiling luminance is smaller and thus might not significantly influence the threshold. The larger the background luminance, the smaller the effect of glare. Another explanation can be found in the sample size; as the desired sample size of 26 participants was not reached, the statistical power might not have been high enough (i.e., post hoc calculated to be .75) to find a significant effect of glare in the conditions with a higher road luminance.

There was, however, a significant positive correlation (r = .21, p < .001) between the measured straylight parameter and the luminance difference thresholds. This means that visual performance decreased

under conditions of glare for people who are more susceptible to straylight and thus experience a larger veiling luminance. The found relationship between age and straylight factor was not surprising and resembled earlier findings by Rozema et al. (2010) and van den Berg et al. (2007).

Control variables like alertness, sleep quality, and time spent driving a car have all been found not to impact the thresholds. Altogether, this highlights that while there is no average effect of glare across all participants, for those with high sensitivity to straylight, which increases strongly with age, glare is a relevant factor in their decreased task performance.

A final interesting finding is the significant positive correlation between the straylight parameter and the measured thresholds ($r = 0.21$). While it intuitively makes sense that for participants with a higher measured sensitivity to glare, the contrast thresholds were higher, this finding is still noteworthy. It shows that the Oculus C-Quant, using a compensation comparison method to determine a straylight threshold, also can provide useful information on contrast thresholds in a completely different psychometric measurement paradigm (QUEST+).

Effects of age under conditions of glare

Focusing on the second sub-research question, we compared the luminance difference thresholds of an old (M = 70.2 years) and young (M = 28.4 years) sample using data from Spieringhs et al. (2023) [Unpublished manuscript]. Clear differences between the two age groups can be found. Except for two conditions, all found differences are statistically different, indicating that for the older sample, the luminance difference threshold is roughly 2.5x higher. This is not surprising, given the characteristics of the aging visual system. When pooling the data of both studies a significant positive correlation ($r = .45$, $p < .001$) between age and threshold was found, showing that the thresholds increase with age. However, due to the nature of both studies, this correlation analysis includes no data in the age group from 40 to 60 years old.

As mentioned, in two of the nine conditions (i.e., 0.66 cd/m^2 and 20.3 arcmin, and 0.66 cd/m^2 and 9.5 arcmin) mean thresholds do not differ statistically between the young and old samples. An explanation for this might be the lack of statistical power due to the set-up of the experiment by Spieringhs et al. (2023) [Unpublished manuscript]. In their experiment, each participant was exposed to only three of nine conditions, while in this experiment, each participant was exposed to all conditions. Another difference between the two studies that might explain this unexpected finding is the exposure time of the targets: 2 seconds in the young sample vs. 3 seconds in the old sample. The reason for the longer exposure time in the old sample is to assure that the older participants, given their reduced reaction times, still had the opportunity to find, identify, and respond to the stimuli. Even with this longer reaction time, older participants still showed an average higher threshold. This threshold might have increased when the 2-second reaction time was used, as participants would be under more time pressure and identify fewer arrows

correctly. In the current study, the average reaction time of the elderly sample was 1.4 s, with 31% of reaction times being larger than 2 s.

Adrian's models

Comparing our measured luminance difference thresholds to those predicted by Adrian's (1989) models, there are moderate linear fits for both the model without ($R^2 = 0.51$) and with ($R^2 = 0.49$) a glare factor. For the model *without* glare factor, the threshold predictions are accurate only for an arrow size of 9.5 arcmin, independent of background luminance. Across all background luminances, it is also overestimating the measured threshold for the smallest arrow size (5.5 arcmin), and underestimating the threshold for the biggest arrow size (20.3 arcmin). For the model *with* a glare factor, predictions are better. In conditions with the larger two arrow sizes, the prediction is accurate, while for the smallest arrow size, there again is a significant overestimation of the threshold.

Similar trends can be found when comparing these results to the study of Spieringhs et al. (2021). In both studies, the Adrian model provides better predictions for larger arrow sizes than for smaller arrow sizes. The main difference between the two works is the overall correspondence between the Adrian model and the predicted threshold; in the work of Spieringhs et al. (2021), the fit between measured and predicted thresholds is significantly higher ($R^2 = 0.75$).

Multiple factors might explain this difference in overall fit. One of them considers the fact that Spieringhs et al. (2021) included a 4th arrow size (3.6 arcmin) in their study. However, this is not a very likely explanation, as in both studies the Adrian model seems to predict less accurately when arrow size decreases. If anything, including this 4th smaller arrow size would have decreased the overall correspondence between predicted and measured thresholds. Another possible explanation for these differences is that Spieringhs et al. (2021) only investigated a part of Adrian's model, as their average age factor was about 1. In this study, using an older sample, this factor was further away from 1: the average age factor was 3.02. As such, this factor has influenced the predicted luminance difference thresholds. The final explanation is that the sample in Spieringhs et al. (2021) was way younger ($M = 28.4$ years) compared to ours ($M = 70.2$ years). The importance of age will be explained in more detail in the upcoming paragraph.

To explain the moderate performance of Adrian's models in this study ($R^2 = 0.51$, and $R^2 = 0.49$), differences between the experiments Adrian based his model on and the current experiment can be highlighted. First of all, Adrian's model is based on data from detection experiments: participants had to indicate whether or not they could detect *any* stimuli, while this work considered an experiment on discrimination. Discrimination can be seen as an extra step of complexity beyond mere detection; besides detecting the presence of an arrow, participants also had to discriminate between two slightly different

variations. Second, Adrian's model is based on experiments using simple stimuli, namely uniformly lit circles on uniformly lit backgrounds. In this experiment, the focus was on more complex shapes in a more complex visual environment. Third, it is important to highlight that the age factor in Adrian's model is based on data from an experiment (Blackwell & Blackwell, 1980) in which the majority of participants (51%) was in the age group of 20 – 30 years. The 70 – 80 age group made up only 11% of their sample. This likely is one of the most important explanations for the overall moderate model fit, as more than 1/3rd of our sample consisted of participants 75+ years old. Since this was such a big part of our sample (and the most interesting part when it comes to investigating the effects of glare), these were included in the analysis, which might not have been entirely fair when purely interested in the performance of Adrian's models.

Concluding, Spieringhs et al. (2021) stated "it shows that the [Adrian] model is more broadly applicable than where it originally was intended for" (p. 18), the results from this study confirm this statement, with the sidenotes that this *a*) only holds for larger target sizes, and *b*) only holds for Adrian's model that takes into account a glare factor.

Image-based DoG models

Two variations of the simple DoG model by Tadmor & Tolhurst (2000) were tested: their original C_{DoG} model, and an adjusted C_{DoG} model with a veiling luminance that was superimposed on the entire input image. As it turned out, superimposing the veiling luminance on the entire image did not result in different C_{DoG} thresholds. The reason is that by superimposing a veiling luminance over the entire image you add a constant luminance for the center and surround Gaussians (Equations 20 - 22), with a similar DoG-filtered image as a result.

In contrast, the two complex DoG models based on the work of Joulan et al. (2011), did provide two different DoG-filtered images, and as such different C_{SDoG} thresholds. This can be explained by the inclusion of a different adaptation luminance (i.e., background + veiling luminance) in the model, in which the veiling luminance is different for each participant.

When investigating the relationship between C_{DoG} thresholds and luminance thresholds, it was found that irrespective of glare, this relationship was linear and only based on arrow size. The slopes being similar (within arrow size groups) in conditions with and without glare hints towards something interesting: this model adheres to the earlier described finding of there being no interaction effect between glare and arrow size. As such, a power law function model was created to predict the luminance difference threshold based on arrow size and C_{DoG} threshold ($R^2 = 1.0$).

For the Joulan model, a similar approach was taken, as similar linear relationships were found between C_{SDoG} thresholds and luminance thresholds, although they were weaker in the conditions with glare

($R^2 = 0.94$) compared to conditions without glare ($R^2 = 1.0$). Here we found the slopes to be dependent on both arrow size and road luminance, compared to only arrow size in the simple DoG model. Another difference was that the slopes within each of the nine road luminance and arrow size conditions differed, depending on whether or not glare was present. A power law function was fitted for each set of slopes, which revealed that exponents were more or less constant across all conditions. The only condition that did not have a similar exponent was that of a road luminance of 0.25 cd/m^2 and glare. As stated earlier, glare has a relatively large impact on the visual scene when the background luminance is only 0.25 cd/m^2, which could therefore have impacted the relationship.

It is important to highlight that for both the simple and complex DoG models, Steven's power law was used as a starting point to model the relation between the measured threshold and arrow size. Using the power law in the context of luminance difference thresholds is not novel, and different combinations of constructs have been investigated. For example, the relation between luminance difference thresholds and background contrast (Legge, 1981) and between perceived contrast and stimulus contrast (Gottesman et al., 1981). Research has also been done on the relation between luminance difference threshold and sizes of disks, but this work did not model it with a power relation (Du Buf, 1987). The building of our prediction model was highly explorative, and as such future research is needed to back it up theoretically and make it more generalizable to other research areas.

Since incorporating glare as a constant veiling luminance over the entire image did not provide a different model compared to the original Tadmor & Tolhurst (2000) model, another approach was taken to incorporate a factor of glare. A prediction model, based on the veiling luminance, was made to predict C_{DoG} thresholds for conditions with glare from C_{DoG} thresholds for conditions without glare, and vice versa (R^2's = 0.58 and 0.56, Equations 43 and 44). Thereafter, these models were combined with the model that predicted luminance thresholds from arrow sizes and C_{DoG} thresholds. This resulted in two final prediction models, one for conditions with glare and one for conditions without glare, that predict with high accuracy (R^2's = 0.98 and 0.96, Equations 45 and 46) the measured luminance difference thresholds from the arrow size, veiling luminance, and C_{DoG} threshold.

For the Joulan model, this extra step was not required, as the model differentiated between conditions with and without glare. In the end, this also resulted in two prediction models, one for conditions with glare and one for conditions without, that predict the luminance difference threshold based on road luminance, arrow size, and C_{SDoG} threshold.

A few final notes regarding the applicability of these DoG models have to be made. First, it is important to highlight that both the Tadmor & Tolhurst (2000) and the Joulan (2011) models are not models that directly predict a luminance difference threshold. Instead, they provide DoG-filtered images, and the

sum of all DoG values in the entire image was used as a proxy for how well contrast would be perceived in different scenarios. Second, the two DoG models are image-forming models, which are most commonly applied in suprathreshold visibility conditions, while in this work they were used in conditions around threshold visibility. Third, the DoG models only simulate visual processing in the lower-order regions of our visual system and therefore do not tell the entire story. Fourth, the set of spatial filters (i.e., the different DoG's) used in the Joulan (2011) models might not be suitable for this context, as Joulan and colleagues' proposed set was built to represent a contrast sensitivity function for situations with an average luminance of 100 cd/m^2 in the image. Our average luminance in the image was way lower. This might be one of the explanations for why the Joulan model (see Figure 37) did not detect the sharp edges of the arrow. Lastly, earlier presented results showed no interaction effect between glare and both road luminance and arrow size. One could therefore question the validity of modeling in the glare as a luminance superimposed on the entire input image. While this makes sense intuitively and corresponds with how people reportedly experience glare, another way of implementing glare on an image might be more suitable.

Limitations

In the previous section, some issues with comparing these results to the results of other studies, and some limitations of the used models have been already described. Therefore, this section will highlight this work's additional, more general, limitation.

The QUEST+ model performed a bit below expectation, as the average fit of the psychometric curves was not ideal. However, other psychometric experiment paradigms also have their disadvantages, and the QUEST+ was chosen as it was the most time-efficient method. This was important, as the older population would not have the cognitive and attentional resources for pro-longed participation in a demanding experiment like this one. Several participants indicated that even in this time-efficient paradigm, they experienced (visual) fatigue. If another psychometric paradigm was chosen, data collection would have been slower, allowing for fatigue to start playing a larger role, thereby reducing the quality of the collected data.

Future research

A first suggestion for future research is to dive deeper into the workings of the Joulan et al. (2011) DoG model. Their proposed set of spatial filters might be finetuned to be more accurate in the context of driving at night. Second, this research can be repeated with varying amounts or locations of glare, as only a single one was used in this work. One can imagine that a stronger or weaker glare would impact the luminance difference threshold. Regarding the location of glare, this study used a glare source coming from above. In

reality, however, there is also glare coming from the headlights of cars ahead. Third, more realistic scenes can be used. For example, the effects of non-uniform backgrounds on the performance of models in this work can be further investigated. Finally, there is one big factor missing in the set-up of this experiment that reduces its ecological validity: a windshield. When on the road, there is this extra medium through which light has to travel, which can induce more scattering of light and potentially more glare. As part of this research, a pilot study was done regarding the effects of a windshield on the luminance difference threshold. The rationale behind, method of, and results of this pilot study are presented in Appendix D.

Conclusion

In this work, the luminance difference thresholds of an elderly population in a night-time driving scenario were investigated. A within-subject two-alternative forced-choice experiment, consisting of three road luminances (0.25, 0.66, and 0.99 cd/m^2), three arrow sizes (5.5, 9.5, 20.3 arcmin), and the absence or presence of glare, was conducted to assess this threshold. In these 18 conditions, participants had to indicate the direction of an arrow that was presented in a scene of a road (the dependent variable). Psychometric curves were fit to proportion-correct data, and the 75%-correct point was used as the luminance difference threshold. This threshold was then a) compared across glare conditions (sub-research question 1), b) compared to data of a younger sample (sub-research question 2), and c) predicted using a psychophysical model and image-based models.

It was found that in the elderly sample, the mean luminance difference threshold under conditions of glare was higher across all background luminance and arrow size conditions. On average, the threshold was 1.3x higher under conditions with glare compared to conditions without glare. However, these differences were only statistically significant in the conditions with a background luminance of 0.25 cd/m^2. Glare thus has the most (negative) impact on visibility levels in situations with a low average luminance in the visual field. The second main finding was that the luminance difference threshold for older people was higher across all conditions compared to the younger sample. This was found by comparing the results of this work with those of Spieringhs and colleagues (2023) [Unpublished manuscript]. There were significant differences in all road luminance and arrow size conditions, with the exception of two 0.66 cd/m^2 conditions. On average, the luminance difference thresholds of the older sample were roughly 2.5x higher than those of the younger sample.

Regarding the investigated models, it was found that the classic model by Adrian (1989) which included a factor for glare, predicted the luminance difference thresholds accurately for the larger two arrows (i.e., 9.5 and 20.3 arcmin). However, the model consistently overestimated the measured thresholds for the smallest arrow size (i.e., 5.5 arcmin). The image-based DoG models by Tadmor & Tolhurst (2000) and Joulan, Hautiere, et al. (2011) were found to be providing metrics that could predict the luminance

difference thresholds with relatively high accuracy based on an input image. However, the resulting prediction models were dependent on the arrow size, road luminance, and veiling luminance, and these variables were required as input to achieve accurate prediction. It turns out that, for all models investigated, many input variables are needed to make accurate predictions of the thresholds. This limits their practical applicability.

Concluding, this work has highlighted the importance of considering the elderly population when designing road lighting. They constitute an ever-growing group of the world population that should not be ignored. The found luminance difference thresholds, under a variety of conditions, can be used to guide road design standards that are appropriate for this demographic. Ultimately, this will result in safer roads for all its users.

References

Ackland, P., Resnikoff, S., & Bourne, R. (2017). World blindness and visual impairment: Despite many successes, the problem is growing. *Community Eye Health*, *30*(100), 71–73.

ADOpy developers. (2020). *Psychometric Function Estimation*. https://docs.adopy.org/en/stable/examples/psi.html

Adrian, W. (1989). Visibility of targets: Model for calculation. *Lighting Research & Technology*, *21*(4), 181–188. https://doi.org/10.1177/096032718902100404

Aslam, T. M., Haider, D., & Murray, I. J. (2007). Principles of disability glare measurement: An ophthalmological perspective. *Acta Ophthalmologica Scandinavica*, *85*(4), 354–360. https://doi.org/10.1111/j.1600-0420.2006.00860.x

Barten, P. G. (1999). *Contrast Sensitivity of the Human Eye and Its Effects on Image Quality*. SPIE. https://doi.org/10.1117/3.353254

Berson, D. (2003). Strange vision: Ganglion cells as circadian photoreceptors. *Trends in Neurosciences*, *26*(6), 314–320. https://doi.org/10.1016/S0166-2236(03)00130-9

Betts, J. G., Young, K. A., Wise, J. A., Johnson, E., Poe, B., Kruse, D. H., Korol, O., Johnson, J. E., Womble, M., & DeSaix, P. (2013). Sensory Perception. In *Anatomy and Physiology*. OpenStax. https://openstax.org/books/anatomy-and-physiology/pages/14-1-sensory-perception

Blackwell, H. R. (1946). Contrast Thresholds of the Human Eye. *Journal of the Optical Society of America*, *36*(11), 624. https://doi.org/10.1364/JOSA.36.000624

Blackwell, O. M., & Blackwell, H. R. (1980). Individual Responses to Lighting Parameters for a Population of 235 Observers of Varying Ages. *Journal of the Illuminating Engineering Society*, *9*(4), 205–232. https://doi.org/10.1080/00994480.1980.10747901

Boulos, E. N., Jack, D., Surowiec, R., Bomback, J. L., Subramanian, S., Simmons, C. J., & Simmons, J. H. (1997). *Fundamental Issues in Automotive Veiling Glare*. 970227. https://doi.org/10.4271/970227

Bourne, R., Steinmetz, J. D., Flaxman, S., Briant, P. S., Taylor, H. R., Resnikoff, S., Casson, R. J., Abdoli, A., Abu-Gharbieh, E., Afshin, A., Ahmadieh, H., Akalu, Y., Alamneh, A. A., Alemayehu, W., Alfaar, A. S., Alipour, V., Anbesu, E. W., Androudi, S., Arabloo, J., … Vos, T. (2021). Trends in prevalence of blindness and distance and near vision impairment over 30 years: An analysis for the Global Burden of Disease Study. *The Lancet Global Health*, *9*(2), e130–e143. https://doi.org/10.1016/S2214-109X(20)30425-3

Brémond, R. (2020). Visual Performance Models in Road Lighting: A Historical Perspective. *LEUKOS*, *17*(3), 212–241. https://doi.org/10.1080/15502724.2019.1708204

Brown, M. B., & Forsythe, A. B. (1974). Robust Tests for the Equality of Variances. *Journal of the American Statistical Association*, *69*(346), 364–367. https://doi.org/10.1080/01621459.1974.10482955

Campbell, F. W., & Maffei, L. (1974). Contrast and Spatial Frequency. *Scientific American*, *231*(5), 106–114. https://doi.org/10.1038/scientificamerican1174-106

Campbell, F. W., & Robson, J. G. (1968). Application of fourier analysis to the visibility of gratings. *The Journal of Physiology*, *197*(3), 551–566. https://doi.org/10.1113/jphysiol.1968.sp008574

Carney, C. E., Buysse, D. J., Ancoli-Israel, S., Edinger, J. D., Krystal, A. D., Lichstein, K. L., & Morin, C. M. (2012). The Consensus Sleep Diary: Standardizing Prospective Sleep Self-Monitoring. *Sleep*, *35*(2), 287–302. https://doi.org/10.5665/sleep.1642

CBS. (2022). *Hoeveel mensen hebben een rijbewijs?* https://www.cbs.nl/nl-nl/visualisaties/verkeer-en-vervoer/verkeer/rijbewijzen

Chaya, T., Matsumoto, A., Sugita, Y., Watanabe, S., Kuwahara, R., Tachibana, M., & Furukawa, T. (2017). Versatile functional roles of horizontal cells in the retinal circuit. *Scientific Reports*, *7*(1), 5540. https://doi.org/10.1038/s41598-017-05543-2

CIE. (1995). *Discomfort Glare in Interior Lighting*. International Commission on Illumination (CIE).

CIE. (2017). *CIE 227:2017—Lighting for Older People and People with Visual Impairment in Buildings*. International Commission on Illumination (CIE). https://doi.org/10.25039/TR.227.2017

Clifford, C. W. G., Webster, M. A., Stanley, G. B., Stocker, A. A., Kohn, A., Sharpee, T. O., & Schwartz, O. (2007). Visual adaptation: Neural, psychological and computational aspects. *Vision Research*, *47*(25), 3125–3131. https://doi.org/10.1016/j.visres.2007.08.023

Davoudian, N., Raynham, P., & Barrett, E. (2014). Disability glare: A study in simulated road lighting conditions. *Lighting Research & Technology*, *46*(6), 695–705. https://doi.org/10.1177/1477153513510168

Demb, J. B., & Singer, J. H. (2015). Functional Circuitry of the Retina. *Annual Review of Vision Science*, *1*(1), 263–289. https://doi.org/10.1146/annurev-vision-082114-035334

Discovery Eye Foundation. (2016). *Structure of the Retina*. https://discoveryeye.org/layers-of-the-retina/

Donners, M. A. H., Geerdinck, L. M., van den Broek-Cools, J. H. F., & Buddemeijer-Lock, A. (2015). *A psychophysical model of discomfort glare in both outdoor and indoor applications*. 28th Session of the CIE, Manchester, United Kingdom.

Du Buf, J. (1987). *Spatial characteristics of brightness and apparent-contrast perception*. https://doi.org/10.6100/IR272991

Fairchild, M. D. (2013). Human Color Vision. In *Color Appearance Models* (pp. 1–37). John Wiley & Sons, Ltd. https://doi.org/10.1002/9781118653128.ch1

Faul, F., Erdfelder, E., Lang, A.-G., & Buchner, A. (2007). G*Power 3: A flexible statistical power analysis program for the social, behavioral, and biomedical sciences. *Behavior Research Methods*, *39*, 175–191.

Fiedler, A. J., Liu, J., Hung, G. K., & Ciuffreda, K. J. (2009). Models of Myopia Development. In *Biomedical Engineering Principles of the Bionic Man* (Vol. 5). World Scientific Publishing Company. https://doi.org/10.1142/6687

Franssen, L., & Coppens, J. E. (2007). *Straylight at the retina: Scattered papers*. https://dare.uva.nl/search?identifier=132e488d-8b77-4740-87f4-48315776d58e

Franssen, L., Tabernero, J., Coppens, J. E., & van den Berg, T. J. T. P. (2007). Pupil Size and Retinal Straylight in the Normal Eye. *Investigative Opthalmology & Visual Science*, *48*(5), 2375. https://doi.org/10.1167/iovs.06-0759

Freund, B., Colgrove, L. A., Burke, B. L., & McLeod, R. (2005). Self-rated driving performance among elderly drivers referred for driving evaluation. *Accident Analysis & Prevention*, *37*(4), 613–618. https://doi.org/10.1016/j.aap.2005.03.002

Galloway, N. R., Amoaku, W. M. K., Galloway, P. H., & Browning, A. C. (2016). Basic Anatomy and Physiology of the Eye. In N. R. Galloway, W. M. K. Amoaku, P. H. Galloway, & A. C. Browning, *Common Eye Diseases and their Management* (pp. 7–16). Springer International Publishing. https://doi.org/10.1007/978-3-319-32869-0_2

Gazzaniga, M. S., Ivry, R. B., & Mangun, G. R. (2014). *Cognitive Neuroscience: The Biology of the Mind* (Fourth edition). W. W. Norton & Company, Inc.

Gottesman, J., Rubin, G. S., & Legge, G. E. (1981). A power law for perceived contrast in human vision. *Vision Research*, *21*(6), 791–799. https://doi.org/10.1016/0042-6989(81)90176-0

Hautière, N., & Dumont, E. (2007). *Assessment of visibility using digital imaging*. 4.

Hess, M., Nauman, E., & Steinkopf, L. (2017). Population Ageing, the Intergenerational Conflict, and Active Ageing Policies – a Multilevel Study of 27 European Countries. *Journal of Population Ageing*, *10*(1), 11–23. https://doi.org/10.1007/s12062-016-9161-3

Hildebrand, G. D., & Fielder, A. R. (2011). Anatomy and Physiology of the Retina. In J. Reynolds & S. Olitsky (Eds.), *Pediatric Retina* (pp. 39–65). Springer Berlin Heidelberg. https://doi.org/10.1007/978-3-642-12041-1_2

Ising, K. (2014). *Pedestrian contrast in black and white*. https://www.meaforensic.com/pedestrian-contrast-in-black-and-white/

JETI. (2022). *JETI - Specbos 1211-2—Broadband Spectroradiometer*. https://www.jeti.com/Products/Spectroradiometer/specbos1211-2

Jones, P. R. (2018). QuestPlus: A MATLAB Implementation of the QUEST+ adaptive Psychometric Method. *Journal of Open Research Software*, *6*(1), 27. https://doi.org/10.5334/jors.195

Joulan, K., Bremond, R., & Robert-Landry, C. (2012). *Method for determining the visibility of objects in a field of view of a driver of a vehicle, taking into account a contrast sensitivity function, driver assistance system, and motor vehicle.* (Patent No. European Pattent 2 747 026).

Joulan, K., Hautière, N., & Brémond, R. (2011). Contrast sensitivity functions for road visibility estimation on digital images. *Proc. 27th Session of the Commission Internationale de l'Eclairage*.

Joulan, K., Hautiere, N., & Bremond, R. (2011). A unified CSF-based framework for edge detection and edge visibility. *CVPR 2011 WORKSHOPS*, 21–26. https://doi.org/10.1109/CVPRW.2011.5981679

Kalloniatis, M., & Luu, C. (2005). Visual Acuity. In *The Organization of the Retina and Visual System*. Salt Lake City (UT): University of Utah Health Sciences. https://www.ncbi.nlm.nih.gov/books/NBK11509/figure/ch25kallspatial.F14/

Kerofsky, L., Jagannath, A., & Reznik, Y. (2015). *User aware video streaming*. 941104. https://doi.org/10.1117/12.2077808

Legge, G. E. (1981). A power law for contrast discrimination. *Vision Research*, *21*(4), 457–467. https://doi.org/10.1016/0042-6989(81)90092-4

Lin, F.-C., Zao, J. K., Tu, K.-C., Wang, Y., Huang, Y.-P., Chuang, C.-W., Kuo, H.-Y., Chien, Y.-Y., Chou, C.-C., & Jung, T.-P. (2012). SNR analysis of high-frequency steady-state visual evoked potentials from the foveal and extrafoveal regions of Human Retina. *2012 Annual International Conference of the IEEE Engineering in Medicine and Biology Society*, 1810–1814. https://doi.org/10.1109/EMBC.2012.6346302

Löfving, B., Billger, M., & Thaung, J. (2015). Visualization of Disability Glare Due to Veiling Luminance. *Energy Procedia*, *78*, 735–740. https://doi.org/10.1016/j.egypro.2015.11.084

Lok, R., Smolders, K. C. H. J., Beersma, D. G. M., & de Kort, Y. A. W. (2018). Light, Alertness, and Alerting Effects of White Light: A Literature Overview. *Journal of Biological Rhythms*, *33*(6), 589–601. https://doi.org/10.1177/0748730418796443

Masland, R. H. (2012). The Neuronal Organization of the Retina. *Neuron*, *76*(2), 266–280. https://doi.org/10.1016/j.neuron.2012.10.002

Mather, G. (2016). *Foundations of Sensation and Perception* (0 ed.). Psychology Press. https://doi.org/10.4324/9781315672236

Ministerie van Infrastructuur en Waterstaat. (2019). *Richtlijn ontwerp autosnelwegen*. Ministerie van Infrastructuur en Waterstaat.

Ministerie van Verkeer en Waterstaat, Rijkswaterstaat. (1991). *Richtlijnen voor de bebakening en markering van wegen*. Ministerie van Verkeer en Waterstaat, Rijkswaterstaat.

NEN 13201-1. (2016). *NEN-EN 13201-1—Road lighting – Part 1: Selection of lighting classes*.

NEN 13201-2. (2016). *NEN-EN 13201-2—Road lighting—Part 2: Performance requirements*.

NEN 13201-3. (2016). *NEN-EN 13201-3—Road lighting—Part 3: Calculation of performance*.

Osterhaus, W. K. E. (2005). Discomfort glare assessment and prevention for daylight applications in office environments. *Solar Energy*, *79*(2), 140–158. https://doi.org/10.1016/j.solener.2004.11.011

Owens, D. A., Sivak, M., Helmers, G., Sato, T., Battle, D., & Traube, E. C. (1992). *Effects of light transmittance and scatter by windshields on nighttime visual performance*. University of Michigan - Transportation Research Institute. https://deepblue.lib.umich.edu/bitstream/handle/2027.42/64071/83109.pdf?sequence=1

Persson, D. (1993). The Elderly Driver: Deciding When to Stop. *The Gerontologist*, *33*(1), 88–91. https://doi.org/10.1093/geront/33.1.88

Pierson, C., Wienold, J., & Bodart, M. (2017). Discomfort glare perception in daylighting: Influencing factors. *Energy Procedia*, *122*, 331–336. https://doi.org/10.1016/j.egypro.2017.07.332

Pierson, C., Wienold, J., & Bodart, M. (2018). Review of Factors Influencing Discomfort Glare Perception from Daylight. *LEUKOS*, *14*(3), 111–148. https://doi.org/10.1080/15502724.2018.1428617

Rijkswaterstaat. (2021). *Actuele verkeersongevallencijfers*. https://www.rijkswaterstaat.nl/wegen/wegbeheer/onderzoek/verkeersveiligheid-en-ongevallencijfers/actuele-verkeersongevallencijfers#cijfers-cbs

Rijkswaterstaat. (2022). *Over ons—Onze organisatie*. https://www.rijkswaterstaat.nl/over-ons/onze-organisatie#:~:text=We%20willen%20leven%20in%20een,zoals%20economie%2C%20milieu%20en%20woongenot.

RIT. (n.d.). *Forced Choice and miscellaneous consideration*. https://www.cis.rit.edu/people/faculty/montag/vandplite/pages/chap_4/ch4p5.html

RIVM. (2019). *Infographic Impact van de vergrijzing*. https://www.rivm.nl/infographic-impact-van-vergrijzing#:~:text=De%20vergrijzing%20heeft%20grote%20impact%20op%20de%20volksgezondheid%20en%20de,zelfstandig%20en%20vaak%20ook%20alleen.

Rozema, J. J., Van den Berg, T. J. T. P., & Tassignon, M.-J. (2010). Retinal Straylight as a Function of Age and Ocular Biometry in Healthy Eyes. *Investigative Opthalmology & Visual Science*, *51*(5), 2795. https://doi.org/10.1167/iovs.09-4056

Schütt, H. H., Harmeling, S., Macke, J. H., & Wichmann, F. A. (2016). Painfree and accurate Bayesian estimation of psychometric functions for (potentially) overdispersed data. *Vision Research*, *122*, 105–123. https://doi.org/10.1016/j.visres.2016.02.002

Sciubba, J. D. (2020). Population Aging as a Global Issue. In J. D. Sciubba, *Oxford Research Encyclopedia of International Studies*. Oxford University Press. https://doi.org/10.1093/acrefore/9780190846626.013.559

Shahid, A., Wilkinson, K., Marcu, S., & Shapiro, C. M. (2011). Karolinska Sleepiness Scale (KSS). In A. Shahid, K. Wilkinson, S. Marcu, & C. M. Shapiro (Eds.), *STOP, THAT and One Hundred Other Sleep Scales* (pp. 209–210). Springer New York. https://doi.org/10.1007/978-1-4419-9893-4_47

Spieringhs, R. M., Smet, K., Heynderickx, I., & Hanselaer, P. (2021). Road Marking Contrast Threshold Revisited. *LEUKOS*, 1–20. https://doi.org/10.1080/15502724.2021.1993893

Stevens, S. S. (1960). The pyschophysics of sensory function. *American Scientist*, *48*(2), 226–253.

SWOV. (2022). *Verkeersdoden in Nederland*. SWOV-factsheets.

Tadmor, Y., & Tolhurst, D. J. (2000). Calculating the contrasts that retinal ganglion cells and LGN neurones encounter in natural scenes. *Vision Research*, *40*(22), 3145–3157. https://doi.org/10.1016/S0042-6989(00)00166-8

TNO. (n.d.). *Defensiekrant 24—Landolt C Gezichtsscheprtekaart*.

van Bommel, W. (2015). *Road Lighting*. Springer International Publishing. https://doi.org/10.1007/978-3-319-11466-8

van den Berg, T. J. T. P., Franssen, L., & Coppens, J. E. (2010). Ocular Media Clarity and Straylight. In *Encyclopedia of the Eye* (pp. 173–183). Elsevier. https://doi.org/10.1016/B978-0-12-374203-2.00230-X

van den Berg, T. J. T. P., IJspeert, J. K., & de Waard, P. W. T. (1991). Dependence of intraocular straylight on pigmentation and light transmission through the ocular wall. *Vision Research*, *31*(7/8), 1361–1367. https://doi.org/10.1016/0042-6989(91)90057-c

van den Berg, T. J. T. P., van Rijn, L. J., Kaper-Bongers, R., Vonhoff, D. J., Völker-Dieben, H. J., Grabner, G., Nischler, C., Emesz, M., Wilhelm, H., & Gamer, D. (2009). Disability Glare in the Aging Eye. Assessment and Impact on Driving. *Journal of Optometry*, *2*(3), 112–118. https://doi.org/10.3921/joptom.2009.112

van den Berg, T. J. T. P., van Rijn, L. J. (René), Michael, R., Heine, C., Coeckelbergh, T., Nischler, C., Wilhelm, H., Grabner, G., Emesz, M., Barraquer, R. I., Coppens, J. E., & Franssen, L. (2007). Straylight Effects with Aging and Lens Extraction. *American Journal of Ophthalmology*, *144*(3), 358-363.e1. https://doi.org/10.1016/j.ajo.2007.05.037

Vesters, M. A. C. (2022). *Applicability of Contrast Perception Models to Elderly Vision in a Driving Scenario*. Eindhoven University of Technology.

Vissenberg, M. C. J. M., Perz, M., Donners, M. A. H., & Sekulovski, D. (2021). A generic glare sensation model based on the human visual system. *Proceedings of the Conference CIE 2021*, 203–212. https://doi.org/10.25039/x48.2021.OP23

Vos, J. J., & van den Berg, T. J. T. P. (1999). Report on disability glare. *CIE Collection*, *135*, 1–9.

Wandell, B. A. (1995). The Retinal Representation. In *Foundations of Vision*. Oxford University Press. https://foundationsofvision.stanford.edu/chapter-5-the-retinal-representation/

Watson, A. B. (2017). QUEST+: A general multidimensional Bayesian adaptive psychometric method. *Journal of Vision*, *17*(3), 1–27.

Watson, A. B., & Pelli, D. G. (1983). Quest: A Bayesian adaptive psychometric method. *Perception & Psychophysics*, *33*(2), 113–120. https://doi.org/10.3758/BF03202828

WHO. (2010). *Ageing: Global population*. https://www.who.int/news-room/questions-and-answers/item/population-ageing#:~:text=Why%20is%20the%20population%20ageing,people%20who%20are%20over%2060.

WHO. (2019). *World report on vision*. World Health Organization. https://www.who.int/publications/i/item/9789241516570

WHO. (2021). *Ageing and health*. https://www.who.int/news-room/fact-sheets/detail/ageing-and-health

WHO. (2022a). *Data portal: All-cause mortality rate in older people (per 100 000 population)*. https://platform.who.int/data/maternal-newborn-child-adolescent-ageing/indicator-explorer-new/mca/all-cause-mortality-rate-in-older-people-(per-100-000-population)

WHO. (2022b). *Data portal: Life expectancy at age 60*. https://platform.who.int/data/maternal-newborn-child-adolescent-ageing/indicator-explorer-new/mca/life-expectancy-at-age-60

WHO. (2022c). *Data portal: Percentage of total population aged 60 years or over*. https://platform.who.int/data/maternal-newborn-child-adolescent-ageing/indicator-explorer-new/mca/percentage-of-total-population-aged-60-years-or-over

Appendices

Appendix A: Matlab code

A1: Running the experiment

```
clear
addpath('C:\Users\X');
callstr = ['set(gcbf,"Userdata",double(get(gcbf,"Currentcharacter"))) ; uiresume '] ;
ud.Hf = figure('keypressfcn',callstr,'Name','test','Menu','none','Toolbar','none','Position',[1981 1 3840 2160]);%0 0
1900 1080,'Position',[1537 1 1536 864] 1981 1 3840 2160
ud.HaL = axes('Units','pixels',...
    'Position',[1 1 3840 2160],'XTick',[],'YTick',[]);%0 0 1900 1080 %1 1 3840 2160

WindowAPI(ud.Hf, 'Button', 'off');
WindowAPI(ud.Hf, 'position', 'full')
WindowAPI(ud.Hf, 'Clip', true);
box off

%% Read in images and determine pixel areas
%central
ud.myim_R = imread('Project4_Scene_12.png');
ud.myim_R_B = ud.myim_R;
ud.myim = ud.myim_R;

%background
ud.backgroundpix_R(:,:,1) = ud.myim_R(:,:,1) == 167 & ud.myim_R(:,:,2) == 167 & ud.myim_R(:,:,3) == 167;
ud.backgroundpix_R(:,:,2) = ud.myim_R(:,:,1) == 167 & ud.myim_R(:,:,2) == 167 & ud.myim_R(:,:,3) == 167;
ud.backgroundpix_R(:,:,3) = ud.myim_R(:,:,1) == 167 & ud.myim_R(:,:,2) == 167 & ud.myim_R(:,:,3) == 167;

%long curb left
ud.myim_R_LL = imread('Project4_R_LL_2.png');
ud.curbpix_R_LL = ud.myim_R_LL <=138;

%long curb right
ud.myim_R_LR = imread('Project4_R_LR_2.png');
ud.curbpix_R_LR = ud.myim_R_LR <=138;

%middle curb
ud.myim_R_M = imread('Project4_R_M_2.png');
ud.curbpix_R_M = ud.myim_R_M <=138;

%road
ud.myim_R_R = imread('Project4_R_R_2.png');
ud.roadpix_R = ud.myim_R_R <=138;
ud.roadpix_R_1 = ud.roadpix_R - ud.curbpix_R_LL;
ud.roadpix_R_2 = ud.roadpix_R_1 - ud.curbpix_R_LR;
ud.roadpix_R_3 = ud.roadpix_R_2 - ud.curbpix_R_M;
ud.roadpix_R_4 = logical(ud.roadpix_R_3);

ud_all = ud.backgroundpix_R + ud.curbpix_R_LL + ud.curbpix_R_LR + ud.curbpix_R_M + ud.roadpix_R_4;
ud_missing = ud_all == 0;

%all curb
ud.curbpix_R_all = ud.curbpix_R_M + ud.curbpix_R_LL + ud.curbpix_R_LR;
```

```
ud.curbpix_R_all_1 = logical(ud.curbpix_R_all);

%road markings pointing left or right at different distances
ud.curbpix6_1 =  imread('Project4_R_La_40m_2.png');
ud.curbpix6 =  ud.curbpix6_1<=138;

ud.curbpix7_1 =  imread('Project4_R_La_60m_2.png');
ud.curbpix7 =  ud.curbpix7_1<=138;

ud.curbpix8_1 =  imread('Project4_R_La_80m_2.png');
ud.curbpix8 =  ud.curbpix8_1<=138;

ud.curbpix9_1 =  imread('Project4_R_La_100m_2.png');
ud.curbpix9 =  ud.curbpix9_1<=138;

ud.curbpix10_1 =  imread('Project4_R_Ra_40m_2.png');
ud.curbpix10 =  ud.curbpix10_1<=138;

ud.curbpix11_1 =  imread('Project4_R_Ra_60m_2.png');
ud.curbpix11 =  ud.curbpix11_1<=138;

ud.curbpix12_1 =  imread('Project4_R_Ra_80m_2.png');
ud.curbpix12 =  ud.curbpix12_1<=138;

ud.curbpix13_1 =  imread('Project4_R_Ra_100m_2.png');
ud.curbpix13 =  ud.curbpix13_1<=138;

% ud.theend_1 = imread('theend.png');
% ud.theend = ud.theend_1 <=138;
%% set start parameters for road markings (not road arrow)
ud.myim(ud.roadpix_R_4) = 131;
ud.myim(ud.backgroundpix_R) = 0;
brightpix = ud.myim > 150;
ud.myim(brightpix) = 0;
ud.curbpix6_1(ud.curbpix6) = 162;
ud.curbpix6_1(ud.curbpix7) = 162;
ud.curbpix6_1(ud.curbpix8) = 162;
ud.curbpix6_1(ud.curbpix9) = 162;
ud.curbpix6_1(ud.curbpix10) = 162;
ud.curbpix6_1(ud.curbpix11) = 162;
ud.curbpix6_1(ud.curbpix12) = 162;
ud.curbpix6_1(ud.curbpix13) = 162;
ud.myim(ud.curbpix_R_all_1) = 162;
ud.myim_b = ud.myim;

% set gray image to equal RGB = 119
ud.myimgray = uint8(ones(2160, 3840, 3)*119);

% show gray image
imshow(ud.myimgray);

% input data before start experiment
ud.number= 'Participant number,';
ud.age= 'Age,';
ud.date= 'Date MMDDYY,';
ud.image= 'Image, ';
```

```
ud.PN=input(ud.number);
ud.Age=input(ud.age);
ud.Date=input(ud.date);

% determine conditions
road = [1 2 3]; %0.25 0.66 0.99 cd/m2
distance = [1 2 3]; %40 60 80 m
arrowD = [1 2]; %left / right
observTim = 3; %3 s


%% initialise quest (for each condition 3 road marking distances x 3 road surface luminance = 9)

F1 = @(x,mu1_1,sigma_1_1,gamma,lambda)gamma+(1 - gamma - lambda).*normcdf(x,mu1_1,sigma_1_1);
F2 = @(x,mu1_2,sigma_1_2,gamma,lambda)gamma+(1 - gamma - lambda).*normcdf(x,mu1_2,sigma_1_2);
F3 = @(x,mu1_3,sigma_1_3,gamma,lambda)gamma+(1 - gamma - lambda).*normcdf(x,mu1_3,sigma_1_3);
F4 = @(x,mu2_1,sigma_2_1,gamma,lambda)gamma+(1 - gamma - lambda).*normcdf(x,mu2_1,sigma_2_1);
F5 = @(x,mu2_2,sigma_2_2,gamma,lambda)gamma+(1 - gamma - lambda).*normcdf(x,mu2_2,sigma_2_2);
F6 = @(x,mu2_3,sigma_2_3,gamma,lambda)gamma+(1 - gamma - lambda).*normcdf(x,mu2_3,sigma_2_3);
F7 = @(x,mu3_1,sigma_3_1,gamma,lambda)gamma+(1 - gamma - lambda).*normcdf(x,mu3_1,sigma_3_1);
F8 = @(x,mu3_2,sigma_3_2,gamma,lambda)gamma+(1 - gamma - lambda).*normcdf(x,mu3_2,sigma_3_2);
F9 = @(x,mu3_3,sigma_3_3,gamma,lambda)gamma+(1 - gamma - lambda).*normcdf(x,mu3_3,sigma_3_3);

%determine stimulus and parameter domain for each road surface luminance
%mu1 = linspace(116, 130, 20);%0.0228 (0.2728; age:65 20.3)   0.3313 (0.5813; age: 80 5.5) range of possible
values for threshold
mu1_1 = linspace(116, 124, 20); %for every distance a new mu
mu1_2 = linspace(116, 124, 20);
mu1_3 = linspace(116, 124, 20);

%mu2 = linspace(131, 145, 20);%0.0407 (0.7007; age:65 20.3)   0.5679 (1.2279; age: 80 5.5)
mu2_1 = linspace(131, 139, 20); %for every distance a new mu
mu2_2 = linspace(131, 139, 20);
mu2_3 = linspace(131, 139, 20);

%mu3 = linspace(139, 152, 20);%0.0542 (1.0442; age:65 20.3)   0.7095 (1.6995; age: 80 5.5)
mu3_1 = linspace(139, 147, 20);
mu3_2 = linspace(139, 147, 20);
mu3_3 = linspace(139, 147, 20);

%sigma_1 = linspace(0.0770, (0.0770*1.5), 3); %sensitivity of the observer . Slope of curve
sigma_1_1 = 1 ./ (sqrt(2*pi)) * linspace(0.0355, (0.0355*1.5), 3);
sigma_1_2 = 1 ./ (sqrt(2*pi)) * linspace(0.0392, (0.0392*1.5), 3);
sigma_1_3 = 1 ./ (sqrt(2*pi)) * linspace(0.0804, (0.0804*1.5), 3);

%sigma_2 = linspace(0.0845, (0.0845*1.5), 3);
sigma_2_1 = 1 ./ (sqrt(2*pi)) * linspace(0.0739, (0.0739*1.5), 3);
sigma_2_2 = 1 ./ (sqrt(2*pi)) * linspace(0.0817, (0.0817*1.5), 3);
sigma_2_3 = 1 ./ (sqrt(2*pi)) * linspace(0.1639, (0.1639*1.5), 3);

%sigma_3 = linspace(0.1287, (0.1287*1.5), 3);
sigma_3_1 = 1 ./ (sqrt(2*pi)) * linspace(0.1215, (0.1215*1.5), 3);
sigma_3_2 = 1 ./ (sqrt(2*pi)) * linspace(0.1327, (0.1327*1.5), 3);
sigma_3_3 = 1 ./ (sqrt(2*pi)) * linspace(0.1418, (0.1418*1.5), 3);
```

```
gamma = 0.5; % 2 choices so fixed at 0.5
lambda = 0.02; %incorrect responses to seen stimuli, due to inattention or response errors.

paramDomain1_1 = {mu1_1, sigma_1_1, gamma, lambda};
paramDomain1_2 = {mu1_2, sigma_1_2, gamma, lambda};
paramDomain1_3 = {mu1_3, sigma_1_3, gamma, lambda};
paramDomain2_1 = {mu2_1, sigma_2_1, gamma, lambda};
paramDomain2_2 = {mu2_2, sigma_2_2, gamma, lambda};
paramDomain2_3 = {mu2_3, sigma_2_3, gamma, lambda};
paramDomain3_1 = {mu3_1, sigma_3_1, gamma, lambda};
paramDomain3_2 = {mu3_2, sigma_3_2, gamma, lambda};
paramDomain3_3 = {mu3_3, sigma_3_3, gamma, lambda};

stimDomain1 = 115:1:255;
stimDomain2 = 130:1:255;
stimDomain3 = 138:1:255;

respDomain =[0 1];

stopRule = 'entropy';
stopCriterion = 3; %2
% QP1, background luminance 0.25 cd/m2 and distance 40 m
QP1 = QuestPlus(F1, stimDomain1, paramDomain1_1, respDomain, stopRule, stopCriterion,0,200);%510
QP1.initialise();
% QP2, background luminance 0.25 cd/m2 and distance 60 m
QP2 = QuestPlus(F2, stimDomain1, paramDomain1_2, respDomain, stopRule, stopCriterion,0,200);
QP2.initialise();
% QP3, background luminance 0.25 cd/m2 and distance 80 m
QP3 = QuestPlus(F3, stimDomain1, paramDomain1_3, respDomain, stopRule, stopCriterion,0,200);
QP3.initialise();
% QP4, background luminance 0.66 cd/m2 and distance 40 m
QP4 = QuestPlus(F4, stimDomain2, paramDomain2_1, respDomain, stopRule, stopCriterion,0,200);
QP4.initialise();
% QP5, background luminance 0.66 cd/m2 and distance 60 m
QP5 = QuestPlus(F5, stimDomain2, paramDomain2_2, respDomain, stopRule, stopCriterion,0,200);
QP5.initialise();
% QP6, background luminance 0.66 cd/m2 and distance 80 m
QP6 = QuestPlus(F6, stimDomain2, paramDomain2_3, respDomain, stopRule, stopCriterion,0,200);
QP6.initialise();
% QP7, background luminance 0.99 cd/m2 and distance 40 m
QP7 = QuestPlus(F7, stimDomain3, paramDomain3_1, respDomain, stopRule, stopCriterion,0,200);
QP7.initialise();
% QP8, background luminance 0.99 cd/m2 and distance 60 m
QP8 = QuestPlus(F8, stimDomain3, paramDomain3_2, respDomain, stopRule, stopCriterion,0,200);
QP8.initialise();
% QP9, background luminance 0.99 cd/m2 and distance 80 m
QP9 = QuestPlus(F9, stimDomain3, paramDomain3_3, respDomain, stopRule, stopCriterion,0,200);
QP9.initialise();

stoppingCrit = 1;

%% run experiment
pause(10)
while ~QP1.isFinished() ||  ~QP2.isFinished() || ~QP3.isFinished() || ~QP4.isFinished() || ~QP5.isFinished() ||
~QP6.isFinished() || ~QP7.isFinished() || ~QP8.isFinished() || ~QP9.isFinished()
```

```
RandBack = [1 2 3];
RandDist = [1 2 3];

if QP1.isFinished() && QP2.isFinished() && QP3.isFinished()
   RandBack = RandBack(RandBack ~= 1);
end

if QP4.isFinished() && QP5.isFinished() && QP6.isFinished()
    RandBack = RandBack(RandBack ~= 2);
end

if QP7.isFinished() && QP8.isFinished() && QP9.isFinished()
    RandBack = RandBack(RandBack ~= 3);
end

if QP1.isFinished() && QP4.isFinished() && QP7.isFinished()
   RandDist = RandDist(RandDist ~= 1);
end

if QP2.isFinished() && QP5.isFinished() && QP8.isFinished()
    RandDist = RandDist(RandDist ~= 2);
end

if QP3.isFinished() && QP6.isFinished() && QP9.isFinished()
    RandDist = RandDist(RandDist ~= 3);
end

Lback = RandBack(randperm(length(RandBack),1));
randDist = RandDist(randperm(length(RandDist),1));

%Lback = randi(3); % get random value between 1 and 3
% set background luminance
switch Lback
   case 1
      ud.myim(ud.roadpix_R_4) = 116;
   case 2
      ud.myim(ud.roadpix_R_4) = 131;
   case 3
      ud.myim(ud.roadpix_R_4) = 139;
end

% randDist = randi(3); % get random value between 1 and 3
randDir = randi(2); % get random value between 1 and 2
% get value from the quest method and then set stimulus value (set luminance of the arrow)
switch Lback
   case 1 %0.25 cd/m2
      switch randDist
         case 1 %40 m
            targ = QP1.getTargetStim();
            if targ < 116
               targ = 116;
            end
            switch randDir
               case 1 %links
                  ud.myim(ud.curbpix6) = targ;
               case 2 %rechts
```

```
                ud.myim(ud.curbpix10) = targ;
            end
        case 2 %60 m
            targ = QP2.getTargetStim();
            if targ < 116
                targ = 116;
            end
            switch randDir
                case 1
                    ud.myim(ud.curbpix7) = targ;
                case 2
                    ud.myim(ud.curbpix11) = targ;
            end
        case 3 %80 m
            targ = QP3.getTargetStim();
            if targ < 116
                targ = 116;
            end
            switch randDir
                case 1
                    ud.myim(ud.curbpix8) = targ;
                case 2
                    ud.myim(ud.curbpix12) = targ;
            end
    end
case 2 %0.66 cd/m2
    switch randDist
        case 1 %40 m
            targ = QP4.getTargetStim();
            if targ < 131
                targ = 131;
            end
            switch randDir
                case 1 %links
                    ud.myim(ud.curbpix6) = targ;
                case 2 %rechts
                    ud.myim(ud.curbpix10) = targ;
            end
        case 2 %60 m
            targ = QP5.getTargetStim();
            if targ < 131
                targ = 131;
            end
            switch randDir
                case 1
                    ud.myim(ud.curbpix7) = targ;
                case 2
                    ud.myim(ud.curbpix11) = targ;
            end
        case 3 %80 m
            targ = QP6.getTargetStim();
            if targ < 131
                targ = 131;
            end
            switch randDir
                case 1
```

```
                ud.myim(ud.curbpix8) = targ;
            case 2
                ud.myim(ud.curbpix12) = targ;
        end
    end
case 3 %0.99 cd/m2
    switch randDist
        case 1 %40 m
            targ = QP7.getTargetStim();
            if targ < 139
                targ = 139;
            end
            switch randDir
                case 1 %links
                    ud.myim(ud.curbpix6) = targ;
                case 2 %rechts
                    ud.myim(ud.curbpix10) = targ;
            end
        case 2 %60 m
            targ = QP8.getTargetStim();
            if targ < 139
                targ = 139;
            end
            switch randDir
                case 1
                    ud.myim(ud.curbpix7) = targ;
                case 2
                    ud.myim(ud.curbpix11) = targ;
            end
        case 3 %80 m
            targ = QP9.getTargetStim();
            if targ < 139
                targ = 139;
            end
            switch randDir
                case 1
                    ud.myim(ud.curbpix8) = targ;
                case 2
                    ud.myim(ud.curbpix12) = targ;
            end
    end
end

% update image
imshow(ud.myim);
ch = 0;
elapsedTime = 0;
set(ud.Hf,'Userdata',[])
% get response
try
    tNow = clock;
    beep
    % wait until left/right key is pressed or until 2 seconds passed
    while ch ~= 28 && ch ~= 29 && elapsedTime <= observTim
        pause(0.001)
        ch = get(ud.Hf,'Userdata') ;
```

```
        elapsedTime = etime(clock,tNow);
        if isempty(ch)
            ch = 200 ; % in case of no answer we give them ch = 200
        end
    end
catch
    % Something went wrong, return and empty matrix.
    ch = NaN;
end

% set answer correct (arrow left + answer left = 1; arrow right +
% answer right = 1; else 0);.
if randDir == 1 && ch == 28 || randDir == 2 && ch == 29
    anscorrect =1;
else
    if ch == 200
    guess = randi(2);
    switch guess
        case 1
            anscorrect =0;
        case 2
            anscorrect = 1;
    end
    else
            anscorrect =0;
    end
end

% update the quest function for corresponding initialisation with
% whether the answer to the stimulus value was correct
switch Lback
    case 1 %0.25 cd/m2
        switch randDist
            case 1 %40 m
                QP1.update(targ, anscorrect);
            case 2 %60 m
                QP2.update(targ, anscorrect);
            case 3 %80 m
                QP3.update(targ, anscorrect);
        end
    case 2 %0.66 cd/m2
        switch randDist
            case 1 %40 m
                QP4.update(targ, anscorrect);
            case 2 %60 m
                QP5.update(targ, anscorrect);
            case 3 %80 m
                QP6.update(targ, anscorrect);
        end
    case 3 %0.99 cd/m2
        switch randDist
            case 1 %40 m
                QP7.update(targ, anscorrect);
            case 2 %60 m
                QP8.update(targ, anscorrect);
            case 3 %80 m
```

```
            QP9.update(targ, anscorrect);
        end
    end

% store data | participant number, age, date of experiment, luminance
    % background, distance arrow, direction arrow, luminance target, choice
    % participant, correct (yes/no)
    stoppingCrit = stoppingCrit+1;
    data = [ud.PN, ud.Age, ud.Date,Lback,randDist,randDir,targ, ch,anscorrect,elapsedTime ];
    dlmwrite('ExperimentDataRAW.csv',data,'-append');
    ch
    ud.myim = ud.myim_b;
    % set back to gray image
    imshow(ud.myimgray);
    pause(2.5)
    if stoppingCrit > 150
        disp("end of experiment max trials")
        break
    end

end
%% analyse data and plot thresholds
% QP1, background luminance 0.25 cd/m2 and distance 40 m
endGuess_mean1 = QP1.getParamEsts('mean');
est_mu1_1 = endGuess_mean1(1); %free parameter % was estimated at 168. Could be done for other arrows by
changing QP...
est_signma = endGuess_mean1(2); %fixed at : 1
est_gamma = endGuess_mean1(3); %fixed at: 0.5
est_lambda = endGuess_mean1(4); %fixed at : 0.02
% QP2, background luminance 0.25 cd/m2 and distance 60 m
endGuess_mean2 = QP2.getParamEsts('mean');
est_mu1_2 = endGuess_mean2(1);
% QP3, background luminance 0.25 cd/m2 and distance 80 m
endGuess_mean3 = QP3.getParamEsts('mean');
est_mu1_3 = endGuess_mean3(1);
% QP4, background luminance 0.66 cd/m2 and distance 40 m
endGuess_mean4 = QP4.getParamEsts('mean');
est_mu2_1 = endGuess_mean4(1);
% QP5, background luminance 0.66 cd/m2 and distance 60 m
endGuess_mean5 = QP5.getParamEsts('mean');
est_mu2_2 = endGuess_mean5(1);
% QP6, background luminance 0.66 cd/m2 and distance 80 m
endGuess_mean6 = QP6.getParamEsts('mean');
est_mu2_3 = endGuess_mean6(1);
% QP7, background luminance 0.99 cd/m2 and distance 40 m
endGuess_mean7 = QP7.getParamEsts('mean');
est_mu3_1 = endGuess_mean7(1);
% QP8, background luminance 0.99 cd/m2 and distance 60 m
endGuess_mean8 = QP8.getParamEsts('mean');
est_mu3_2 = endGuess_mean8(1);
% QP9, background luminance 0.99 cd/m2 and distance 80 m
endGuess_mean9 = QP9.getParamEsts('mean');
est_mu3_3 = endGuess_mean9(1);

%endscreen
```

```
data2 = [ud.PN, ud.Age,
ud.Date,est_mu1_1,est_mu1_2,est_mu1_3,est_mu2_1,est_mu2_2,est_mu2_3,est_mu3_1,est_mu3_2,est_mu3_3, ];
dlmwrite('ExperimentDataThresholds.csv',data2,'-append');
disp("end of experiment")
%imshow(ud.theend);
```

A2: Calculating the luminance difference thresholds

```
clear
close all
addpath('C:\Users\XXX\');
addpath('C:\Users\XXX\');

filename = 'C:\Users\XXX';
M = readmatrix(filename);

%Replace the condition indicators for actual values to allow intuitive use
%of the code later on.
M(M(:,4)==1, 4) = 0.25;
M(M(:,4)==2, 4) = 0.66;
M(M(:,4)==3, 4) = 0.99;
M(M(:,5)==1, 5) = 40;
M(M(:,5)==2, 5) = 60;
M(M(:,5)==3, 5) = 80;

%Fix for some incorrectly coded responses.
M(isnan(M(:,1)),:) = [];
M(:,11)= zeros(length(M),1);
M(M(:,8)==28 & M(:,6)==1 | M(:,8)==29 & M(:,6)==2,11) = 1;

%Correction for participant 18, who sometimes used 31 where 29 was intended.
M(M(:,8)==28 & M(:,6)==1 | M(:,8)==31 & M(:,6)==2,11) = 1;

%Nonresponse trials: set value to 0.5
M(M(:,8) == 200, 11) = 0.5;



%%%%%%%%%%%%% OWN INPUT HERE %%%%%%%%%%%%%

lumLB = [0.25 0.66 0.99];
dist = [40 60 80];
participant = [18 19 20 21 22 23 24 25 26 27 28 29 30 31 32 34 35 36 181 191 201 211 221 231 241 251 261 271
281 291 301 311 321 341 351 361];

%%%%%%%%%%%%% OWN INPUT HERE %%%%%%%%%%%%%


%% Individual observers
if 1
   for l = 1:length(participant)
      for k = 1:3
         for j = 1:3

            %Conditions
            con1 = M(:,1) == participant(l);      %particpant number
            con2 = M(:,4) == lumLB(k);            %road luminance (0.25, 0.66, 0.99)
            con3 = M(:,5) == dist(j);             %arrow distance (40, 60, 80)


            %Save only the required rows as new dataet.
            all_con = con1 & con2 & con3;
```

```
D = M(all_con,:);

%Delete the unnessecary columns: we only need the luminance value, amount
%correct at this value, total trials at this value
D = D(:,[7 11]);
D;
%Now we only have the luminance value (in RGB), and the correct/incorrect


%Make the dataset ready for psignifit: level, #correct, #total
levels = unique(D(:,1));
counts = histc(D(:,1), levels);

nr_correct = [];

for i = 1:length(levels)
    corr_sum = sum(D(D(:,1)==levels(i),2));
    nr_correct = [nr_correct; corr_sum];
end

input_data = [levels, nr_correct, counts];


%Now the input_data can be used to create the psychometric
%curve.
%First: Convert RGB to luminance values
lum = f(double(input_data(:,1)));
input_data(:,1) = lum;
input_data


%Now we can use psignfit.
options = struct;
options.sigmoidName = 'norm';
options.expType     = '2AFC';

result = psignifit(input_data,options);
%plotPsych(result);
%print(['Result_29_' num2str(k) '_' num2str(j) '_' num2str(l)],'-dpng','-r600');

Threshold(k,j,l) = getThreshold(result,0.75)-lumLB(k);
ThresholdDwn(k,j,l) = result.conf_Intervals(1,1,1)-lumLB(k);
ThresholdUp(k,j,l) = result.conf_Intervals(1,2,1)-lumLB(k);

B1 = nr_correct./counts;
A1 = lum;
F1 = result.psiHandle(A1);
[R2 Rsq] = rsquared(repelem(A1, counts),repelem(B1,counts),repelem(F1,counts));
R2psychcurves(k,j,l) = R2;
R2psychcurves2(k,j,l) = Rsq;

%Add some more data from the raw dataset to the processed
%threshold data.
age(l) = unique(M(M(:,1)==participant(l),2));
```

```
            data = [participant(l), age(l), lumLB(k), dist(j), Threshold(k,j,l), ThresholdDwn(k,j,l), ThresholdUp(k,j,l),
R2psychcurves(k,j,l), R2psychcurves2(k,j,l)];
            dlmwrite('final_thresholds.csv',data,'-append');
        end
    end
  end
end
%% Average observer
if 0
  for k = 1:3
    for j = 1:3
      %Conditions
      con4 = M(:,4) == lumLB(k);    %road luminance (0.25, 0.66, 0.99)
      con5 = M(:,5) == dist(j);      %arrow distance (40, 60, 80)

      %Save only the required rows as new dataet.
      all_con = con4 & con5;
      D = M(all_con,:);

      %Delete the unnessecary columns: we only need the luminance value, amount
      %correct at this value, total trials at this value
      D = D(:,[7 11]);
      D;

      %Make the dataset ready for psignifit: level, #correct, #total
      levels = unique(D(:,1));
      counts = histc(D(:,1), levels);

      nr_correct = [];

      for i = 1:length(levels)
        corr_sum = sum(D(D(:,1)==levels(i),2));
        nr_correct = [nr_correct; corr_sum];
      end

      input_data = [levels, nr_correct, counts];

      %Now the input_data can be used to create the psychometric
      %curve.
      %First: Convert RGB to luminance values
      lum = f(double(input_data(:,1)));
      input_data(:,1) = lum;
      input_data

      %Now we can use psignfit.
      options = struct;
      options.fixedPars = NaN(5,1);
      options.fixedPars(3) = .01;
      options.sigmoidName = 'norm';
      options.expType     = '2AFC';

      result = psignifit(input_data,options);
      plotPsych(result);
      Threshold(k,j) = getThreshold(result,0.75)-lumLB(k);
      ThresholdDwn(k,j) = result.conf_Intervals(1,1,1)-lumLB(k);
      ThresholdUp(k,j) = result.conf_Intervals(1,2,1)-lumLB(k);
```

```
        data = [lumLB(k), dist(j), Threshold(k,j), ThresholdDwn(k,j), ThresholdUp(k,j)];
        dlmwrite('avg_observer.csv',data,'-append');
      end
    end
end


%%


function [R2 Rsq] = rsquared(A,B,f)
Bbar = mean(B);
SStot = sum((B - Bbar).^2);
SSreg = sum((f - Bbar).^2);
SSres = sum((B - f).^2);
R2 = 1 - SSres/SStot;
R = corrcoef(A,B);
Rsq = R(1,2).^2;
end

function y = f(x)   %RGB values to luminance values

%  Reference paper:
%  Spieringhs, R.M., Smet, K., Heynderickx, I., Hanselaer, P. 2021.
%  Road Marking Contrast Threshold Revisited. LEUKOS.
%
%   f(x) = p1*x^2 + p2*x + p3
%   Coefficients (with 95% confidence bounds):
%     p1 =   0.0006363  (0.0005671, 0.0007055)
%     p2 =     -0.1301  (-0.1484, -0.1119)
%     p3 =       6.782  (5.58, 7.983)

p1 =   0.0006363;
p2 =     -0.1301;
p3 =       6.782;
y = p1*x.^2 + p2.*x + p3;
end
```

A3: Applying Adrian's model

```
%Calculate threshold according to the Adrian (1989) model.
filename = 'C:\Users\XXX';
M = readmatrix(filename);

%Add row for arrow size (in arcminutes)
M(:, size(M,2)+1)= zeros(length(M),1);
M(M(:,4)==40, size(M,2)) = 20.3;
M(M(:,4)==60, size(M,2)) = 9.5;
M(M(:,4)==80, size(M,2)) = 5.5;

%Add row for glare angle (in degrees)
M(:, size(M,2)+1)= zeros(length(M),1);
M(M(:,4)==40, size(M,2)) = 22.39;
M(M(:,4)==60, size(M,2)) = 21.58;
M(M(:,4)==80, size(M,2)) = 21.48;

%Calculate different Adrian thresholds for each row:

for i = 1:length(M)
  threshAdNoGlare(i) = rms_contrastAdNoGlare(M(i,3), M(i,9), M(i,2), 3, 1);
     threshAdGlare(i) = rms_contrastAdGlare(M(i,3), M(i,9), M(i,2), 3, 1, 12.6, M(i,10));
        threshAdPSF(i) = rms_contrastAdPSF(M(i,3), M(i,9), M(i,2), 3, 1, 12.6, M(i,10), M(i,8));
end

%Export dataset to .csv
M(:, size(M,2)+1) = threshAdNoGlare;
M(:, size(M,2)+1) = threshAdGlare;
M(:, size(M,2)+1) = threshAdPSF;
writematrix(M,'data_with_adrian.csv')


%Original Adrian (1989) model WITHOUT glare
function [Lt, Cth] = rms_contrastAdNoGlare(Lb, Angle, Age, tobs, pos)
%Created by RMSpieringhs 18/12/19 based on the Adrian contrast model.
%Modified by TRC van Hoesel 7/11/22 to include presence of a glare
%source.
%Last updated 28/11/22.
%% Output (Cth, Lt):
%Cth contrast threshold
%Lt target luminance in cd/m2
%% Input (Lb, Angle, Age, tobs, pos):
%Lb in cd/m2 (Lb must be higher than 0.0042) Background luminance
%Angle of object in min
%Age in years (must be between 22 and 76)
%t in sec
%if pos = 1 positive contrast
%if pos = 0 negative contrast


try
%% check input
if Lb < 0.0042
   disp('Lb should not be negative and be higher than 0.0042')
else
```

```
end

if Age < 23 || Age > 75
   disp('age must be between 22 and 76')
else
end

%% calc AF
if Age <= 23
   AF = 1;
else
   if Age <= 64
      AF = (((Age-19)^2)/2160)+0.99;
   else
      AF = (((Age-56.6)^2)/116.3)+1.43;
   end
end

%% calc Tobs

g1 = log10(Angle)+0.523;
g = 0.36-(0.0972*((g1^2)/((g1^2)-2.513*g1+2.7895)));

h1 = log10(Lb)+6;
h = 0.355-(0.1217*((h1.^2)/((h1.^2)-10.4*h1+52.28)));

f = (((g^2)+(h^2))^0.5)/2.1;

Tobs = (f+tobs)/tobs;


%% calc Cth

if pos == 1

   Fcp = 1;
   if Lb < 0.6
      b = 10^(-0.072+0.3372*log10(Lb)+(0.0866*(log10(Lb)^2)));
      c = 10^(-1.256+0.319*log10(Lb));
   else
      b = log10(4.2841*(Lb^0.1556))+(0.1684*(Lb^0.5867));
      %4.2841 in this formula instead of the original 4.1925 from Adrian (1989).
      % See "van Bommel (2015). Road Lighting, Appendix B".

      c = 0.05946*(Lb^0.466);
   end

   Cth = (2.6/Lb)*(((b/Angle)+c)^2)*Fcp*AF*Tobs;

   Lt = Cth*Lb ;%+ Lb;

else

   Fcp = 1;
   if Lb < 0.6
      b = 10^(-0.072+0.3372*log10(Lb)+(0.0866*(log10(Lb)^2)));
```

```
        c = 10^(-1.256+0.319*log10(Lb));
    else
        b = log10(4.2841*(Lb^0.1556))+(0.1684*(Lb^0.5867));
        %4.2841 in this formula instead of the original 4.1925 from Adrian (1989).
        % See "van Bommel (2015). Road Lighting, Appendix B".

        c = 0.05946*(Lb^0.466);
    end

    Cth = (2.6/Lb)*(((b/Angle)+c)^2)*Fcp*AF*Tobs;

    if Lb < 0.1
    d = 10^(-10^(-1*(0.075*((log10(Lb)+1)^2)+0.0245)));
    else
    d = 10^(-10^(-1*(0.125*((log10(Lb)+1)^2)+0.0245)));
    end
    e = 0.6*(Lb^-0.1488);
    Fcp = 1 - ((d*(Angle^(-1*e)))/(2.4*Cth*Lb));

    Cth = (2.6/Lb)*(((b/Angle)+c)^2)*Fcp*AF*Tobs;

    Lt = Cth*Lb ;%+ Lb;

end
catch
   help rms_contrastAd
   return
end
end

%Original Adrian (1989) model WITH glare
function [Lt, Cth] = rms_contrastAdGlare(Lb, Angle, Age, tobs, pos, eyeillu, glareangle)
%Created by RMSpieringhs 18/12/19 based on the Adrian contrast model.
%Modified by TRC van Hoesel 7/11/22 to include presence of a glare
%source.
%Last updated 28/11/22.
%% Output (Cth, Lt):
%Cth contrast threshold
%Lt target luminance in cd/m2
%% Input (Lb, Angle, Age, tobs, pos):
%Lb in cd/m2 (Lb must be higher than 0.0042) Background luminance
%Angle of object in min
%Age in years (must be between 22 and 76)
%t in sec
%if pos = 1 positive contrast
%if pos = 0 negative contrast

%In presence of a glare source: use the following arguments
%eyeillu: illumination at the eye from the glare source (lx)
%glareangle: angle between center of the glare source and the fixation line, 20 degrees als ze naar oneindig kijken.
        %precies midden scherm: 20 degrees.
        %80m: 21.48, 60m: 21.85, 40m: 22.39
%If no glare source present, set both values to 0.
% [Lt, Cth] = rms_contrastAd(0.99, 20.3, 70, 3, 1, 12.6, 15)

try
```

```
%% check input
if Lb < 0.0042
   disp('Lb should not be negative and be higher than 0.0042')
else
end

if Age < 23 || Age > 75
   disp('age must be between 22 and 76')
else
end

%% add veiling luminance for disability glare
if eyeillu ~= 0 && glareangle ~= 0
   k = (0.0752 * Age - 1.883)^2 + 9.2;    %age-dependent constant
   Lseq = k * (eyeillu/(glareangle^2));   %veiling luminance
   Lb = Lb+Lseq;

   %eerst checken hoe deze het doet, hoe is de fit.
   %daarna kunnen we nog andere manieren van veiling luminances bekijken
   %en toeveogen.
end


%% calc AF
if Age <= 23
   AF = 1;
else
   if Age <= 64
      AF = (((Age-19)^2)/2160)+0.99;
   else
      AF = (((Age-56.6)^2)/116.3)+1.43;
   end
end

%% calc Tobs

g1 = log10(Angle)+0.523;
g = 0.36-(0.0972*((g1^2)/((g1^2)-2.513*g1+2.7895)));

h1 = log10(Lb)+6;
h = 0.355-(0.1217*((h1.^2)/((h1.^2)-10.4*h1+52.28)));

f = (((g^2)+(h^2))^0.5)/2.1;

Tobs = (f+tobs)/tobs;


%% calc Cth

if pos == 1

   Fcp = 1;
   if Lb < 0.6
      b = 10^(-0.072+0.3372*log10(Lb)+(0.0866*(log10(Lb)^2)));
      c = 10^(-1.256+0.319*log10(Lb));
   else
```

```
        b = log10(4.2841*(Lb^0.1556))+(0.1684*(Lb^0.5867));
        %4.2841 in this formula instead of the original 4.1925 from Adrian (1989).
        % See "van Bommel (2015). Road Lighting, Appendix B".

        c = 0.05946*(Lb^0.466);
    end

    Cth = (2.6/Lb)*(((b/Angle)+c)^2)*Fcp*AF*Tobs;

    Lt = Cth*Lb ;%+ Lb;

else

    Fcp = 1;
    if Lb < 0.6
        b = 10^(-0.072+0.3372*log10(Lb)+(0.0866*(log10(Lb)^2)));
        c = 10^(-1.256+0.319*log10(Lb));
    else
        b = log10(4.2841*(Lb^0.1556))+(0.1684*(Lb^0.5867));
        %4.2841 in this formula instead of the original 4.1925 from Adrian (1989).
        % See "van Bommel (2015). Road Lighting, Appendix B".

        c = 0.05946*(Lb^0.466);
    end

    Cth = (2.6/Lb)*(((b/Angle)+c)^2)*Fcp*AF*Tobs;

    if Lb < 0.1
    d = 10^(-10^(-1*(0.075*((log10(Lb)+1)^2)+0.0245)));
    else
    d = 10^(-10^(-1*(0.125*((log10(Lb)+1)^2)+0.0245)));
    end
    e = 0.6*(Lb^-0.1488);
    Fcp = 1 - ((d*(Angle^(-1*e)))/(2.4*Cth*Lb));

    Cth = (2.6/Lb)*(((b/Angle)+c)^2)*Fcp*AF*Tobs;

    Lt = Cth*Lb ;%+ Lb;

end
catch
   help rms_contrastAd
   return
end
end
```

A4: Applying the simple *DoG* model

```
clear;
%load('imageArrow.mat')
addpath('C:\Users\XXX');
filename = 'C:\Users\XXX.csv';
M = readmatrix(filename);
%L = a;   %loads arrow image, represented as 150x150 matrix

%% Reading in arrow images
% Read in images of arrows at different distances, resize it to 150x150
% reading in the RGB images of the arrows at three different distances (40, 60, 80 m)

sizePX = 186:335;
sizePX2 = 291:440;
    curbpix6_0 =  imread('Project4_R_La_40m_2.png');
    curbpix6_3 = curbpix6_0(850:1250,1590:2350,:);
    curbpix6_1 = curbpix6_3(sizePX,sizePX2,:);
    curbpix6 =  curbpix6_1<=138;
    curbpix6_2 = curbpix6_1>138;

    curbpix7_0 =  imread('Project4_R_La_60m_2.png');
    curbpix7_3 = curbpix7_0(850:1250,1590:2350,:);
    curbpix7_1 = curbpix7_3(sizePX,sizePX2,:);
    curbpix7 =  curbpix7_1<=138;
    curbpix7_2 = curbpix7_1>138;

    curbpix8_0 =  imread('Project4_R_La_80m_2.png');
    curbpix8_3 = curbpix8_0(850:1250,1590:2350,:);
    curbpix8_1 = curbpix8_3(sizePX,sizePX2,:);
    curbpix8 =  curbpix8_1<=138;
    curbpix8_2 = curbpix8_1>138;

    roadBack1 = 116;
    roadBack2 = 131;
    roadBack3 = 139;

    pixelscurb1 = curbpix6_1;
    idpixelscurb1 = curbpix6;   %Pixels corresponding to arrow
    idpixelback1 = curbpix6_2;  %Pixels corresponding to background

    pixelscurb2 = curbpix7_1;
    idpixelscurb2 = curbpix7;
    idpixelback2 = curbpix7_2;

    pixelscurb3 = curbpix8_1;
    idpixelscurb3 = curbpix8;
    idpixelback3 = curbpix8_2;


    o=5;   %Indicating column of measured thresholds
    p=1;
    data_final = [];
    Lv_data_final = [];

while p < length(M)
```

```
LT1 = M(p,o); % 0.25 cd/m2 20.3 arcmin
Lv1 = PSF(M(p,2), M(p,10), M(p,8), 12.6);  %Calculating the veiling luminance for this participant and condition
p=p+1;

LT2 = M(p,o); % 0.25 cd/m2 9.5 arcmin
Lv2 = PSF(M(p,2), M(p,10), M(p,8), 12.6);
p=p+1;

LT3 = M(p,o); % 0.25 cd/m2 5.5 arcmin
Lv3 = PSF(M(p,2), M(p,10), M(p,8), 12.6);
p=p+1;

LT4 = M(p,o); % 0.66 cd/m2 20.3 arcmin
Lv4 = PSF(M(p,2), M(p,10), M(p,8), 12.6);
p=p+1;

LT5 = M(p,o); % 0.66 cd/m2 9.5 arcmin
Lv5 = PSF(M(p,2), M(p,10), M(p,8), 12.6);
p=p+1;

LT6 = M(p,o); % 0.66 cd/m2 5.5 arcmin
Lv6 = PSF(M(p,2), M(p,10), M(p,8), 12.6);
p=p+1;

LT7 = M(p,o); % 0.99 cd/m2 20.3 arcmin
Lv7 = PSF(M(p,2), M(p,10), M(p,8), 12.6);
p=p+1;

LT8 = M(p,o); % 0.99 cd/m2 9.5 arcmin
Lv8 = PSF(M(p,2), M(p,10), M(p,8), 12.6);
p=p+1;

LT9 = M(p,o); % 0.99 cd/m2 5.5 arcmin
Lv9 = PSF(M(p,2), M(p,10), M(p,8), 12.6);
p=p+1;


%LT1 - LT9: the measured luminance thresholds of the participants
% + the corresponding Lv for each participant!
lummap1 = f(double(pixelscurb1));
lummap1(idpixelscurb1)= ( LT1) + f(116) + Lv1;  % + Lv1 adds the veiling luminance on the image
lummap1(idpixelback1)= f(116) + Lv1;            % + Lv1 adds the veiling luminance on the image
lummap1 = lummap1(:,:,1);

lummap2 = f(double(pixelscurb2));
lummap2(idpixelscurb2) = ( LT2) + f(116) + Lv2;
lummap2(idpixelback2)= f(116) + Lv2;
lummap2 = lummap2(:,:,1);

lummap3 = f(double(pixelscurb3));
lummap3(idpixelscurb3)= ( LT3) + f(116) + Lv3;
lummap3(idpixelback3)= f(116) + Lv3;
lummap3 = lummap3(:,:,1);

lummap4 = f(double(pixelscurb1));
lummap4(idpixelscurb1)= ( LT4) + f(131) + Lv4;
```

```
    lummap4(idpixelback1)= f(131) + Lv4;
    lummap4 = lummap4(:,:,1);

    lummap5 = f(double(pixelscurb2));
    lummap5(idpixelscurb2)= ( LT5) + f(131) + Lv5;
    lummap5(idpixelback2)= f(131) + Lv5;
    lummap5 = lummap5(:,:,1);

    lummap6 = f(double(pixelscurb3));
    lummap6(idpixelscurb3)= ( LT6) + f(131) + Lv6;
    lummap6(idpixelback3)= f(131) + Lv6;
    lummap6 = lummap6(:,:,1);

    lummap7 = f(double(pixelscurb1));
    lummap7(idpixelscurb1)= ( LT7) + f(139) + Lv7;
    lummap7(idpixelback1)= f(139) + Lv7;
    lummap7 = lummap7(:,:,1);

    lummap8 = f(double(pixelscurb2));
    lummap8(idpixelscurb2)= ( LT8) + f(139) + Lv8;
    lummap8(idpixelback2)= f(139) + Lv8;
    lummap8 = lummap8(:,:,1);

    lummap9 = f(double(pixelscurb3));
    lummap9(idpixelscurb3)= ( LT9) + f(139) + Lv9;
    lummap9(idpixelback3)= f(139) + Lv9;
    lummap9 = lummap9(:,:,1);
%%


rc = 1;   %Set radius of center and surround receptive fields.
rs = 2;
n = round(length(ceil(3*-rs):1:ceil(3*rs))/2);     %Define matrix size of receptive fields (13 by 13 in this case)
for i = ceil(3*-rs):1:ceil(3*rs)                  %Indicators that run from -6 to 6, in order to fill all cells of the matrix
    for j = ceil(3*-rs):1:ceil(3*rs)
        RFc2(n+i,n+j) = exp(-((i./abs(rc)).^2)-((j./abs(rc)).^2));
         %center is at n+i,n+i = 7+0,7+0 = 7,7. Then the indices are used
         %to nagivate around the matrix.
        RFc = round(RFc2,5);

        RFs2(n+i,n+j) = ((abs(rc)./abs(rs)).^2).*exp(-((i./abs(rs)).^2)-((j./abs(rs)).^2));   %the rc/rs factor at the start,
then similar to center field
        RFs = round(RFs2,5);
    end
end

RFs3 = RFs;
round(sum(RFc-RFs,'all'),5)    %Substract surround from center field, round to 5 decimals
if sum(RFc-RFs,'all') ~= 0     %Check if sum of all elements in the subtraction-matrix is 0
    RFs3(n-1,n) = RFs(n-1,n) +round(sum(RFc-RFs,'all')/4,5);    %Changes the four values around the central cell
(7,7), +0.0002 each.
    RFs3(n,n-1) = RFs(n,n-1) +round(sum(RFc-RFs,'all')/4,5);
    RFs3(n+1,n) = RFs(n+1,n) +round(sum(RFc-RFs,'all')/4,5);    %Now, the sum of all elements in the surround RF
matrix are 0
    RFs3(n,n+1) = RFs(n,n+1) +round(sum(RFc-RFs,'all')/4,5);
    RFs = round(RFs3,5);
```

```
   sum(RFc-RFs,'all')
end

kernel = round(RFc-RFs,5);

%[DoG, C1, C2, C3, RFcS, RFsS] = DoG_TT_opt(L,1,2);
DoG1=abs(convolve2(lummap1,kernel,'replicate'));%'same'));


%Plot with original image and DoG filtered image
%figure;
%subplot(1,2,1)  %Original image
%imagesc(lummap1)
%caxis manual
%caxis([0 1]);

%subplot(1,2,2)    %%DOG image
%imagesc(DoG1)
%caxis manual
%caxis([0 0.7]);
%colorbar;

DoGT1(1) = sum(DoG1,'all');      %Sum of all DoG values per pixel (150x150).

DoG2 = abs(convolve2(lummap2,kernel,'replicate'));
DoGT2 = sum(DoG2,'all');

DoG3 = abs(convolve2(lummap3,kernel,'replicate'));
DoGT3 = sum(DoG3,'all');

DoG4 = abs(convolve2(lummap4,kernel,'replicate'));
DoGT4 = sum(DoG4,'all');

DoG5 = abs(convolve2(lummap5,kernel,'replicate'));
DoGT5 = sum(DoG5,'all');

DoG6 = abs(convolve2(lummap6,kernel,'replicate'));
DoGT6 = sum(DoG6,'all');

DoG7 = abs(convolve2(lummap7,kernel,'replicate'));
DoGT7 = sum(DoG7,'all');

DoG8 = abs(convolve2(lummap8,kernel,'replicate'));
DoGT8 = sum(DoG8,'all');

DoG9 = abs(convolve2(lummap9,kernel,'replicate'));
DoGT9 = sum(DoG9,'all');

data = [DoGT1,DoGT2,DoGT3,DoGT4,DoGT5,DoGT6,DoGT7,DoGT8,DoGT9];
data_final = [data_final data];

Lv_data = [Lv1, Lv2, Lv3, Lv4, Lv5, Lv6, Lv7, Lv8, Lv9];
Lv_data_final = [Lv_data_final Lv_data];
%dlmwrite('TDoGModelNewTrial.csv',data,'-append','precision','%.3f');

end
```

```
M(:, size(M,2)+1) = data_final;
M(:, size(M,2)+1) = Lv_data_final;
writematrix(M,'data_with_simpleDoG.csv')


function Lv = PSF(Age, glareangle, pigfac, eyeillu)
   Lv = eyeillu * ((1-
(0.08*((Age/70)^4)))*(((9.2*(10^6))/((1+((glareangle/0.0046)^2))^1.5))+((1.5*(10^5))/((1+((glareangle/0.045)^2))^
1.5))) + (1+(1.6*((Age/70)^4)))*(((400)/((1+((glareangle/0.1)^2))) + (3*(10^-8)*(glareangle^2))) +
pigfac*((((1300)/((1+((glareangle/0.1)^2))^1.5))+((0.8)/((1+((glareangle/0.1)^2))^0.5))))) + 2.5*(10^-3)*pigfac);
end

function y = f(x)   %RGB values to luminance values
%  Reference paper:
%  Spieringhs, R.M., Smet, K., Heynderickx, I., Hanselaer, P. 2021.
%  Road Marking Contrast Threshold Revisited. LEUKOS.
%
%   f(x) = p1*x^2 + p2*x + p3
%   Coefficients (with 95% confidence bounds):
%     p1 =   0.0006363  (0.0005671, 0.0007055)
%     p2 =     -0.1301  (-0.1484, -0.1119)
%     p3 =       6.782  (5.58, 7.983)

p1 =   0.0006363;
p2 =     -0.1301;
p3 =       6.782;
y = p1*x.^2 + p2.*x + p3;
end

%--------------------------------------------------------------------------

function y = convolve2(x, m, shape, tol)
%CONVOLVE2 Two dimensional convolution.
%   Y = CONVOLVE2(X, M) performs the 2-D convolution of matrices X and
%   M. If [mx,nx] = size(X) and [mm,nm] = size(M), then size(Y) =
%   [mx+mm-1,nx+nm-1]. Values near the boundaries of the output array are
%   calculated as if X was surrounded by a border of zero values.
%
%   Y = CONVOLVE2(X, M, SHAPE) where SHAPE is a string returns a
%   subsection of the 2-D convolution with size specified by SHAPE:
%
%       'full'      - (default) returns the full 2-D convolution
%
%       'valid'     - returns only those parts of the convolution
%                     that can be computed without padding; size(Y) =
%                     [mx-mm+1,nx-nm+1] when size(X) > size(M)
%
%       'same'      - returns the central part of the convolution
%                     that is the same size as X using zero padding
%
%       'wrap' or
%       'circular'  - as for 'same' except that instead of using
%                     zero-padding the input X is taken to wrap round as
%                     on a toroid
%
```

```
%       'reflect' or
%       'symmetric' - as for 'same' except that instead of using
%                     zero-padding the input X is taken to be reflected at
%                     its boundaries
%
%       'replicate' - as for 'same' except that instead of using
%                     zero-padding the rows at the array boundary are
%                     replicated
%
%   CONVOLVE2 is fastest when mx > mm and nx > nm - i.e. the first
%   argument is the input and the second is the mask.
%
%   If the rank of the mask M is low, CONVOLVE2 will decompose it into a
%   sum of outer product masks, each of which is applied efficiently as
%   convolution with a row vector and a column vector, by calling CONV2.
%   The function will often be faster than CONV2 or FILTER2 (in some
%   cases much faster) and will produce the same results as CONV2 to
%   within a small tolerance.
%
%   Y = CONVOLVE2(... , TOL) where TOL is a number in the range 0.0 to
%   1.0 computes the convolution using a reduced-rank approximation to
%   M, provided this will speed up the computation. TOL limits the
%   relative sum-squared error in the effective mask; that is, if the
%   effective mask is E, the error is controlled such that
%
%       sum(sum( (M-E) .* (M-E) ))
%       -------------------------    <=  TOL
%           sum(sum( M .* M ))
%
%   See also CONV2, FILTER2, EXINDEX

% Copyright David Young, Feb 2002, revised Jan 2005, Jan 2009, Apr 2011,
% Feb 2014

% Deal with optional arguments
narginchk(2,4);
if nargin < 3
   shape = 'full';    % shape default as for CONV2
   tol = 0;
elseif nargin < 4
   if isnumeric(shape)
      tol = shape;
      shape = 'full';
   else
      tol = 0;
   end
end;

% Set up to do the wrap & reflect operations, not handled by conv2
if ismember(shape, {'wrap' 'circular' 'reflect' 'symmetric' 'replicate'})
   x = extendarr(x, m, shape);
   shape = 'valid';
end

% do the convolution itself
y = doconv(x, m, shape, tol);
```

```
end

%-------------------------------------------------------------------

function y = doconv(x, m, shape, tol)
% Carry out convolution
[mx, nx] = size(x);
[mm, nm] = size(m);

% If the mask is bigger than the input, or it is 1-D already,
% just let CONV2 handle it.
if mm > mx || nm > nx || mm == 1 || nm == 1
   y = conv2(x, m, shape);
else
   % Get svd of mask
   if mm < nm; m = m'; end        % svd(..,0) wants m > n
   [u,s,v] = svd(m, 0);
   s = diag(s);
   rank = trank(m, s, tol);
   if rank*(mm+nm) < mm*nm         % take advantage of low rank
      if mm < nm;  t = u; u = v; v = t; end  % reverse earlier transpose
      vp = v';
      % For some reason, CONV2(H,C,X) is very slow, so use the normal call
      y = conv2(conv2(x, u(:,1)*s(1), shape), vp(1,:), shape);
      for r = 2:rank
         y = y + conv2(conv2(x, u(:,r)*s(r), shape), vp(r,:), shape);
      end
   else
      if mm < nm; m = m'; end     % reverse earlier transpose
      y = conv2(x, m, shape);
   end
end
end

%-------------------------------------------------------------------

function r = trank(m, s, tol)
% Approximate rank function - returns rank of matrix that fits given
% matrix to within given relative rms error. Expects original matrix
% and vector of singular values.
if tol < 0 || tol > 1
   error('Tolerance must be in range 0 to 1');
end
if tol == 0            % return estimate of actual rank
   tol = length(m) * max(s) * eps;
   r = sum(s > tol);
else
   ss = s .* s;
   t = (1 - tol) * sum(ss);
   r = 0;
   sm = 0;
   while sm < t
      r = r + 1;
      sm = sm + ss(r);
   end
end
```

```
end

%---------------------------------------------------------------------

function y = extendarr(x, m, shape)
% Extend x so as to wrap around on both axes, sufficient to allow a
% "valid" convolution with m to return a result the same size as x.
% We assume mask origin near centre of mask for compatibility with
% "same" option.

[mx, nx] = size(x);
[mm, nm] = size(m);

mo = floor((1+mm)/2); no = floor((1+nm)/2);  % reflected mask origin
ml = mo-1;            nl = no-1;             % mask left/above origin
mr = mm-mo;           nr = nm-no;            % mask right/below origin

% deal with shape option terminology - was inconsistent with exindex
switch shape
   case 'wrap'
      shape = 'circular';
   case 'reflect'
      shape = 'symmetric';
end
y = exindex(x, 1-ml:mx+mr, 1-nl:nx+nr, shape);

end

function arr = exindex(arr, varargin)
%EXINDEX extended array indexing
%   ARROUT = EXINDEX(ARRIN, S1, S2, ...) indexes a virtual array made by
%   extending ARRIN with zeros in all directions, using subscripts S1, S2
%   etc.
%
%   ARROUT = EXINDEX(ARRIN, S1, R1, S2, R2, ...) extends ARRIN using rule
%   R1 on the first dimension, R2 on the second dimension etc.
%
%   ARROUT = EXINDEX(ARRIN, S1, S2, ..., R) extends ARRIN using rule R on
%   every dimension.
%
%   Subscripts
%   ----------
%
%   Broadly, if V is the virtual extended array, ARROUT = V(S1, S2, ...)
%
%   The elements of the subscript arguments S1, S2 etc must be integers.
%   They need not be positive and are not restricted in any way by the size
%   of ARRIN. Logical indexing and linear indexing are not supported.
%
%   There must be at least one subscript argument for each dimension of
%   ARRIN as reported by NDIMS, except that row and column vectors may have
%   1 or 2 subscripts. A single subscript is taken to refer to the
%   dimension along which the vector lies, as in normal vector indexing.
%   Scalars require 2 subscripts. If there are more subscripts than
%   dimensions, ARRIN is taken to have trailing singleton dimensions, as in
%   normal array indexing.
```

```
%
%   The number of dimensions of ARROUT will be the number of subscript
%   arguments, though trailing singleton dimensions will, as usual, be
%   suppressed. The size of ARROUT is given by the normal Matlab rules for
%   the result of indexing into ARRIN: that is
%
%       size(ARROUT) = size( ARRIN(ones(size(S1)), ones(size(S2)), ...) )
%
%   A subscript argument may be the string ':'. This behaves like a colon
%   in ordinary subscripting: a colon for the K'th subscript stands for
%   1:size(ARRIN, K). The 'end' keyword is not supported.
%
%   Rules
%   -----
%
%   Each rule may be one of the following:
%
%   A scalar cell: ARRIN is padded with elements equal to the contents of
%   the cell. The class of the cell contents must be compatible with the
%   class of ARRIN.
%
%       If different constants are used on different dimensions, padding is
%       done in the order of the subscripts. For example, a 2D array is
%       extended first in the row index direction and then in the column
%       index direction. For all other cases, the order in which dimensions
%       are extended has no effect.
%
%   'circular': ARRIN is extended with copies of itself; i.e. V is tiled
%   with ARRIN.
%
%   'symmetric': ARRIN is extended with copies of itself with reflection at
%   its boundaries; i.e. V is tiled with [ARRIN fliplr(ARRIN);
%   flipud(ARRIN) fliplr(flipud(ARRIN))].
%
%   'replicate': ARRIN is extended by copying its border elements; i.e. an
%   element of V is equal to the nearest element of ARRIN.
%
%   If no rule is given, padding is with zeros.
%
%   Examples
%   --------
%
%   Pad a 2D matrix with K extra rows and columns with reflection on both
%   axes:
%
%       b = exindex(a, 1-k:size(a,1)+k, 1-k:size(a,2)+k, 'symmetric');
%
%   Circularly shift a 2D matrix by R rows downwards and C columns
%   rightwards:
%
%       b = exindex(a, 1-r:size(a,1)-r, 1-c:size(a,2)-c, 'circular');
%
%   Force a row or column vector to be 1024 elements long, trimming or
%   padding with zeros as necessary:
%
%       u = exindex(v, 1:1024);
```

```
%
%   The same, with a non-zero padding value:
%
%       u = exindex(v, 1:1024, {-1});   % note constant in cell
%
%   Truncate or extend all the rows of a matrix to 1024 columns:
%
%       b = exindex(a, ':', 1:1024);
%
%   Extend a 2-D array into the third dimension by copying it:
%
%       b = exindex(a, ':', ':', 1:3, 'replicate');
%
%   Pad a 1-D cell array with cells containing the empty matrix:
%
%       cellout = exindex(cellin, 0:10, {{[]}});
%
%   See also: padarray, circshift, repmat

% Copyright David Young 2010

% Sort out arguments
[exindices, rules, nd, sz] = getinputs(arr, varargin{:});
consts = cellfun(@iscell, rules);  % Check for constants, as can be
constused = any(consts);           % more efficient if there are none

% Setup for constant padding
if constused
   tofill = cell(1, nd);
end

% Main loop over subscript arguments, transforming them into valid
% subscripts into arr using the rule for each dimension
if constused
   for i = 1:nd
      [exindices{i}, tofill{i}] = extend(exindices{i}, rules{i}, sz(i));
   end
else % no need for information for doing constants
   for i = 1:nd
      exindices{i} = extend(exindices{i}, rules{i}, sz(i));
   end
end

% Create the new array by indexing into arr. If there are no constants,
% this does the whole job
arr = arr(exindices{:});

% Fill areas that need constants
if constused
   % Get full range of output array indices
   ranges = arrayfun(@(x) {1:x}, size(arr));
   for i = nd:-1:1    % order matters
      if consts(i)
         ranges{i} = tofill{i};      % don't overwrite original
         c = rules{i};               % get constant and fill ...
         arr(ranges{:}) = c{1};      % we've checked c is scalar
```

```
            ranges{i} = ~tofill{i};     % don't overwrite
        end
    end
end

end

% ---------------------------------------------------------------------

function [exindices, rules, nd, sz] = getinputs(arr, varargin)
% Sort out and check arguments. Inputs are as given in the help comments
% for exindex. Outputs are cell arrays; each element of exindices is a
% set of integer extended indices which has been checked for validity; each
% element of rules is a rule which has not been checked for validity.

% Use index/rules arguments only to establish no. dimensions - ndims(arr)
% is no use, as trailing singleton dimensions truncated and vectors can be
% 2D or 1D
nd = length(varargin);
if nd == 0
    error('exindex:missingargs', 'Not enough arguments');
elseif nd == 1
    exindices = varargin;
    rules = {{0}};
elseif ~(isnumeric(varargin{2}) || strcmp(varargin{2}, ':'))
    % have alternating indices and rule
    nd = nd/2;
    if round(nd) ~= nd
        error('exindex:badnumargs', ...
            'Odd number of arguments after initial index/rule pair');
    end
    exindices = varargin(1:2:end);
    rules = varargin(2:2:end);
elseif nd > 2 && ~(isnumeric(varargin{end}) || strcmp(varargin{end}, ':'))
    % have a general rule at end
    nd = nd - 1;
    exindices = varargin(1:nd);
    [rules{1:nd}] = deal(varargin{end});
else
    % no rule is specified
    exindices = varargin;
    [rules{1:nd}] = deal({0});
end

% Sort out mismatch of apparent array size and number of dimensions
% indexed
sz = size(arr);
ndarr = ndims(arr);
if nd < ndarr
    if nd == 1 && ndarr == 2
        % Matlab allows vectors to be indexed with a single subscript and
        % to retain their shape. In all other cases (including scalars) a
        % single subscript causes the output to take the same shape as the
        % subscript array - we can't deal with this.
        if sz(1) == 1 && sz(2) > 1
            % have a row vector
```

```
            exindices = [{1} exindices {1}];
            rules = [rules rules];  % 1st rule doesn't matter
        elseif sz(2) == 1 && sz(1) > 1
            % have a column vector
            exindices = [exindices {1}];
            rules = [rules rules];  % 2nd rule doesn't matter
        else
            error('exindex:wantvector', ...
                'Only one index but array is not a vector');
        end
    else
        error('exindex:toofewindices', ...
            'Array has more dimensions than there are index arguments');
    end
    nd = 2;
elseif nd > ndarr
    % Effective array size
    sz = [sz ones(1, nd-ndarr)];
end

% Expand any colons now to simplify checking.
% It's tempting to allow the 'end' keyword here: easy to substitute the
% size of the dimension. However, to be worthwhile it would be necessary to
% use evalin('caller',...) so that expressions using end could be given as
% in normal indexing. This would mean moving the code up to exindex itself,
% and evalin makes for inefficiency and fragility, so this hasn't been
% done.
colons = strcmp(exindices, ':');
if any(colons)  % saves a little time
    exindices(colons) = arrayfun(@(x) {1:x}, sz(colons));
end

% Check the indices (rules are checked as required in extend)
checkindex = @(ind) validateattributes(ind, {'numeric'}, ...
    {'integer'}, 'exindex', 'index');
cellfun(checkindex, exindices);

end

% ------------------------------------------------------------------------

function [ind, tofill] = extend(ind, rule, s)
% The core function: maps extended array subscripts into valid input array
% subscripts.

if ischar(rule)    % pad with rule

    tofill = [];  % never used
    switch rule
        case 'replicate'
            ind = min( max(1,ind), s );
        case 'circular'
            ind = mod(ind-1, s) + 1;
        case 'symmetric'
            ind = mod(ind-1, 2*s) + 1;
            ott = ind > s;
```

```
            ind(ott) = 2*s + 1 - ind(ott);
        otherwise
            error('exindex:badopt', 'Unknown option');
    end

elseif iscell(rule) && isscalar(rule)     % pad with constant

    % The main messiness is due to constant padding. This can't be done
    % with indexing into the original array, but we want the indexing
    % structure to be preserved, so for now we index to element 1 on each
    % dimension, and record the indices of the regions that need to be
    % fixed.

    tofill = ind < 1 | ind > s;
    ind(tofill) = 1;

else

    error('exindex:badconst', 'Expecting string or scalar cell');

end

end
```

A5: Applying the complex *DoG* model

```
clear;
addpath('C:\Users\XXX');
filename = 'C:\XXX.csv';
M = readmatrix(filename);

% reading in the RGB images of the arrows at three different distances (40, 60, 80 m)
sizePX = 186:335;%161:360;%186:335;
sizePX2 = 291:440;%266:465;%291:440;
   curbpix6_0 =  imread('Project4_R_La_40m_2.png');
   curbpix6_3 = curbpix6_0(850:1250,1590:2350,:);
   curbpix6_1 = curbpix6_3(sizePX,sizePX2,:);
   curbpix6 =  curbpix6_1<=138;
   curbpix6_2 = curbpix6_1>138;

   curbpix7_0 =  imread('Project4_R_La_60m_2.png');
   curbpix7_3 = curbpix7_0(850:1250,1590:2350,:);
   curbpix7_1 = curbpix7_3(sizePX,sizePX2,:);
   curbpix7 =  curbpix7_1<=138;
   curbpix7_2 = curbpix7_1>138;

   curbpix8_0 =  imread('Project4_R_La_80m_2.png');
   curbpix8_3 = curbpix8_0(850:1250,1590:2350,:);
   curbpix8_1 = curbpix8_3(sizePX,sizePX2,:);
   curbpix8 =  curbpix8_1<=138;
   curbpix8_2 = curbpix8_1>138;

   roadBack1 = 116;
   roadBack2 = 131;
   roadBack3 = 139;

   pixelscurb1 = curbpix6_1;
   idpixelscurb1 = curbpix6;
   idpixelback1 = curbpix6_2;

   pixelscurb2 = curbpix7_1;
   idpixelscurb2 = curbpix7;
   idpixelback2 = curbpix7_2;

   pixelscurb3 = curbpix8_1;
   idpixelscurb3 = curbpix8;
   idpixelback3 = curbpix8_2;


   %LT = luminance thresholds
   o=5;   %Indicating column of measured thresholds
   p=1;
   data_final = [];

while p < length(M)
   LT1 = M(p,o); % 0.25 cd/m2 20.3 arcmin
   Lv1 = PSF(M(p,2), M(p,10), M(p,8), 12.6);
   p=p+1;
```

```
LT2 = M(p,o); % 0.25 cd/m2 9.5 arcmin
Lv2 = PSF(M(p,2), M(p,10), M(p,8), 12.6);
p=p+1;

LT3 = M(p,o); % 0.25 cd/m2 5.5 arcmin
Lv3 = PSF(M(p,2), M(p,10), M(p,8), 12.6);
p=p+1;

LT4 = M(p,o); % 0.66 cd/m2 20.3 arcmin
Lv4 = PSF(M(p,2), M(p,10), M(p,8), 12.6);
p=p+1;

LT5 = M(p,o); % 0.66 cd/m2 9.5 arcmin
Lv5 = PSF(M(p,2), M(p,10), M(p,8), 12.6);
p=p+1;

LT6 = M(p,o); % 0.66 cd/m2 5.5 arcmin
Lv6 = PSF(M(p,2), M(p,10), M(p,8), 12.6);
p=p+1;

LT7 = M(p,o); % 0.99 cd/m2 20.3 arcmin
Lv7 = PSF(M(p,2), M(p,10), M(p,8), 12.6);
p=p+1;

LT8 = M(p,o); % 0.99 cd/m2 9.5 arcmin
Lv8 = PSF(M(p,2), M(p,10), M(p,8), 12.6);
p=p+1;

LT9 = M(p,o); % 0.99 cd/m2 5.5 arcmin
Lv9 = PSF(M(p,2), M(p,10), M(p,8), 12.6);
p=p+1;

% Create luminance maps, with the RGP map as input.
lummap1 = f(double(pixelscurb1));
lummap1(idpixelscurb1)= ( LT1) + f(116) + Lv1;   % + Lv1 adds the veiling luminance on the image
lummap1(idpixelback1)= f(116) + Lv1;             % + Lv1 adds the veiling luminance on the image
lummap1 = lummap1(:,:,1);

lummap2 = f(double(pixelscurb2));
lummap2(idpixelscurb2) = ( LT2) + f(116) + Lv2;
lummap2(idpixelback2)= f(116) + Lv2;
lummap2 = lummap2(:,:,1);

lummap3 = f(double(pixelscurb3));
lummap3(idpixelscurb3)= ( LT3) + f(116) + Lv3;
lummap3(idpixelback3)= f(116) + Lv3;
lummap3 = lummap3(:,:,1);

lummap4 = f(double(pixelscurb1));
lummap4(idpixelscurb1)= ( LT4) + f(131) + Lv4;
lummap4(idpixelback1)= f(131) + Lv4;
lummap4 = lummap4(:,:,1);

lummap5 = f(double(pixelscurb2));
lummap5(idpixelscurb2)= ( LT5) + f(131) + Lv5;
lummap5(idpixelback2)= f(131) + Lv5;
```

```
lummap5 = lummap5(:,:,1);

lummap6 = f(double(pixelscurb3));
lummap6(idpixelscurb3)= ( LT6) + f(131) + Lv6;
lummap6(idpixelback3)= f(131) + Lv6;
lummap6 = lummap6(:,:,1);

lummap7 = f(double(pixelscurb1));
lummap7(idpixelscurb1)= ( LT7) + f(139) + Lv7;
lummap7(idpixelback1)= f(139) + Lv7;
lummap7 = lummap7(:,:,1);

lummap8 = f(double(pixelscurb2));
lummap8(idpixelscurb2)= ( LT8) + f(139) + Lv8;
lummap8(idpixelback2)= f(139) + Lv8;
lummap8 = lummap8(:,:,1);

lummap9 = f(double(pixelscurb3));
lummap9(idpixelscurb3)= ( LT9) + f(139) + Lv9;
lummap9(idpixelback3)= f(139) + Lv9;
lummap9 = lummap9(:,:,1);


I1 = RMS_Joulan(lummap1,3.8e-04,1.0776);
Jt1 = sum(I1,'all');
fprintf('Calculated 1/9 for case %d.\n',p);

I2 = RMS_Joulan(lummap2,3.8e-04,1.0776);
Jt2 = sum(I2,'all');
fprintf('Calculated 2/9 for case %d.\n',p);

I3 = RMS_Joulan(lummap3,3.8e-04,1.0776);
Jt3 = sum(I3,'all');
fprintf('Calculated 3/9 for case %d.\n',p);

I4 = RMS_Joulan(lummap4,3.8e-04,1.0776);
Jt4 = sum(I4,'all');
fprintf('Calculated 4/9 for case %d.\n',p);

I5 = RMS_Joulan(lummap5,3.8e-04,1.0776);
Jt5 = sum(I5,'all');
fprintf('Calculated 5/9 for case %d.\n',p);

I6 = RMS_Joulan(lummap6,3.8e-04,1.0776);
Jt6 = sum(I6,'all');
fprintf('Calculated 6/9 for case %d.\n',p);

I7 = RMS_Joulan(lummap7,3.8e-04,1.0776);
Jt7 = sum(I7,'all');
fprintf('Calculated 7/9 for case %d.\n',p);

I8 = RMS_Joulan(lummap8,3.8e-04,1.0776);
Jt8 = sum(I8,'all');
fprintf('Calculated 8/9 for case %d.\n',p);

I9 = RMS_Joulan(lummap9,3.8e-04,1.0776);
```

```
    Jt9 = sum(I9,'all');
    fprintf('Calculated 9/9 for case %d.\n',p);


    data = [Jt1, Jt2, Jt3, Jt4, Jt5, Jt6, Jt7, Jt8, Jt9];
    data_final = [data_final data];

end

M(:, size(M,2)+1) = data_final;
writematrix(M,'data_with_Joulan_with_veiling.csv')


function Lv = PSF(Age, glareangle, pigfac, eyeillu)
    Lv = eyeillu * ((1-
(0.08*((Age/70)^4)))*(((9.2*(10^6))/((1+((glareangle/0.0046)^2))^1.5))+((1.5*(10^5))/((1+((glareangle/0.045)^2))^
1.5))) + (1+(1.6*((Age/70)^4)))*(((400)/((1+((glareangle/0.1)^2))) + (3*(10^-8)*(glareangle^2))) +
pigfac*((((1300)/((1+((glareangle/0.1)^2))^1.5))+((0.8)/((1+((glareangle/0.1)^2))^0.5))))) + 2.5*(10^-3)*pigfac);
end

function y = f(x)   %RGB values to luminance values
%  Reference paper:
%  Spieringhs, R.M., Smet, K., Heynderickx, I., Hanselaer, P. 2021.
%  Road Marking Contrast Threshold Revisited. LEUKOS.
%
%   f(x) = p1*x^2 + p2*x + p3
%   Coefficients (with 95% confidence bounds):
%     p1 =   0.0006363  (0.0005671, 0.0007055)
%     p2 =     -0.1301  (-0.1484, -0.1119)
%     p3 =       6.782  (5.58, 7.983)

p1 =   0.0006363;
p2 =     -0.1301;
p3 =       6.782;
y = p1*x.^2 + p2.*x + p3;
end

function I2 = RMS_Joulan(L,px,Dist) %input: luminance map, pixel size, radius of center receptive field
% Reference papers and pattent:
% 1) Joulan K., Hautiere N., Bremond R. 2011.
%   Contrast sensitivity functions for road visibility estimation in digital images.
%   Proceedings of 27th CIE Session; 2011 July 10-15;
%
% 2) Joulan K., Hautiere N., Bremond R. 2011.
%    A unified CSF-based framework for edge detection and edge visibility.
%    Proceedings of the CVPR 2011 Workshops; 2011 June
%
% 3) Joulan K., Bremond R., Robert-Landry, C. 2012.
%    Method for determining the visibility of objects in a field of view of a
%    driver of a vehicle, taking into account a contrast sensitivity
%    function, driver assistance system, and motor vehicle.
%    (European Pattent 2 747 026).

%characteristics of the DoG Filters representing the human visual system
f = [2.9 7.7 1 0.4 1.5 0.1];   %spatial frequency (cpd)
```

```
sC = (1./f).*sqrt(log(3)/2);   %standard deviation of Gaussian center-field
sS = 3.*sC;                    %standard deviation of Gaussian surround-field

rc = Dist;                  %radius center receptive field
Lav=mean(mean(L));          %mean luminance on the map

WF = [392.20 169.26 134.46 45.83 22.98 17.21];  %weightings for the different DOGs

I1 = (1/Lav).*L;            %adaptation luminance = inverse of the mean luminance

%sigma (standard deviation of Gaussians) converted to pixels
sigmaS=sS.*pi./180.*rc./px;
sigmaC=sC.*pi./180.*rc./px;

for i = 1:6
SDOG(i,:,:)=KernelS(I1,sigmaS(i),sigmaC(i),WF(i));
end
I2 = sum(SDOG);
end

function [signalmap2,kernel] = KernelS(map,sigmaS,sigmaC,WF)
rs=2*(ceil((sigmaS*4+1)/2)-1)+1;
c=(rs+1)/2;
%Set limits (for the radius) of the Gaussian for the surround receptive
%field. The Gaussian has long tails, at which the value =~ 0. We dont want
%to have an influence of these almost-0 tails.

[x,y]=meshgrid(1:1:rs);

%normalized Gaussian for center receptive field
exponentS = ((c-x).^2)./(2*sigmaS^2) + ((c-y).^2)./(2*sigmaS^2);
gaussS =exp(-exponentS);
normS=sum(sum(gaussS));
gaussS=gaussS/normS;

%normalized Gaussian for surround receptive field
exponentC = ((c-x).^2)./(2*sigmaC^2) + ((c-y).^2)./(2*sigmaC^2);
gaussC =exp(-exponentC);
normC=sum(sum(gaussC));
gaussC=gaussC/normC;

kernel=WF.*(gaussC-gaussS)./max(max((gaussC-gaussS)));

map2=zeros(size(map)+2)+min(min(map));
map2(2:end-1,2:end-1)=map;
signalmap=single(convolve2(map2,kernel,'replicate'));
signalmap2=signalmap(2:end-1,2:end-1);
end

function y = convolve2(x, m, shape, tol)
%CONVOLVE2 Two dimensional convolution.
%   Y = CONVOLVE2(X, M) performs the 2-D convolution of matrices X and
%   M. If [mx,nx] = size(X) and [mm,nm] = size(M), then size(Y) =
%   [mx+mm-1,nx+nm-1]. Values near the boundaries of the output array are
%   calculated as if X was surrounded by a border of zero values.
%
```

```
%   Y = CONVOLVE2(X, M, SHAPE) where SHAPE is a string returns a
%   subsection of the 2-D convolution with size specified by SHAPE:
%
%     'full'      - (default) returns the full 2-D convolution
%
%     'valid'     - returns only those parts of the convolution
%                   that can be computed without padding; size(Y) =
%                   [mx-mm+1,nx-nm+1] when size(X) > size(M)
%
%     'same'      - returns the central part of the convolution
%                   that is the same size as X using zero padding
%
%     'wrap' or
%     'circular'  - as for 'same' except that instead of using
%                   zero-padding the input X is taken to wrap round as
%                   on a toroid
%
%     'reflect' or
%     'symmetric' - as for 'same' except that instead of using
%                   zero-padding the input X is taken to be reflected at
%                   its boundaries
%
%     'replicate' - as for 'same' except that instead of using
%                   zero-padding the rows at the array boundary are
%                   replicated
%
%   CONVOLVE2 is fastest when mx > mm and nx > nm - i.e. the first
%   argument is the input and the second is the mask.
%
%   If the rank of the mask M is low, CONVOLVE2 will decompose it into a
%   sum of outer product masks, each of which is applied efficiently as
%   convolution with a row vector and a column vector, by calling CONV2.
%   The function will often be faster than CONV2 or FILTER2 (in some
%   cases much faster) and will produce the same results as CONV2 to
%   within a small tolerance.
%
%   Y = CONVOLVE2(... , TOL) where TOL is a number in the range 0.0 to
%   1.0 computes the convolution using a reduced-rank approximation to
%   M, provided this will speed up the computation. TOL limits the
%   relative sum-squared error in the effective mask; that is, if the
%   effective mask is E, the error is controlled such that
%
%      sum(sum( (M-E) .* (M-E) ))
%      --------------------------    <=  TOL
%          sum(sum( M .* M ))
%
%   See also CONV2, FILTER2, EXINDEX

% Copyright David Young, Feb 2002, revised Jan 2005, Jan 2009, Apr 2011,
% Feb 2014

% Deal with optional arguments
narginchk(2,4);
if nargin < 3
   shape = 'full';    % shape default as for CONV2
   tol = 0;
```

```
elseif nargin < 4
   if isnumeric(shape)
      tol = shape;
      shape = 'full';
   else
      tol = 0;
   end
end

% Set up to do the wrap & reflect operations, not handled by conv2
if ismember(shape, {'wrap' 'circular' 'reflect' 'symmetric' 'replicate'})
   x = extendarr(x, m, shape);
   shape = 'valid';
end

% do the convolution itself
y = doconv(x, m, shape, tol);
end

%--------------------------------------------------------------------------

function y = doconv(x, m, shape, tol)
% Carry out convolution
[mx, nx] = size(x);
[mm, nm] = size(m);

% If the mask is bigger than the input, or it is 1-D already,
% just let CONV2 handle it.
if mm > mx || nm > nx || mm == 1 || nm == 1
   y = conv2(x, m, shape);
else
   % Get svd of mask
   if mm < nm; m = m'; end        % svd(..,0) wants m > n
   [u,s,v] = svd(m, 0);
   s = diag(s);
   rank = trank(m, s, tol);
   if rank*(mm+nm) < mm*nm         % take advantage of low rank
      if mm < nm;  t = u; u = v; v = t; end  % reverse earlier transpose
      vp = v';
      % For some reason, CONV2(H,C,X) is very slow, so use the normal call
      y = conv2(conv2(x, u(:,1)*s(1), shape), vp(1,:), shape);
      for r = 2:rank
         y = y + conv2(conv2(x, u(:,r)*s(r), shape), vp(r,:), shape);
      end
   else
      if mm < nm; m = m'; end     % reverse earlier transpose
      y = conv2(x, m, shape);
   end
end
end

%--------------------------------------------------------------------------

function r = trank(m, s, tol)
% Approximate rank function - returns rank of matrix that fits given
% matrix to within given relative rms error. Expects original matrix
```

```
% and vector of singular values.
if tol < 0 || tol > 1
   error('Tolerance must be in range 0 to 1');
end
if tol == 0            % return estimate of actual rank
   tol = length(m) * max(s) * eps;
   r = sum(s > tol);
else
   ss = s .* s;
   t = (1 - tol) * sum(ss);
   r = 0;
   sm = 0;
   while sm < t
      r = r + 1;
      sm = sm + ss(r);
   end
end
end

%---------------------------------------------------------------------

function y = extendarr(x, m, shape)
% Extend x so as to wrap around on both axes, sufficient to allow a
% "valid" convolution with m to return a result the same size as x.
% We assume mask origin near centre of mask for compatibility with
% "same" option.

[mx, nx] = size(x);
[mm, nm] = size(m);

mo = floor((1+mm)/2); no = floor((1+nm)/2);  % reflected mask origin
ml = mo-1;           nl = no-1;           % mask left/above origin
mr = mm-mo;          nr = nm-no;          % mask right/below origin

% deal with shape option terminology - was inconsistent with exindex
switch shape
   case 'wrap'
      shape = 'circular';
   case 'reflect'
      shape = 'symmetric';
end
y = exindex(x, 1-ml:mx+mr, 1-nl:nx+nr, shape);

end

function arr = exindex(arr, varargin)
%EXINDEX extended array indexing
%   ARROUT = EXINDEX(ARRIN, S1, S2, ...) indexes a virtual array made by
%   extending ARRIN with zeros in all directions, using subscripts S1, S2
%   etc.
%
%   ARROUT = EXINDEX(ARRIN, S1, R1, S2, R2, ...) extends ARRIN using rule
%   R1 on the first dimension, R2 on the second dimension etc.
%
%   ARROUT = EXINDEX(ARRIN, S1, S2, ..., R) extends ARRIN using rule R on
%   every dimension.
```

```
%
%   Subscripts
%   ----------
%
%   Broadly, if V is the virtual extended array, ARROUT = V(S1, S2, ...)
%
%   The elements of the subscript arguments S1, S2 etc must be integers.
%   They need not be positive and are not restricted in any way by the size
%   of ARRIN. Logical indexing and linear indexing are not supported.
%
%   There must be at least one subscript argument for each dimension of
%   ARRIN as reported by NDIMS, except that row and column vectors may have
%   1 or 2 subscripts. A single subscript is taken to refer to the
%   dimension along which the vector lies, as in normal vector indexing.
%   Scalars require 2 subscripts. If there are more subscripts than
%   dimensions, ARRIN is taken to have trailing singleton dimensions, as in
%   normal array indexing.
%
%   The number of dimensions of ARROUT will be the number of subscript
%   arguments, though trailing singleton dimensions will, as usual, be
%   suppressed. The size of ARROUT is given by the normal Matlab rules for
%   the result of indexing into ARRIN: that is
%
%       size(ARROUT) = size( ARRIN(ones(size(S1)), ones(size(S2)), ...) )
%
%   A subscript argument may be the string ':'. This behaves like a colon
%   in ordinary subscripting: a colon for the K'th subscript stands for
%   1:size(ARRIN, K). The 'end' keyword is not supported.
%
%   Rules
%   -----
%
%   Each rule may be one of the following:
%
%   A scalar cell: ARRIN is padded with elements equal to the contents of
%   the cell. The class of the cell contents must be compatible with the
%   class of ARRIN.
%
%       If different constants are used on different dimensions, padding is
%       done in the order of the subscripts. For example, a 2D array is
%       extended first in the row index direction and then in the column
%       index direction. For all other cases, the order in which dimensions
%       are extended has no effect.
%
%   'circular': ARRIN is extended with copies of itself; i.e. V is tiled
%   with ARRIN.
%
%   'symmetric': ARRIN is extended with copies of itself with reflection at
%   its boundaries; i.e. V is tiled with [ARRIN fliplr(ARRIN);
%   flipud(ARRIN) fliplr(flipud(ARRIN))].
%
%   'replicate': ARRIN is extended by copying its border elements; i.e. an
%   element of V is equal to the nearest element of ARRIN.
%
%   If no rule is given, padding is with zeros.
%
```

```
%   Examples
%   --------
%
%   Pad a 2D matrix with K extra rows and columns with reflection on both
%   axes:
%
%       b = exindex(a, 1-k:size(a,1)+k, 1-k:size(a,2)+k, 'symmetric');
%
%   Circularly shift a 2D matrix by R rows downwards and C columns
%   rightwards:
%
%       b = exindex(a, 1-r:size(a,1)-r, 1-c:size(a,2)-c, 'circular');
%
%   Force a row or column vector to be 1024 elements long, trimming or
%   padding with zeros as necessary:
%
%       u = exindex(v, 1:1024);
%
%   The same, with a non-zero padding value:
%
%       u = exindex(v, 1:1024, {-1});   % note constant in cell
%
%   Truncate or extend all the rows of a matrix to 1024 columns:
%
%       b = exindex(a, ':', 1:1024);
%
%   Extend a 2-D array into the third dimension by copying it:
%
%       b = exindex(a, ':', ':', 1:3, 'replicate');
%
%   Pad a 1-D cell array with cells containing the empty matrix:
%
%       cellout = exindex(cellin, 0:10, {{[]}});
%
%   See also: padarray, circshift, repmat

% Copyright David Young 2010

% Sort out arguments
[exindices, rules, nd, sz] = getinputs(arr, varargin{:});
consts = cellfun(@iscell, rules);  % Check for constants, as can be
constused = any(consts);           % more efficient if there are none

% Setup for constant padding
if constused
   tofill = cell(1, nd);
end

% Main loop over subscript arguments, transforming them into valid
% subscripts into arr using the rule for each dimension
if constused
   for i = 1:nd
      [exindices{i}, tofill{i}] = extend(exindices{i}, rules{i}, sz(i));
   end
else % no need for information for doing constants
   for i = 1:nd
```

```
        exindices{i} = extend(exindices{i}, rules{i}, sz(i));
    end
end

% Create the new array by indexing into arr. If there are no constants,
% this does the whole job
arr = arr(exindices{:});

% Fill areas that need constants
if constused
    % Get full range of output array indices
    ranges = arrayfun(@(x) {1:x}, size(arr));
    for i = nd:-1:1    % order matters
        if consts(i)
            ranges{i} = tofill{i};      % don't overwrite original
            c = rules{i};               % get constant and fill ...
            arr(ranges{:}) = c{1};      % we've checked c is scalar
            ranges{i} = ~tofill{i};     % don't overwrite
        end
    end
end

end

% ---------------------------------------------------------------------

function [exindices, rules, nd, sz] = getinputs(arr, varargin)
% Sort out and check arguments. Inputs are as given in the help comments
% for exindex. Outputs are cell arrays; each element of exindices is a
% set of integer extended indices which has been checked for validity; each
% element of rules is a rule which has not been checked for validity.

% Use index/rules arguments only to establish no. dimensions - ndims(arr)
% is no use, as trailing singleton dimensions truncated and vectors can be
% 2D or 1D
nd = length(varargin);
if nd == 0
    error('exindex:missingargs', 'Not enough arguments');
elseif nd == 1
    exindices = varargin;
    rules = {{0}};
elseif ~(isnumeric(varargin{2}) || strcmp(varargin{2}, ':'))
    % have alternating indices and rule
    nd = nd/2;
    if round(nd) ~= nd
        error('exindex:badnumargs', ...
            'Odd number of arguments after initial index/rule pair');
    end
    exindices = varargin(1:2:end);
    rules = varargin(2:2:end);
elseif nd > 2 && ~(isnumeric(varargin{end}) || strcmp(varargin{end}, ':'))
    % have a general rule at end
    nd = nd - 1;
    exindices = varargin(1:nd);
    [rules{1:nd}] = deal(varargin{end});
else
```

```
    % no rule is specified
    exindices = varargin;
    [rules{1:nd}] = deal({0});
end

% Sort out mismatch of apparent array size and number of dimensions
% indexed
sz = size(arr);
ndarr = ndims(arr);
if nd < ndarr
    if nd == 1 && ndarr == 2
        % Matlab allows vectors to be indexed with a single subscript and
        % to retain their shape. In all other cases (including scalars) a
        % single subscript causes the output to take the same shape as the
        % subscript array - we can't deal with this.
        if sz(1) == 1 && sz(2) > 1
            % have a row vector
            exindices = [{1} exindices {1}];
            rules = [rules rules];  % 1st rule doesn't matter
        elseif sz(2) == 1 && sz(1) > 1
            % have a column vector
            exindices = [exindices {1}];
            rules = [rules rules];  % 2nd rule doesn't matter
        else
            error('exindex:wantvector', ...
                'Only one index but array is not a vector');
        end
    else
        error('exindex:toofewindices', ...
            'Array has more dimensions than there are index arguments');
    end
    nd = 2;
elseif nd > ndarr
    % Effective array size
    sz = [sz ones(1, nd-ndarr)];
end

% Expand any colons now to simplify checking.
% It's tempting to allow the 'end' keyword here: easy to substitute the
% size of the dimension. However, to be worthwhile it would be necessary to
% use evalin('caller',...) so that expressions using end could be given as
% in normal indexing. This would mean moving the code up to exindex itself,
% and evalin makes for inefficiency and fragility, so this hasn't been
% done.
colons = strcmp(exindices, ':');
if any(colons)  % saves a little time
    exindices(colons) = arrayfun(@(x) {1:x}, sz(colons));
end

% Check the indices (rules are checked as required in extend)
checkindex = @(ind) validateattributes(ind, {'numeric'}, ...
    {'integer'}, 'exindex', 'index');
cellfun(checkindex, exindices);

end
```

```
% --------------------------------------------------------------------

function [ind, tofill] = extend(ind, rule, s)

% The core function: maps extended array subscripts into valid input array
% subscripts.

if ischar(rule)    % pad with rule
   tofill = [];  % never used
   switch rule
      case 'replicate'
         ind = min( max(1,ind), s );
      case 'circular'
         ind = mod(ind-1, s) + 1;
      case 'symmetric'
         ind = mod(ind-1, 2*s) + 1;
         ott = ind > s;
         ind(ott) = 2*s + 1 - ind(ott);
      otherwise
         error('exindex:badopt', 'Unknown option');
   end

elseif iscell(rule) && isscalar(rule)     % pad with constant

   % The main messiness is due to constant padding. This can't be done
   % with indexing into the original array, but we want the indexing
   % structure to be preserved, so for now we index to element 1 on each
   % dimension, and record the indices of the regions that need to be
   % fixed.

   tofill = ind < 1 | ind > s;
   ind(tofill) = 1;
else
   error('exindex:badconst', 'Expecting string or scalar cell');

end
end
```

Appendix B: Questionnaire

Vragenlijst Experiment "Contrast Perceptie Op De Weg"

1. Hoe oud bent u?

…….... jaar

2. Wat is de kleur van uw ogen?

……....

3. Draagt u een bril of contactlenzen?

Ja, namelijk :

…….....
.....
(wat is de sterkte, heeft u een cilindrische afwijking?)

Nee

4. Heeft u operaties aan uw oog ondergaan (bijvoorbeeld een staaroperatie of laserbehandeling)?

Ja, namelijk:

…….....
.....

Nee

5. Heeft u andere afwijkingen aan uw ogen?

Ja, namelijk:

…….....
.....

Nee

6. Hoe alert voelt u zich op dit moment?

1. Extreem alert
2. Heel alert
3. Alert
4. Ietwat alert
5. Niet alert, maar ook niet slaperig
6. Enkele tekenen van slaperigheid
7. Slaperig, maar het kost geen moeite om wakker te blijven
8. Slaperig, en het kost wat moeite om wakker te blijven
9. Erg slaperig, vecht tegen de slaap

7. Hoe zou u uw slaapkwaliteit van afgelopen nacht beoordelen?

1. Heel slecht
2. Slecht
3. Oké
4. Goed
5. Heel goed

8. Heeft u vandaag cafeïnehoudende producten genuttigd, zoals koffie of thee?

Ja, namelijk:

…….....
.....
(wat, en hoeveel?)

Nee

9. Heeft u een rijbewijs?

Ja, voor ……. jaar.

Nee (dit is het einde van de vragenlijst voor u)

10. Hoeveel dagen in de week rijdt u gemiddeld auto?

…… (1 tot 7)

11. Op een gemiddelde dag waarop u autorijdt, voor hoe lang rijdt u dan?

…… (uren/minuten)

Questionnaire Experiment "Contrast Perception On The Road"

1. What is your age?

…….... years

2. What is your eye color?

……....

3. Do you wear glasses or contact lenses to correct your vision?

Yes, namely:

…….....
.....

(prescription: minus or plus how much, cylinder, etc.)

No

4. Have you undergone any eye surgery (for example cataract surgery or laser vision correction)?

Yes, namely:

…….....
.....

No

5. Do you have any other known visual deficiencies?

Yes, namely:

…….....
.....

No

6. How alert do you feel at this moment?

1. Extremely alert
2. Very alert
3. Alert
4. Rather alert
5. Neither alert nor sleepy
6. Some signs of sleepiness
7. Sleepy, but no effort to keep awake
8. Sleepy, but some effort to keep awake
9. Very sleepy, fighting sleep

7. How would you rate the quality of your sleep?

1. Very poor
2. Poor
3. Fair
4. Good
5. Very good

8. Have you consumed any caffeine containing products, like coffee or tea, today?

Yes, namely:

…….....
.....

(what, how much?)

No

9. Do you have a driver's license?

Yes, for ……. years.

No (you have finished the questionnaire)

10. On average, how many days of the week do you drive a car?

…… (1 to 7)

11. On an average day of driving a car, how long do you drive it?

…… (minutes/hours)

Appendix C: Informed consent forms

TU/e EINDHOVEN UNIVERSITY OF TECHNOLOGY

Informatieformulier voor proefpersonen

Dit document geeft u informatie over het onderzoek 'Contrast perceptie op de weg'. Voordat het onderzoek begint is het belangrijk dat u kennisneemt van de werkwijze die bij dit onderzoek gevolgd wordt en dat u instemt met vrijwillige deelname. Lees dit document a.u.b. aandachtig door.

Doel en nut van het onderzoek

Het doel van dit onderzoek is om de zichtbaarheid van wegmarkeringen (pijlen) te meten, in situaties waar verblinding optreed. De verkregen informatie wordt gebruikt om de contrast perceptie van de onderzoeksgroep te beschrijven, en hoe deze perceptie afhangt van verschillende verlichtingsscenarios.
Het onderzoek wordt uitgevoerd door Tom van Hoesel, een master student begeleid door Raymond Cuijpers van de Human-Technology Interaction groep aan de Technische Universiteit Eindhoven.

Procedure

Bij aanvang zullen verschillende korte oogtesten worden uitgevoerd. Dit zijn een kleurenblindheidstest, een scherpte test (u kunt deze kennen van de oogarts), en een test om te kijken hoe gevoelig u bent voor verblinding. Deze scherptetest zal beslissen of uw zicht scherp genoeg is om te kunnen deelnemen aan dit experiment. Bij deze verblindingstest zult u met één oog in een apparaat kijken naar twee knipperende halve circels. Hierbij zal u moeten aangeven of de linker of rechter halve circel sneller knippert. Omdat u met deze test waarschijnlijk niet bekend bent, zal er voor de echte test mogelijkheid zijn om dit een keer te oefenen. Daarna zal u een korte vragenlijst krijgen waarin verschillende dingen gevraagd worden over uw zicht (draagt u een bril, heeft u operaties aan uw oog gehad, etc.), over hoe hoevaak u zich in het verkeer bevindt, en over uw alertheid.
Na deze vragenlijst begint het experiment en zal u plaatnemen voor een tv scherm waarop een wegdek te zien zal zijn. Op dit wegdek staat een wegmarkering: een pijl die naar links of naar rechts wijst. U heeft per scène 2 seconden de tijd om met behulp van de pijltjes op het toetsenbord aan te geven of deze pijl naar links of naar rechts wijst. Als u twijfelt, zult u moeten gokken. Het is van belang dat u tijdens deze procedure zo snel en accuraat mogelijk antwoord. Terwijl u verschillende scènes beoordeelt, zal een LED-lampje in uw gezicht schijnen. Het beoordelen van de verschillende scènes zal zo'n 20 tot 30 minuten duren.
Na dit experiment zal er ruimte zijn voor vragen en opmerkingen, en wordt u gecompenseerd voor uw deelname.

Risico's

Zowel de vragenlijst als eerste twee oogtesten brengen geen risico's met zich mee. De verblindingstest kan enigszins oncomfortabel zijn, omdat u gedurende een korte periode gefocust naar knipperende lichten zult moeten kijken.

Tijdens het beoordelen van de pijl/wegdek scènes, kan het voorkomen dat u moe wordt van het focussen. Ook kan het voorkomen dat u geïrriteerd of overprikkeld raakt door het LED-lampje dat op uw gezicht schijnt of door de wisselende scènes op het scherm voor u.

Verder brengt dit onderzoek geen risico's of nadelige bijwerkingen op de langere termijn met zich mee. Mocht u zich toch op wat voor manier ook oncomfortabel voelen gedurende het experiment, dan kunt u dit aangeven en een pauze nemen, of volledig stoppen met het onderzoek.

Duur
De instructies, metingen en debriefing duren ongeveer 1 uur.

Participanten
U bent geselecteerd omdat u als participant geregistreerd staat in de participanten database van de Human-Technology Interaction group van de Technische Universiteit Eindhoven.

Vrijwilligheid
Uw deelname is geheel vrijwillig. U kunt zonder opgaaf van redenen weigeren mee te doen aan het onderzoek en uw deelname op welk moment dan ook afbreken. Ook kunt u nog achteraf (binnen 24 uur) weigeren dat uw gegevens voor het onderzoek mogen worden gebruikt. Dit alles blijft te allen tijde zonder nadelige gevolgen.

Vergoeding
De vergoeding bedraagt 10 euro wanneer u het volledige experiment voltooid (met €2,00 extra indien u niet op de TU/e of Fontys Eindhoven studeert of werkt).
In het geval dat uit de scherptetest blijkt dat u niet scherp genoeg ziet om te kunnen deelnemen aan dit experiment, zal uw vergoeding 2 euro bedragen (met €2,00 extra indien u niet op de TU/e of Fontys Eindhoven studeert of werkt).
In beide gevallen zal de betaling contant gedaan worden.

Confidentiality and use, storage, and sharing of data.
Bij alle onderzoeken van Human-Technology Interaction wordt gewerkt volgens de ethische code van het NIP (Nederlands Instituut voor Psychologen) en deze studie is goedgekeurd door de Ethische Commissie van de HTI groep.

In de studie zullen persoonlijke (uw leeftijd, ooggezondheid, rijervaring) en experimentele data (uw links/rechts indicatie van de pijlen op de weg) worden verzameld, geanalyseerd, en opgeslagen. Het doel van het verzamelen, analyseren en opslaan van deze data is om de onderzoeksvraag te beantwoorden en de resultaten te publiceren in wetenschappelijke literatuur. Om uw privacy te beschermen verzamelen wij geen data die u kunnen identificeren. In het geval uit de scherptetest blijkt dat uw zicht niet scherp genoeg is om deel te nemen, zal alle data die tot op dat punt zijn verzameld worden weggegooid.

Deze studie bedraagt een samenwerking tussen de Technische Universiteit Eindhoven en de KU Leuven (België). De verzamelde data zal daarom ook gedeeld worden met de KU Leuven. De data wordt gecodeerd en wordt buiten de genoemde universiteiten niet gedeeld. De data zal geen informatie bevatten die u kan identificeren.

Er zullen geen video of audio opnames gemaakt worden die u kunnen identificeren.

Nadere inlichtingen
Als u nog verdere informatie wilt over dit onderzoek, dan kunt u zich wenden tot Tom van Hoesel (email: t.r.c.v.hoesel@student.tue.nl).
Voor eventuele klachten over dit onderzoek kunt u terecht bij de begeleidend docent, Raymond Cuijpers (r.h.cuijpers@tue.nl). U kunt onregelmatigheden op het gebied van wetenschappelijke integriteit rapporteren bij vertrouwenspersonen van de TU/e.

Geïnformeerde toestemming

Contrast perceptie op de weg

- Ik heb de informatie van het bijbehorende informatieformulier voor deelnemers gelezen en begrepen.

- Ik heb de gelegenheid gekregen om vragen te stellen. Mijn vragen zijn voldoende beantwoord en ik had voldoende tijd om te beslissen of ik meedoe.

- Ik weet dat mijn deelname volledig vrijwillig is. Ik weet dat ik kan weigeren deel te nemen en dat ik mijn deelname op elk moment tijdens de studie kan stopzetten, zonder opgaaf van redenen. Ik weet dat ik de toestemming om mijn gegevens te gebruiken kan intrekken tot 24 uur nadat de gegevens zijn vastgelegd.

- Ik ga ermee akkoord om vrijwillig deel te nemen aan dit onderzoek uitgevoerd door de onderzoeksgroep Human Technology Interaction van de Technische Universiteit Eindhoven in samenwerking met de KU Leuven.

- Ik weet dat geen informatie die kan worden gebruikt om mij of mijn reacties in dit onderzoek persoonlijk te identificeren, zal worden gedeeld met iemand buiten het onderzoeksteam.

Certificaat van toestemming

Ik, (NAAM) .....
wil en geef toestemming en consent om deel te nemen aan dit onderzoek.

_____ _____

Handtekening van de participant Datum

Information form for participants

This document gives you information about the study "Contrast perception on the road". Before the study begins, it is important that you learn about the procedure followed in this study and that you give your informed consent for voluntary participation. Please read this document carefully.

Aim and benefit of the study

The aim of this study is to measure the visibility of road-mark arrows at different distances and under different lighting scenarios, under conditions of glare. This information is used to compare how these different factors impact contrast perception and to make models that can predict this.
This study is performed by Tom van Hoesel, a master student supervised by Raymond Cuijpers of the Human-Technology Interaction group at Eindhoven University of Technology.

Procedure

At the start, you will be given a short questionnaire asking various things regarding your vision (do you wear glasses, have you undergone eye-surgery, etc.), regarding your participation in traffic, and regarding your alertness.
Then, several short eye tests will be administered. These are a color blindness test, a visual acuity test, and a test to measure how sensitive you are to glare. The visual acuity test will decide whether or not your vision is clear enough to participate in this experiment. In case you cannot participate, you will also be compensated for your time (see "Compensation"). In the glare test, you will look into a device with one eye. You will see two blinking half-circles, and have to indicate whether the left or right half-circle is blinking faster. Since you probably are not familiar with this test, there will be an opportunity to practice this procedure.
After these tests the experiment starts, and you will be seated in front of a TV screen showing a road. On this road is a roadmark: an arrow pointing either to the left or to the right. You will have 2 seconds per scene to indicate, using the arrows on the keyboard, whether this arrow is pointing left or right. When in doubt, you will have to guess to the best of your abilities. It is important that you answer as quickly and accurately as possible during this procedure. While you are assessing different scenes, a small LED light will shine in your face. Judging the different scenes will take about 20 to 30 minutes.
After the experiment, there will be the opportunity for comments or questions, and you will be compensated for your participation.

Risks

Both the questionnaire and first two eye tests pose no risks. The glare test may be somewhat uncomfortable, because you will have to focus on flashing lights for a short period of time. While reviewing the arrow/road scenes, you might experience fatigue caused by focusing. You may also become annoyed or overstimulated by the LED light shining on your face, or by the changing scenes on the screen in front of you.
Besides the aforementioned, this study does not involve any (long-term) risks or adverse side effects. Should you nevertheless feel uncomfortable in any way during the experiment, you can report it to the experimenter and take a break, or stop the study altogether.

Duration

The instructions, measurements and debriefing will take approximately 1 hour.

TU/e EINDHOVEN UNIVERSITY OF TECHNOLOGY

Participants

You were selected because you were registered as participant in the participant database of the Human Technology Interaction group of the Eindhoven University of Technology.

Voluntary

Your participation is completely voluntary. You can refuse to participate without giving any reasons and you can stop your participation at any time during the study. You can also withdraw your permission to use your data up to 24 hours after they were recorded. None of this will have any negative consequences for you whatsoever.

Compensation

When you finish the complete experiment, you will be paid 10 euros (plus an additional €2.00 if you do not study or work at the TU/e or Fontys Eindhoven).
In case your visual acuity is not sufficient for participation in this experiment, you will be paid 2 euros (plus an additional €2.00 if you do not study or work at the TU/e or Fontys Eindhoven).

In both cases, payments will be done in cash.

Confidentiality and use, storage, and sharing of data.

All research conducted at the Human-Technology Interaction Group adheres to the Code of Ethics of the NIP (Nederlands Instituut voor Psychologen – Dutch Institute for Psychologists), and this study has been approved by the Ethical Review Board of the department.

In this study personal data (your age, eye-health, traffic participation) and experimental data (choices regarding the roadmark arrow directions) will be recorded, analyzed, and stored. The goal of collecting, analyzing, and storing this data is to answer the research question and publish the results in the scientific literature. To protect your privacy, no information that can be used to personally identify you will be collected.
In case your visual acuity is not sufficient to participate, all data collected up to that point will be discarded.

This study is a cooperation between the Eindhoven University of Technology and the KU Leuven (Belgium). The collected data is therefore shared with the KU Leuven. The data is encoded and is not shared outside the universities. You cannot be identified by the data.

No video or audio recordings are made that could identify you.

Further information

If you want more information about this study, you can contact Tom van Hoesel (contact email: t.r.c.v.hoesel@student.tue.nl).

If you have any complaints about this study, please contact the supervisor, Raymond Cuijpers (r.h.cuijpers@tue.nl). You can report irregularities related to scientific integrity to confidential advisors of the TU/e.

Informed consent form

Contrast perception on the road

- I have read and understood the information of the corresponding information form for participants.

- I have been given the opportunity to ask questions. My questions are sufficiently answered, and I had sufficient time to decide whether I participate.

- I know that my participation is completely voluntary. I know that I can refuse to participate and that I can stop my participation at any time during the study, without giving any reasons. I know that I can withdraw permission to use my data up to 24 hours after the data have been recorded.

- I agree to voluntarily participate in this study carried out by the research group Human Technology Interaction of the Eindhoven University of Technology in cooperation with the KU Leuven.

- I know that no information that can be used to personally identify me or my responses in this study will be shared with anyone outside of the research team.

Certificate of consent

I, (NAME) .....
want and provide consent to participate in this study.

_____ _____

Participant's Signature Date

Appendix D: Pilot study on the influence of a windshield on luminance difference thresholds

Introduction. When it comes to driving a car, there is another factor influencing the amount of glare that influences your contrast perception: the windshield. This layer of glass between you and the road acts as an extra medium through which glare can occur. The perception of a veiling luminance on the windshield can occur as a result of two processes: the windshield can reflect sunlight from the dashboard cover, and dirt on or damage in the windshield can scatter sunlight (Boulos et al., 1997). Research shows that light scattering due to dirt is especially negatively impacting nighttime visibility, effects of which are stronger in conditions of glare (Owens et al., 1992). Because of this, using a mock-up windshield provided by Rijkswaterstaat, a small pilot study was done to investigate the effects of a dirty windshield on the luminance difference threshold.

Method. The method was exactly the same as used in the rest of this work, except for the presence or absence of a windshield as an additional factor. The sample size for this pilot was small (n = 2, male, aged 24 and 28), and therefore no statistical inferences will be drawn. The used windshield was that of a Nissan Note (Pilkington M1250), and was placed at an angle of 30 degrees in front of the participant. Figure 41 shows this setup-up, together with the point-of-view from the perspective of the participant, showing the extra veiling luminance caused by the glare source interacting with the windshield.

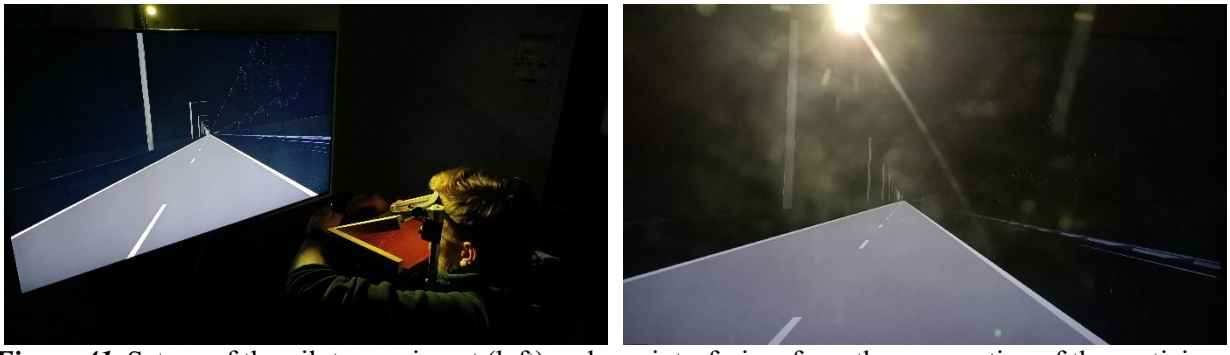

Figure 41. Set-up of the pilot experiment (left) and a point-of-view from the perspective of the participant (right).

Results. Figure 42 shows the mean luminance difference thresholds for the different conditions. It becomes evident that in the condition with both glare and a windshield, the thresholds are consistently higher across all arrow sizes and road luminances. The luminance difference threshold for conditions without a windshield also seems to be lower than those conditions with a windshield.

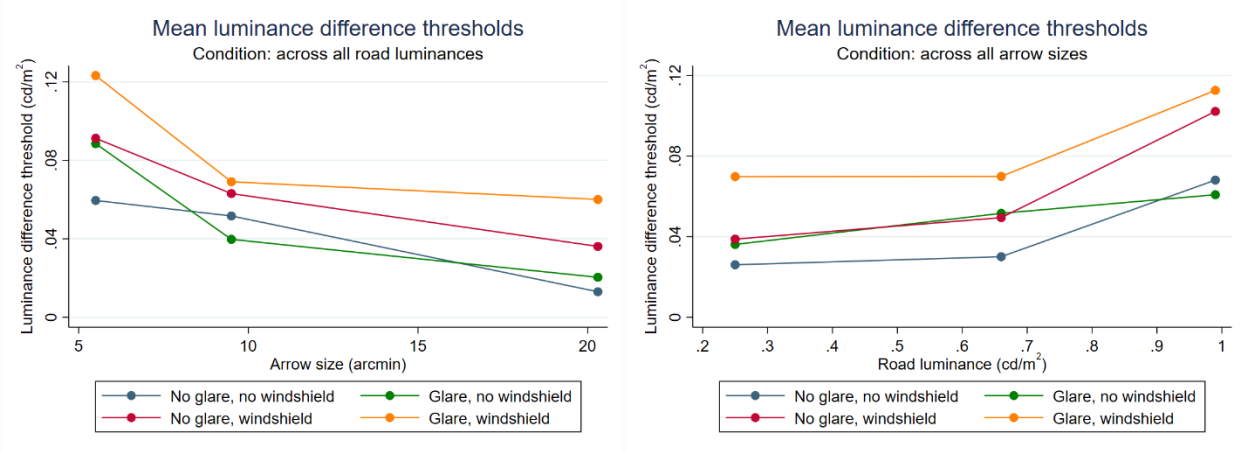

Figure 42. Mean luminance difference thresholds in the pilot, across all glare, windshield, road luminance, and arrow size conditions.

Discussion. As expected, the presence of a windshield increases the luminance difference threshold. However, comparing the conditions "*no glare, windshield*" with "*glare, no windshield*" the results hint at an interesting phenomenon: as separate factors, the presence of a dirty windshield might be more detrimental to contrast perception than the presence of glare. It will be very interesting to see how these numbers would change with age, given the characteristics of aging visual systems.

As a final note, it goes without saying that these results and conclusions are highly preliminary, and should only be used to inspire future investigation.